Few-Body Physics in Quantum Gases

Dissertation

zur

Erlangung des Doktorgrades (Dr. rer. nat.)

der

Mathematisch–Naturwissenschaftlichen Fakultät

der

Rheinischen Friedrich–Wilhelms–Universität Bonn

vorgelegt von

Kerstin Helfrich

aus

Aschaffenburg

Bonn 2011

Angefertigt mit Genehmigung der
Mathematisch-Naturwissenschaftlichen Fakultät der
Rheinischen Friedrich-Wilhelms-Universität Bonn

Diese Dissertation ist auf dem Hochschulschriftenserver der ULB Bonn unter
`http://hss.ulb.uni-bonn.de/diss_online` elektronisch publiziert.

1. Gutachter: Prof. Dr. Hans-Werner Hammer

2. Gutachter: Prof. Dr. Achim Rosch

Tag der Promotion: 14.10.2011

Erscheinungsjahr: 2011

Abstract

Few-body effects play an important role for the understanding of ultracold quantum gases. We make use of an effective field theory approach to investigate various aspects of universal few-body physics close to a Feshbach resonance. That is the regime where the scattering length is large compared to all other length scales of the system and thus determines the observables. It is also the regime where the Efimov effect whose main characteristic is the occurrence of a sequence of three-body bound states becomes important. At unitarity, i.e., for diverging scattering length, the ratio of binding energies of neighboring states approaches a constant. The existence of those trimers can be captured by a single three-body parameter and influences observables such as recombination rates.
Starting from adequate Lagrangians, we derive atom-dimer scattering amplitudes that contain all information of interest about the three-particle systems. With this method, we first investigate the scattering of atoms and dimers at finite temperature in the presence of the Efimov effect. We calculate the dimer relaxation rate and obtain good agreement with available experimental data. Furthermore, heteronuclear mixtures exhibiting large interspecies scattering length are studied in detail. If bosons are the majority species, the Efimov effect occurs in an S-wave channel and we are able to compute three-body recombination and dimer relaxation rates. The results are compared to the outcome of two existing experiments. For mainly fermionic systems, the Efimov effect is only present in an overall P-wave and three-body recombination at threshold vanishes. However, in mixtures of atoms and dimers, scattering cross sections and dimer relaxation show the typical Efimov behavior of log-periodicity. We also consider two-dimensional Bose gases, where the Efimov effect does not occur. For those systems, we derive an equation including the first non-universal corrections and deduce three-body observables such as binding energies and atom-dimer scattering parameters.

Parts of this thesis have been published in the following articles and conference proceedings:

- K. Helfrich and H.-W. Hammer, *Resonant atom-dimer relaxation in ultracold atoms*, Europhys. Lett. **86**, 53003 (2009).
- K. Helfrich and H.-W. Hammer, *The heteronuclear Efimov effect*, Proceedings of the 19th International IUPAP Conference on Few-Body Problems in Physics, Bonn, Germany, EPJ Web of Conferences 3, 02007 (2010).
- K. Helfrich, H.-W. Hammer, and D.S. Petrov, *Three-body problem in heteronuclear mixtures with resonant interspecies interaction*, Phys. Rev. A **81**, 042715 (2010).
- K. Helfrich and H.-W. Hammer, *Resonant three-body physics in two spatial dimensions*, Phys. Rev. A **83**, 052703 (2011).
- K. Helfrich and H.-W. Hammer, *Three bosons in two dimensions*, in *Strong interactions: From methods to structures*, Mini proceedings of the 474. WE-Heraeus-Seminar "Strong interactions: From methods to structures", Bad Honnef, Germany, arXiv:1104.0847 [hep-ph] (2011).
- K. Helfrich and H.-W. Hammer, *On the Efimov Effect in Higher Partial Waves*, J. Phys. B: At. Mol. Opt. Phys. **44**, 215301 (2011).

Contents

Notation and Conventions

Here, we introduce parameters and variables that are important throughout the whole thesis. This should simplify the reading of the work and serve as reference.

Variable	Description
a	Scattering length
a_0	Bohr radius, $a_0 = 5.29177209 \cdot 10^{-11}$ m
a_- $(a < 0)$	Scatt. length for which the Efimov trimer hits the three-atom threshold
a_* $(a > 0)$	Scatt. length for which the Efimov trimer hits the atom-dimer threshold
a_{0*} $(a > 0)$	Scatt. length for which the three-body recombination rate is minimal
a_+ $(a > 0)$	Scatt. length for which the three-body recombination rate is maximal
A	Atom
$\mathcal{A}$	Off-shell scattering amplitude
d	Auxiliary dimer field
D	Dimer
D	Number of spatial dimensions
$D(P_0, \vec{P})$	Dimer propagator (energy, momentum)
E	Total energy, normally: three-body energy
$E_{\mathrm{D/T/4}}$	Binding energies of the two-, three and four-body system
f	Scattering amplitude
$g_{2/3}$	Bare two- and three-body coupling constants
$\vec{k}$, k	Wave vector, wave number, $k = \lvert\vec{k}\rvert$
k_{br}	Dimer breakup wave number
k_{B}	Boltzmann constant, $k_{\mathrm{B}} = 1.38065 \cdot 10^{-23}$ J/K
ℓ	Typical length scale of a system
ℓ_{vdW}	Van der Waals length
L	Total angular momentum quantum number
m	Mass of the particles
m_i	Mass of the particles of species i
M	Mass of the heteronuclear dimer, $M = m_1 + m_2$
n	Index of Efimov branches
n_*	Index of one Efimov trimer used to fix the other Efimov branches
$n_{\mathrm{A/D}}$	Number density of atoms/dimers
$N_{\mathrm{A/D}}$	Number of atoms/dimers
r	Effective range
s_L	Transcendental number determining the scaling factor for general L, depends on δ; for three identical bosons with three resonant interactions: $s_0 \approx 1.00624$
T	Trimer
T	Temperature

Variable	Description
α_d	Three-body recombination rate into deep dimers
α_s	Three-body recombination rate into shallow dimers (only for $a > 0$)
α_tot	Total three-body recombination rate
β	Dimer relaxation rate into deep dimers
δ	Mass ratio, $\delta = m_1/m_2$
ϵ	Small parameter, $\epsilon \to 0^+$ implied
η_*	Width parameter, closely connected to the lifetime of the Efimov trimers
γ_E	Euler-Mascheroni constant, $\gamma_\mathrm{E} = 0.5772156649$
κ	Binding wave number
κ_*	Binding wave number of the Efimov trimer labeled n_*
Λ	Momentum cutoff
Λ_c	Complex momentum cutoff, $\Lambda_\mathrm{c} = \Lambda \mathrm{e}^{i\eta_*/s_L}$
μ	Reduced mass of the heteronuclear two-particle system, $\mu = m_1 m_2/M$
μ_AD	Reduced mass of the atom-dimer system, $\mu_\mathrm{AD} = m_2 M/(m_2 + M)$
σ	Scattering cross section
$\sigma_\mathrm{AD}^{(\mathrm{el/inel/tot})}$	Elastic/inelastic/total atom-dimer scattering cross section
ψ_i	Bosonic or fermionic field of particle i

Note that throughout the whole work, $\hbar = 1$ is used when convenient but restored for the final results. Therefore, the terms 'wave number' and 'momentum' are used interchangeably. Furthermore, as we are interested in applications to ultracold atomic gases, bosons are often called *atoms*, except in Chapter 6 where fermionic atoms play a central role. This distinction will be clearly stated. Two-body bound states are denoted as *dimers*, three-body bound states as *trimers*, and four-body bound states as *tetramers*.

Chapter 1

Introduction

Since the invention of the laser more than half a century ago, the field of (cold) atomic gases has advanced in large steps. The laser opened new possibilities for spectroscopy and allowed for the cooling, trapping and manipulation of atoms, either in large ensembles or on the single atom level. Quite a few of the newly developed techniques were also honored by Nobel prizes, e.g., in 1997 for laser cooling and in 2005 for the frequency comb techniques. One of the most prominent achievements was the realization of a Bose-Einstein condensate (BEC). The existence of such a condensed state in which the particles occupy exactly the same quantum state and are thus described by a single wave function was already predicted in 1924 by Bose and Einstein [Bo24, Ei24]. Such weakly interacting BECs could finally be realized in 1995 in gases of rubidium by Wieman, Cornell and coworkers [An$^+$95], in sodium by Ketterle's group [Da$^+$95], and in lithium by Hulet and colleagues [BSTH95]. Shortly afterwards, DeMarco and Jin also achieved the formation of a degenerate Fermi gas [DJ99], and other atomic species were condensed. By now, at least 17 types of atoms, magnons, phonons, and molecules were used for BECs and at least three elements were brought to Fermi degeneracy [ucan]. However, the manipulation and investigation of these extreme quantum states still requires ongoing research.

Bose-Einstein condensation and superfluidity are examples for many-body effects in ultracold atomic gases. For the understanding of these quantum systems, few-body effects play an equally important role. The scattering of particles, the formation of bound states etc. influence the behavior of the whole ensemble. It is therefore vital to investigate both aspects of physics and their interplay. One of the most intriguing facets of few-body physics is the Efimov effect involving three particles. It was already predicted by Vitaly Efimov in 1970 [Ef70], but it took 35 years until signatures of it could be observed in an ultracold atom experiment in Grimm's group [Kr$^+$06]. The effect occurs in systems with large *two-body scattering length* a which can be thought of as a measure of the strength of the two-body interaction. For more than ten years now, it has been experimentally possible to adjust the scattering length of atoms with the help of a magnetic field via *Feshbach resonances* [In$^+$98]. This tunability is crucial for the detection of the Efimov effect. For its most prominent feature is the formation of a series of three-body bound states, called Efimov trimers. They exhibit a *geometric spectrum*, i.e., if a is multiplied by a *scaling factor* λ, one finds the next trimer state whose size is a factor of λ larger. At $a^{-1} = 0$, the energies of neighboring trimers differ by a factor of λ^2. For three identical bosons, $\lambda \approx 22.7$ was derived. So for diverging scattering length

and vanishing energy, there is an accumulation point of, in principle, an infinite number of such Efimov trimers. It is intuitively clear that the existence of such molecules influences the behavior of the whole ensemble of cold atoms. They can, e.g., lead to enhanced scattering rates and therefore expel atoms from the trap. The resulting losses can be large enough to obstruct the experiments, and apparently did so during the first attempts in creating BECs.

The fact that large scattering lengths are necessary for the Efimov effect to occur might seem like an obstacle at first. It turns out, however, that this makes it even more interesting from a theoretical point of view. If a is large, the system enters the so-called *universal regime* where the scattering length is the only important length scale present and where the details of the underlying short-range interaction do not play a role. Therefore, the observed effects are universal, i.e., they are present in any system exhibiting a large scattering length whether it is intrinsically large or induced. An example for this is the universal two-body bound state present in systems with a large positive scattering length. For nuclear physics with naturally large scattering lengths between the nucleons, the bound state is the deuteron with its very small binding energy. Helium atoms are an example for atoms that naturally exhibit a large a, and the helium dimer is also only very slightly bound. Because the Efimov effect is a three-particle phenomenon, one more parameter is needed beside the scattering length for a full description of the system. The so-called *three-body parameter* cannot be easily determined theoretically, but has to be taken from experiment. In principle, these two parameters then suffice to describe the trimer bound states or observables such as recombination rates in the universal regime. By now, the Efimov effect has been seen in ten experiments (for a fairly recent review, see Ref. [FG10]). Some of those prove the existence of the effect unambiguously, as they have been able to measure at least two Efimov features showing the universal scaling by a factor of 22.7.

Around the time of the first experimental confirmation of the Efimov effect [Kr$^+$06], a real surge of theoretical publications concerning the Efimov effect in general and the description of the data points for temperatures as high as 250 nK set in. For the recombination rates taken at $T = 10\,\mathrm{nK}$, universal predictions at zero temperature could successfully be used [NM99, EGB99, BBH00, BH04, BH07b]. These were not valid at higher temperature, however, and the finite-temperature effects had to be included. This was done by various groups in various ways. D'Incao and coworkers made use of a model with a two-body potential. This potential contains two parameters that can be tuned to support one or two bound states [DSE04, DGE09]. Massignan and Stoof investigated scattering states in a model with four parameters that is valid for atoms close to Feshbach resonances [MS08]. Universal approaches were also used to calculate the three-body recombination rates for negative scattering length including finite temperature effects. Jonsell derived the rate in the adiabatic hyperspherical approximation [Jo06] and Yamashita et al. used the resonance approximation [YFT07]. For the case of positive scattering length, simplifying assumptions could be made such that some universal scaling functions could be neglected [BKP07, Sh07, PS08]. Most of these approaches were taken further, e.g., for the description of the newer experiments, and are still investigated. However, some of the methods mentioned contain uncontrolled approximations.

A tool well suited to describe universal physics and gain control over higher order contributions is effective field theory (EFT). It makes use of the largely different scales that are present in systems interacting resonantly, i.e., via a large scattering length. The interaction can then be incorporated as a contact potential. This corresponds to the already mentioned

principle of universality, that it is not necessary to know the exact underlying short-range potential. Only the long-range part must be reproduced. This requirement can be fulfilled with the help of a renormalization procedure where the parameters in the potential are matched to physical quantities. The framework of how to use EFT to describe resonantly interacting atoms in ultracold quantum gases and derive observables has been known for more than ten years [BHvK99a, BHvK99b]. In these references, Bedaque and coworkers introduced the incorporation of a three-body parameter to obtain a method suitable for the description of the Efimov effect and implemented it successfully. Next-to-leading order calculations including effective-range effects have also been conducted in the low-energy EFT for three-body systems [PJP09, JPP10, JPP11]. Effective field theories are also used throughout various other domains of physics such as nuclear or condensed matter physics.

As the field of ultracold gases is such an active field of research at the moment, this brings along an interesting aspect: there is a very fruitful interplay between experiment and theory. This is true for the many-body community with the investigation of BECs, superfluidity, or systems similar to condensend matter systems, and also for the few-body community where a lot of effort goes into the investigation of the Efimov effect. Therefore, the last three years were a very good time to do research on the Efimov effect with the help of EFTs.

The focus of this work is on the detailed treatment of four slightly different aspects of universal few-body effects. Two of the projects were directly triggered by experiments whereas the other two are mainly giving predictions for experiments that are currently being conducted or at least feasible in the near future. The scattering of atoms and dimers in a gas of atoms and dimers is calculated for non-vanishing temperatures making use of the Bose-Einstein distribution that the atoms must obey. For systems consisting of two different atomic species, heteronuclear mixtures, all relevant observables for the S-wave Efimov effect present in mostly bosonic systems are derived. If fermions are the majority species, only the P-wave Efimov effect can occur and manifests itself in the atom-dimer scattering observables. Furthermore, as the fourth project, universal three-body observables are computed for a two-dimensional bosonic gas.

The results found in this thesis allow for a more adapted description of systems exhibiting a large scattering length. We here focus on ultracold atomic gases. The exact knowledge of few-body processes is important for the understanding of quantum systems, e.g., in many-body atomic experiments, for the simulation of condensed matter effects with cold gases in lattices, or for quantum computation. An example for the fruitful interplay between few- and many-body physics is the calculation by van Stecher and colleagues concerning four fermion systems [vSG07, vSGB07]. The results can be seen as a first approximation to the BCS–BEC (Bardeen-Cooper-Schrieffer – Bose-Einstein-condensation) crossover. Furthermore, the universal nature of our results suggests that a direct application to, e.g., nuclear or hadronic physics is also possible as long as a large scattering length is present.

The outline of this thesis is as follows: we start by summarizing information necessary for the understanding of this work in Chapter 2. This includes experimental techniques, an introduction to two- and three-body scattering, and a more detailed description of the Efimov effect and its appearance in experiments. In Chapter 3, an introduction to effective field theories is given together with the explicit application to two- and three-body scattering. In the three subsequent chapters, we investigate the Efimov effect in various respects. Atom-dimer scattering at finite temperatures is described in Chapter 4. In Chapters 5 and 6,

the heteronuclear Efimov effect is investigated, in the S-wave case and for higher angular momenta, respectively. Then we turn to two-dimensional systems in Chapter 7 with a focus on three-body observables. We conclude with a summary and an outlook on possible future projects in Chapter 8.

Chapter 2

Motivation and Physical Background

To start with, we collect and shortly present the background information that is necessary for the work described in this thesis. Besides, references for further reading are given. In Section 2.1, we describe key experimental techniques used in cold atom experiments. Then, the most important facts about two-body and three-body scattering are given in Sections 2.2 and 2.3. Subsequently, the Efimov effect, which is central to this thesis, is introduced in the last section.

2.1 Experimental Techniques

It is worthwhile to mention a few experimental techniques that are used in ultracold atomic physics. However, we cannot give a full theoretical description here but rather concentrate on reviewing the general concepts. This should allow for an intuitive understanding. For more details on the historical developments, the techniques, and the experimental realization, see, for example, the reviews [KDSK99, KZ08].

2.1.1 Cooling Techniques

The first cooling step in an experiment with ultracold neutral atoms is *Doppler cooling*. It relies on the fact that atoms can be thought of as two-level systems with a ground state and an excited state. The principle is quite simple and can be best explained with a sketch, see Fig. 2.1. The incoming laser light (red wavy lines) has the frequency ν_L and is slightly red-detuned from the atom's (blue circle) resonance frequency ν_A which is associated with the transition from ground state to excited state, i.e., $\nu_\mathrm{L} < \nu_\mathrm{A}$. If the atom now moves at a velocity v such that $\nu_\mathrm{A} = \nu_\mathrm{L}(1 + \frac{v}{c})$, it can absorb a photon which transfers its momentum to the atom. The now excited atom decays back into its ground state by spontaneous emission. This fluorescent radiation has no preferred direction (see Fig. 2.1 b)) and in this step, on average, no net momentum is transferred. In total, the atom now has a smaller velocity in the direction of the laser beam and thus lower temperatures are achieved. If instead of

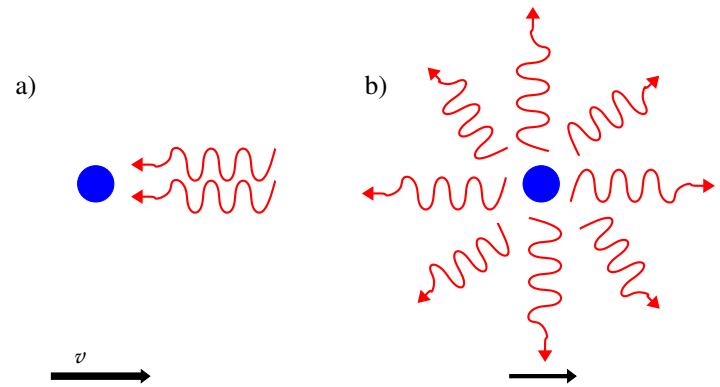

Figure 2.1: Principle of Doppler cooling. a) Atom before absorption and b) after absorption, emitting fluorescence.

one laser beam six lasers are used (two for each spatial direction) and the cooling cycle is repeated successively, this represents a very effective cooling mechanism leading to an *optical molasses*. Drawbacks are the necessity to tune the laser frequency such that it can stay on resonance with the slowing atoms and that the force is velocity dependent. Moreover, there is a minimal temperature that can be achieved, the *Doppler limit*. It is usually of the order of hundreds of μK and is connected to the linewidth of the cooling transition.

In order to further cool the atomic gas, other techniques are available, such as, e.g., *Raman* and *Sisyphus cooling*. With those it is possible to achieve temperatures close to the *recoil limit* where the thermal energy equals the energy of an atom with a momentum equal to the photon momentum. Typical values are of the order of hundreds of nK. To get to the lowest possible temperatures, *evaporative cooling* is used. The principle behind this cooling technique is the same that cools down a cup of coffee. In the steam, the fastest and thus hottest molecules can escape from the ensemble. The residual molecules rethermalize and the ensemble thus has a lower temperature than before. In atomic gases, the evaporation can be achieved by lowering the trap depth which allows the fastest atoms to escape. This is normally realized as forced evaporation by applying a radio-frequency (rf) pulse such that the (hyperfine) spin of the hottest atoms is flipped. These atoms are no longer trapped and are lost to the system (see also Subsection 2.1.2). As with the cup of coffee, the residual atoms rethermalize via scattering processes and a colder ensemble is obtained. An example of the Maxwell-Boltzmann distributions before and after the evaporation can be seen in Fig. 2.2. Pictorially speaking, the tail of the hotter (red) distribution gets cut off in the evaporative process (shaded area). During rethermalization, the non-shaded area under the curve has to be preserved and thus the graph is shifted to the cooler (blue) distribution. Temperatures that can be achieved are of the order of tens of nK. The obvious disadvantage of this cooling method is that most of the atoms are lost in the process. However, if the particle number is chosen to be large enough at the beginning of the experiment, sufficient numbers of atoms can be achieved. Typically, the number of atoms in the experiment is about 10^{10} before and only about 10^5 after the evaporation process.

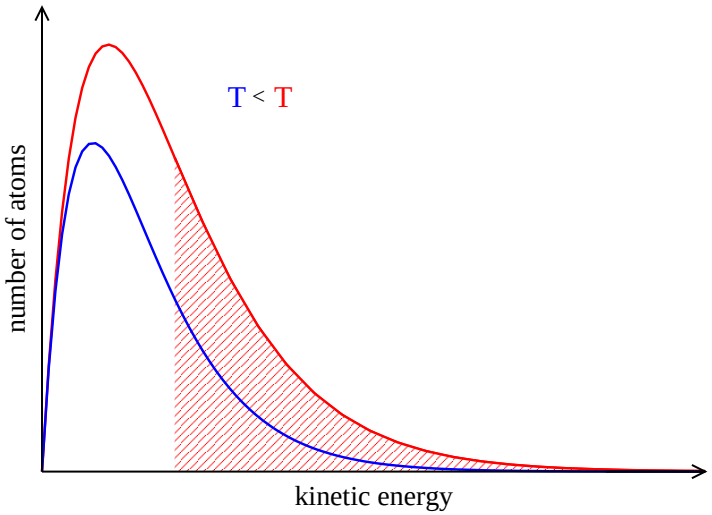

Figure 2.2: Example of Maxwell-Boltzmann distributions before (red) and after evaporative cooling (blue). The shaded area represents the number of particles that are evaporated.

2.1.2 Atom Traps

To investigate atomic gases in detail, they not only need to be cooled down but also trapped. Generally speaking, atoms can be trapped by electromagnetic fields as they interact with the atoms. This is realized by magnetic, optic, or combined traps. The principle of magnetic trapping relies on the Zeeman effect which describes the coupling of atomic levels to an outer magnetic field. The potential energy of an atom in the hyperfine state F with magnetic quantum number m_F for small magnetic fields is given by

$$E(F, m_F) = E(F) + m_F \, g_F \, \mu_\mathrm{B} \, B \,, \tag{2.1}$$

where μ_B is the Bohr magneton, g_F the Landé factor, and $E(F)$ the energy for $B = 0$. We picture the situation of an $F = 2$ state in a harmonic B-field (black) in Fig. 2.3. The $m_F = 1, 2$ (red) states can be trapped as it is energetically favorable for them to stay at the center of the trap (*low-field seekers*) whereas the other (blue) states cannot be trapped (*high-field seekers*). It is important to avoid *Majorana flops*, i.e., spin flips from states that can be trapped into states which cannot be trapped. They can occur spontaneously when the magnetic field vanishes at the center of the trap because there is a non-vanishing overlap of the states. This is fixed by an offset magnetic field or magnetic or optic *endcaps*. However, rf induced spin flips can be used in forced evaporation to cool the sample. Such an rf pulse is indicated in the lower panel of Fig. 2.3 (see also Subsection 2.1.1). Note that this is only a simplified picture neglecting the fact that one has to consider *dressed states* of the atoms with the radiation field for a more precise description of the procedure.

The most important magnetic trap is the *magneto-optical trap* (MOT). It combines magnetic trapping due to two coils in an *anti-Helmholtz configuration* with cooling via six laser beams. The lasers can be polarized in a way that the atoms get pushed back into the center if they move outwards. In the experiments, MOTs are often used as the first stage as they

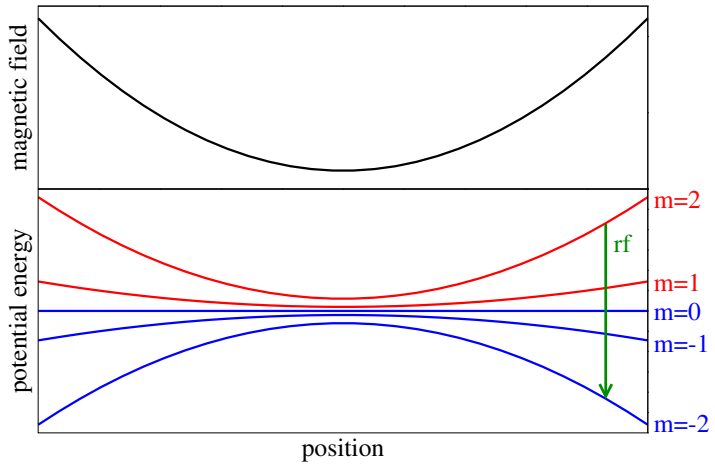

Figure 2.3: Schematic view of the Zeeman effect. The upper panel shows a harmonic magnetic field vs. position. In the lower panel, the potential energies of the Zeeman-split levels of an $F = 2$ state are plotted vs. position. Also indicated is an rf pulse (green) inducing a spin flip from a trapped ($m = 2$) to an untrapped ($m = -2$) state.

have various advantages: they can be loaded with background gas, directly cool the sample because of their *dissipative* nature, and are relatively simple to set up. Note that due to the presence of the magnetic field, typical temperatures achieved in a MOT are hundreds of μK.

However, if further manipulation of the atoms with magnetic fields is planned (see also Subsection 2.1.4), they have to be transferred into an all-optical *dipole* trap. Dipole traps are realized by one or more strongly focused, off-resonant laser beams. The electric field induces an electric dipole moment in the atoms. The resulting dipole force is proportional to the gradient of the light intensity, and for red-detuned lasers, the atoms are attracted towards high intensities. They therefore gather in the focus region. Due to the Gaussian waist of the beam, they are also transversally trapped. As dipole traps are *conservative*, no further cooling is achieved. The *trapping frequencies* in the different spatial directions are related to the laser intensity and indirectly proportional to the beam waist. So a tight confinement corresponds to high laser intensity, high trapping frequency, and small trapping volume.

Sophisticated trapping geometries allow for very specialised experiments, the most prominent example being *optical lattices*. Two counterpropagating laser beams create, with their sinusoidal interference pattern, a periodic potential for the atoms. Depending on the number of dimensions that are confined in this way, one-, two-, or three-dimensional lattices can be realized. Two examples are pictured schematically in Fig. 2.4. This is also how lower-dimensional systems can be created. For example, for a two-dimensional system, a one-dimensional lattice is needed. The trapped atoms are then in pancake shaped volumes close to each other. By removing all but one such pancake, it is possible to investigate an essentially two-dimensional atom gas.

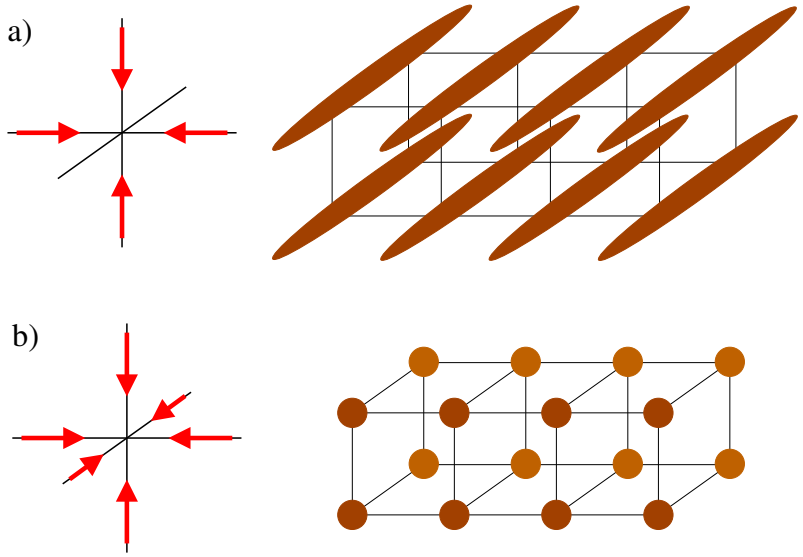

Figure 2.4: Examples of optical lattices. a) A two-dimensional lattice is realized by four laser beams (red arrows) and creates one-dimensional tubes, and b) a three-dimensional lattice (six laser beams) creates essentially crystalline order.

2.1.3 Imaging

Imaging techniques fall into two main categories: destructive and non-destructive. As the name indicates, the first technique destroys the atomic sample which thus has to be prepared anew for each shot. The second allows for in-situ observation of the processes of interest but is in general harder to achieve or has lower contrast.

Many experiments use *absorption imaging*, a destructive method, combined with *time-of-flight* measurements. After the preparation and manipulation of the sample, the trap is switched off. Gravity drags the atoms downward and, especially after tight confinement, the cloud expands. It is allowed to do so for a certain amount of time (typically a few ms) and then a (resonant) probe beam is shone on the atoms. The resulting absorption picture is recorded with a CCD camera. According to Beer's law, the transmission is attenuated exponentially and the "shadow" of the cloud therefore allows for the deduction of the number of atoms present. Analyzing the resulting pictures also allows for the determination of the sample's temperature (see also Subsection 2.1.5). Subsequently, the cycle can be repeated with the same or changed parameter settings. Note that instead of measuring the absorption behind the sample, it is also possible to measure fluorescence of the sample on a camera placed at the side.

There are many mechanisms for obtaining dispersive, non-destructive images. We only mention one of them, the *phase-contrast method*. To acquire information about the phase of the transmitted light, the unscattered light has to be manipulated, i.e., phase-shifted. Then one can make use of the resulting interference of scattered and unscattered signal to deduce the phase. It is possible to take many sequential shots and thus observe the sample directly and to obtain the sought-after information from it.

2.1.4 Feshbach Resonances

Feshbach resonances arise due to the coupling of different interatomic potential channels and result in a change of the scattering length. It can be pictured as in Fig. 2.5 a). Assume the black interatomic potential to be the one describing two incoming atoms in the spin triplet state, whereas the red potential describes the singlet state supporting a bound state at E_{bound}. The molecular and the scattering states are coupled by the hyperfine interaction. They have different magnetic moments, meaning that their relative position can be changed by an external magnetic field (due to the Zeeman effect, see Eq. (2.1)). The potential can then be tuned in such a way that the energy of the incoming particles approximately equals the bound state energy, i.e., $E_{\text{in}} \approx E_{\text{bound}}$. That is exactly the resonant situation depicted in Fig. 2.5 a). The atoms "feel" each other and stay close together (in a quasi-bound state) for a relatively long time, or in other words, the scattering length becomes large. The resulting variation of the scattering length with the magnetic field can be seen in Fig. 2.5 b), where Δ denotes the width and B_0 the position of the resonance. The background (intrinsic) scattering length is given by a_{bg}. The magnetic field dependent scattering length can be well approximated by the empirical formula

$$a = a_{\text{bg}} \left(1 - \frac{\Delta}{B - B_0}\right) . \tag{2.2}$$

For alkali atoms, a_{bg} typically is of the order of a hundred a_0. For the experimental realization, *broad* Feshbach resonances are preferred. They allow for an easier and more controlled tuning of the scattering length. Theoretically, they can be reduced to a single-channel model and are easier to handle.

Feshbach resonances can also be used to create molecules by adiabatically tuning the magnetic field from the negative scattering length side to the resonance and then lowering the molecular potential. This association mechanism is especially important for fermions where the BCS–

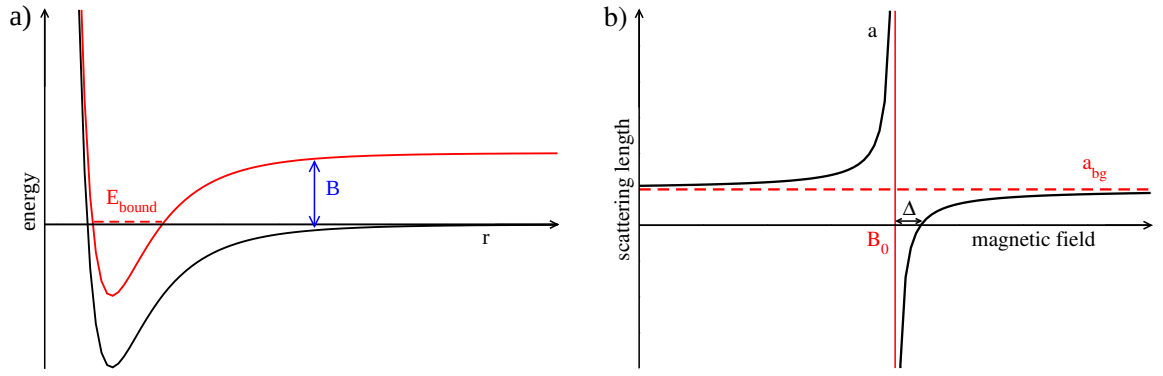

Figure 2.5: Principle of a Feshbach resonance. a) The distance between two potentials can be tuned with the help of a magnetic field, B (blue arrow). If the bound state energy of the closed (red) potential matches the energy of the incoming particles in the open channel (black), a coupling occurs. b) Scheme of the variation of the scattering length (black) in the vicinity of a Feshbach resonance at B_0.

BEC crossover is investigated. In summary, we can state that Feshbach resonances are an essential tool for experiments in ultracold quantum gases. Without this "knob" to tune the scattering length, a lot of experiments would not be as interesting and rich in insights as they are now.

2.1.5 Observables and Other Aspects

For completeness, we quickly mention the typical observables of a cold atom experiment here. They are derived from pictures of the sample, see also Subsection 2.1.3. Particle numbers can be directly related to the optical densities of the images. Therefore, particle losses that occur, for example, close to resonances can be seen in sequential pictures. By also monitoring the time evolution, loss rates can be obtained. The most important loss rate for this thesis, the three-body recombination rate, is introduced in Subsection 2.4.1. The spatial expansion of a cloud during time-of-flight is related to the kinetic energy of the atoms and thus their temperature. With these observables, the systems of interest can be described in detail.

In real experiments, there are a few other aspects that have to be considered. Some imaging methods can, for example, induce heating in the samples that has to be taken into account. Also, as the atoms are not ideal two-level systems, other levels can be populated in the cooling process which cannot be excited by the cooling laser. Therefore, another laser is needed to pump the atoms back into the original ground state and thus back into the cooling cycle.

In total, however, the experimental and technical progress of the last two decades has been enormous and an incredible control of ultracold atoms can be achieved. This is what makes them the ideal testing ground for universal physics.

2.2 Two-Body Scattering

Scattering in general and two-body scattering in particular plays an important role throughout this thesis. Therefore, we want to review some of the basics of scattering theory here for the simplest case of S-wave scattering in three dimensions. More general concepts can be found in the following chapters.
We consider elastic scattering of two particles interacting via a short-range potential along the z-axis in the center-of-mass frame. The wave function can be described in the asymptotic limit by the sum of an incoming plane wave and a scattered spherical wave,

$$\Psi(\vec{r}) = e^{ikz} + f_k(\theta)\,\frac{e^{ikr}}{r}\,, \tag{2.3}$$

where θ describes the scattering angle. The momenta of the particles are given by $\pm\hbar\vec{k}$ and the total energy is given by $E = 2\frac{\hbar^2k^2}{2m}$. This asymptotic form defines the scattering amplitude $f_k(\theta)$ which encodes all relevant information about the scattering process. For distinguishable particles, the differential elastic scattering cross section is given by

$$\frac{d\sigma}{d\Omega}(E) = |f_k(\theta)|^2\,. \tag{2.4}$$

In the low-energy limit, the scattering amplitude approaches a constant value, namely the scattering length,

$$f_k(\theta) \to -a \quad \text{for} \quad k \to 0\,. \tag{2.5}$$

At small enough energies, only the S-wave scattering channel contributes leading to angle-independent results. The scattering amplitude is related to the S-matrix via

$$f_k = \frac{1}{2ik}(S-1)\,. \tag{2.6}$$

To satisfy unitarity (i.e., probability conservation), the scattering amplitude can be written in terms of the scattering phase shift,

$$f_k = \frac{1}{k\cot\delta(k) - ik}\,. \tag{2.7}$$

Together with Eq. (2.5), this leads to the low-energy expansion of the scattering phase shift known as the *effective range expansion*,

$$k\cot\delta(k) = -\frac{1}{a} + \frac{1}{2}rk^2 + \sum_{i=0}^{\infty} P_i k^{2i+4}\,, \tag{2.8}$$

where r and P_i denote the effective range and various shape parameters, respectively. At small enough energies, the shape parameters do not have to be taken into account and in most of the cases we want to consider, even the effective range term can be neglected. If two-body bound states are present, they can be found as the poles of f_k in the upper half-plane of the complex momentum k. It is then useful to define a real binding momentum κ as the pole position with $\kappa > 0$. Furthermore, the total scattering cross section is linked to the forward scattering amplitude via the optical theorem, i.e.,

$$\sigma^{(\mathrm{tot})}(E) = \frac{8\pi}{k}\mathrm{Im}f_k(\theta=0)\,. \tag{2.9}$$

We want to consider systems exhibiting a *large* scattering length, i.e., $a \gg \ell$ where ℓ is the natural length scale of the system. For atoms, it is typically given by the van der Waals length

$$\ell_{\mathrm{vdW}} = \left(mC_6/\hbar^2\right)^{1/4}\,, \tag{2.10}$$

where C_6 is the van der Waals coefficient. For alkalis, the van der Waals length is of the order of a hundred a_0. A large scattering length can arise accidentally as it is the case for helium with $a_{\mathrm{He}} = 197^{+15}_{-34}\,a_0$ [Gri$^+$00] and $\ell_{\mathrm{vdW}} = 10.2\,a_0$ [BH06]. Or it can be achieved by fine-tuning a parameter of the interaction potential, which is the mechanism used in Feshbach resonances discussed in Subsection 2.1.4.

2.3 Three-Body Scattering

To describe the scattering of three particles of equal mass, it is convenient to introduce hyperspherical coordinates. We can only give a short outline of the procedure here and we

closely follow Ref. [BH06], where further details and references can be found. We start by defining Jacobi coordinates,

$$\vec{r}_{12} = \vec{r}_1 - \vec{r}_2 \quad \text{and} \quad \vec{r}_{3,12} = \vec{r}_3 - \frac{1}{2}(\vec{r}_1 + \vec{r}_2)\,. \tag{2.11}$$

This is only one set of Jacobi coordinates using the relative vector between atoms 1 and 2 and the relative vector between the third particle and the center-of-mass of the other two particles. The other two sets are obtained by a cyclic permutation of the subscripts $\{1, 2, 3\}$. As usual, we do not need to consider the (total) center-of-mass coordinate. The hyperradius R is given as the root-mean-square radius,

$$R^2 = \frac{1}{3}\left(r_{12}^2 + r_{23}^2 + r_{13}^2\right) = \frac{1}{2}\,r_{12}^2 + \frac{2}{3}\,r_{3,12}^2\,. \tag{2.12}$$

The hyperradius is only small if all three two-particle separations are small. The Delves hyperangle α_3 is defined as

$$\alpha_3 = \arctan\left(\frac{\sqrt{3}\,r_{12}}{2\,r_{3,12}}\right)\,, \tag{2.13}$$

ranging from 0 to $\pi/2$. When α_3 is close to 0, particle 3 is far away from the other two, whereas the hyperangle is close to $\pi/2$ when the third particle is close to the others. Similar transformations for the heteronuclear case in momentum space can be found in Appendix B.1.

The Schrödinger equation for three identical particles and an interaction potential V is given by

$$\left(-\frac{\hbar^2}{2m}\sum_{i=1}^{3}\nabla_i^2 + V(\vec{r}_1, \vec{r}_2, \vec{r}_3)\right)\Psi = E\Psi\,. \tag{2.14}$$

We now make use of several assumptions. The potential is translation invariant and given as a sum of two-body potentials that depend only on the separation vectors. Then, the wave function also is decomposed into a sum of three wave functions only depending on the Jacobi coordinates. This leads to the *Faddeev equations*. We consider the low-energy case and can thus concentrate on S-wave scattering. Making use of a *hyperspherical expansion* of the wave functions and neglecting off-diagonal coupling terms is known as the *adiabatic hyperspherical approximation*. Then, the hyperspherical potentials and boundary conditions can be deduced and the equations can be solved numerically.

We are interested in the resonant limit, i.e., particles interacting with a very large scattering length. There, the adiabatic hyperspherical approximation is accurate. Furthermore, we consider the small-distance region $R \sim \ell$ because for scattering and bound states, all three particles have to approach each other. The equation corresponding to the lowest hyperspherical potential, which is the only one that can support bound states, is

$$\frac{\hbar^2}{2m}\left[-\frac{\partial^2}{\partial R^2} - \frac{s_0^2 + 1/4}{R^2}\right] f(R) = E f(R)\,, \tag{2.15}$$

where s_0 is determined by the transcendental equation

$$\cosh\left(s_0\frac{\pi}{2}\right) - \frac{8}{\sqrt{3}s_0}\sinh\left(s_0\frac{\pi}{6}\right) = 0\,. \tag{2.16}$$

This yields $s_0 \approx 1.00624$. Note that more details on the derivation of s_0 can be found in Section 6.2 and Appendix A.3. If the energy can also be neglected, Eq. (2.15) for $s_0 \geq 0$ corresponds to the Schrödinger equation describing a particle in a $1/r^2$ potential and the "fall to the center" phenomenon [LL85]. It depicts the situation for a particle with a discrete energy spectrum that is unbounded from below such that for $E \to -\infty$, the particle has to be infinitesimally close to the center of the potential. This corresponds to the situation for the Efimov effect. The solution to Eq. (2.15) is given by

$$f(R) = R^{1/2} K_{is_0}(\sqrt{2}\kappa R)\,, \tag{2.17}$$

where $K_{is_0}(z)$ is a Bessel function with imaginary index and κ is the binding momentum of an Efimov trimer. In the following section, the Efimov effect and its implications for cold atom experiments are described more thoroughly. A derivation in the framework of effective field theory is given in Section 3.4.

2.4 The Efimov Effect

In this section, the Efimov effect, which is a crucial part of this thesis, is introduced in detail. We first give the theoretical description which can also be found in Refs. [BH06, BH07b]. Note that the derivation of the results is shown in Section 3.4 and Chapters 5 and 6. Then, we list the experiments that have seen the Efimov effect up to now.

2.4.1 Theoretical Description

As shortly mentioned before, the Efimov effect was already predicted in 1970 by Vitaly Efimov [Ef70]. Its main feature, also described in the introduction, is the occurrence of a geometric spectrum of three-body bound states, also called trimers. In the limit of diverging scattering length, $a \to \infty$, and for identical bosons, the binding energy of the nth trimer is given by

$$E_{\mathrm{T}}^{(n)} = \left(e^{-2\pi/s_0}\right)^{n-n_*} \hbar^2 \kappa_*^2/m\,, \tag{2.18}$$

where κ_* is the binding wave number of the state labeled n_*. This leads to an accumulation point at $E = 0$ and a discrete scale invariance with a scaling factor of $\lambda = e^{\pi/s_0} \approx 22.7$. Away from unitarity, there is only a finite number of bound states [Ef73],

$$N \approx \frac{s_0}{\pi} \ln \frac{|a|}{r}\,. \tag{2.19}$$

Other corrections due to a non-vanishing effective range are calculated in Refs. [Ef93, HLP07, PJP09, JPP10, JPP11], but we do not need to consider them in detail here. An illustration of the binding energies of Efimov trimers is shown in Fig. 2.6, where AAA denotes the energy region of possible three-atom scattering and AD the region of atom-dimer scattering. The nth Efimov state appears at the three-particle scattering threshold at $a = a_-^{(n)}$, crosses the unitarity limit at $1/a = 0$ with the energy given in Eq. (2.18), and vanishes at $a = a_*^{(n)}$ through the atom-dimer threshold, which for identical bosons is given by $-E_{\mathrm{D}} = -\hbar^2/(ma^2)$, see also Eq. (3.9). Note that for notational simplicity, we often omit the superscript (n), and

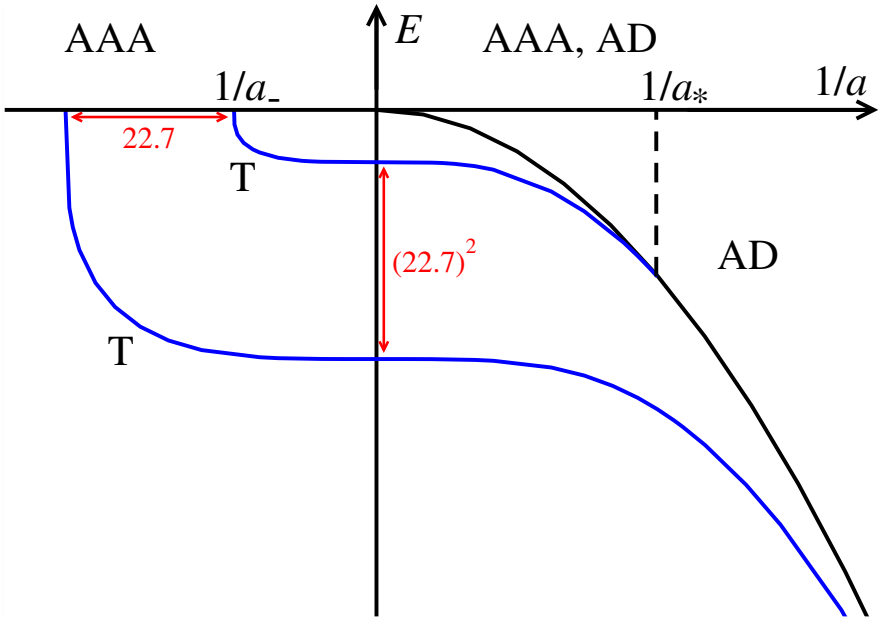

Figure 2.6: Dependence of the binding energies E_{T} (solid blue lines) of the trimers (T) on the inverse scattering length $1/a$. The parameters a_- and a_* specify where the trimer states hit the three-atom and atom-dimer thresholds (E_{D}, solid black line), respectively. See text for more details.

that the quantities in Fig. 2.6 are scaled by a power of $1/4$, allowing to show two trimers. At $E = 0$ and $1/a = 0$, there is an accumulation point of an infinite number of Efimov trimers, but they are not depicted in the figure. Besides, the exact position of the Efimov trimers and hence the threshold crossings at a_- and a_* cannot be determined by theory. However, if one such three-body datum is known, the others are also fixed and can be determined.

The presence of Efimov trimers can be detected with the help of recombination rates. They are also discussed in Subsection 2.4.2 for the already conducted experiments and especially in Chapters 4-6. Nevertheless, we here mention a few general properties and show the formulae for three identical bosons that have been derived previously. They are important for the following chapters of this thesis. The three-body recombination event rate α is defined via the rate equation

$$\frac{d}{dt}n = -3\,\alpha\,n^3\,, \tag{2.20}$$

where n denotes the particle density. The equation describes the scattering of three atoms into a dimer and a third atom. Due to the released binding energy, the dimer and the atom get expelled from the trap, so in total three atoms are lost. The three-body recombination rates for positive and negative scattering lengths and atom-dimer scattering cross sections show a log-periodic dependence on $a\kappa_*$ due to the sequence of Efimov states. For the binding momentum, we know $\kappa_* \propto a_*^{-1} \propto a_-^{-1}$. So once one of these three-body parameters (e.g., a resonance position) is fixed (or known from experiment), the others are also fixed. Factors of e^{π/s_0} are implicitly included in all statements.

In cold atomic systems, Efimov trimers are not stable but rather decay into more deeply bound molecules, also called *deep dimers* in the following. These deep dimers are always present in alkali gases. It is not possible to include those states explicitly but we can incorporate the collective effect of the presence of deep dimers in a single parameter, η_*. It can be included by the simple replacement [BH04]

$$\kappa_* \;\rightarrow\; \kappa_* \, e^{i\eta_*/s_0} \,, \tag{2.21}$$

and it is connected to the lifetime and thus the width of the Efimov trimers [BH06],

$$\Gamma_\mathrm{T} \approx \frac{4\eta_*}{s_0} \left(E_\mathrm{T} + E_\mathrm{D}\right) . \tag{2.22}$$

In the picture of hyperspherical potentials, η_* is also called the *inelasticity parameter* and $(1 - e^{-4\eta_*})$ describes the fraction of the probability that flows inelastically into the deep dimer-atom scattering state [BH06].

For $a < 0$, only three-body recombination into deep dimers can occur. Overall, the recombination rate follows an a^4 scaling with pronounced peaks at the positions a_- [HHP10],

$$\alpha_\mathrm{d} = \frac{64\pi^2(4\pi - 3\sqrt{3}) \coth(\pi s_0) \sinh(2\eta_*)}{\sin^2[s_0 \ln(a/a_-)] + \sinh^2 \eta_*} \, \frac{\hbar a^4}{m} \,. \tag{2.23}$$

For $a > 0$, the situation is more complex as the three-body recombination can occur into the shallow, universal dimer and into the deep dimers. The recombination rates again show an a^4 scaling with minima at a_{0*}. These *Stückelberg oscillations* are due to an interference effect between different recombination pathways [NM99, EGB99]. Without deep dimers, the minima of α_s are real zeros which are washed out due to the deep dimers. The formulae are given by [HHP10],

$$\alpha_\mathrm{s} = \frac{128\pi^2(4\pi - 3\sqrt{3})(\sin^2[s_0 \ln(a/a_{0*})] + \sinh^2 \eta_*)}{\sinh^2(\pi s_0 + \eta_*) + \cos^2[s_0 \ln(a/a_{0*})]} \, \frac{\hbar a^4}{m} \,, \tag{2.24}$$

and

$$\alpha_\mathrm{d} = \frac{128\pi^2(4\pi - 3\sqrt{3}) \coth(\pi s_0) \cosh\eta_* \sinh\eta_*}{\sinh^2(\pi s_0 + \eta_*) + \cos^2[s_0 \ln(a/a_{0*})]} \, \frac{\hbar a^4}{m} \,. \tag{2.25}$$

Note that the rate α_d/a^4 depends only very weakly on a since $\sinh^2 \pi \gg 1$. Furthermore, atom-dimer scattering is also present [BH06],

$$\sigma_\mathrm{AD}^{(\mathrm{el})} = 84.9 \frac{\sin^2[s_0 \ln(a/a_*) - 0.97] + \sinh^2 \eta_*}{\sin^2[s_0 \ln(a/a_*)] + \sinh^2 \eta_*} \, a^2 \,. \tag{2.26}$$

These observables are plotted in Fig. 2.7 for $\eta_* = 0.05$, $\hbar = 1$, and $m = 1$. The solid black lines show the three-body recombination rate and the solid blue line the atom-dimer scattering cross section. The dashed grey lines simply indicate the a^4 scaling. Peaks of the three-body recombination rates (a_- and a_+) are highlighted with red dash-dotted lines whereas the green dash-dotted lines show the position of a_{0*}. Ratios of adjacent minima or maxima are $e^{\pi/s_0} \approx 22.7$ and the mixed ratio of a neighboring pair of maximum and minimum is $a_+/a_{0*} = e^{\pi/(2s_0)} \approx 4.76$. Across the resonance, the maxima are symmetric, i.e., $a_+/|a_-| = 1$. Note that for three identical bosons, accidentally $a_+/a_* \approx 1$, but this is not

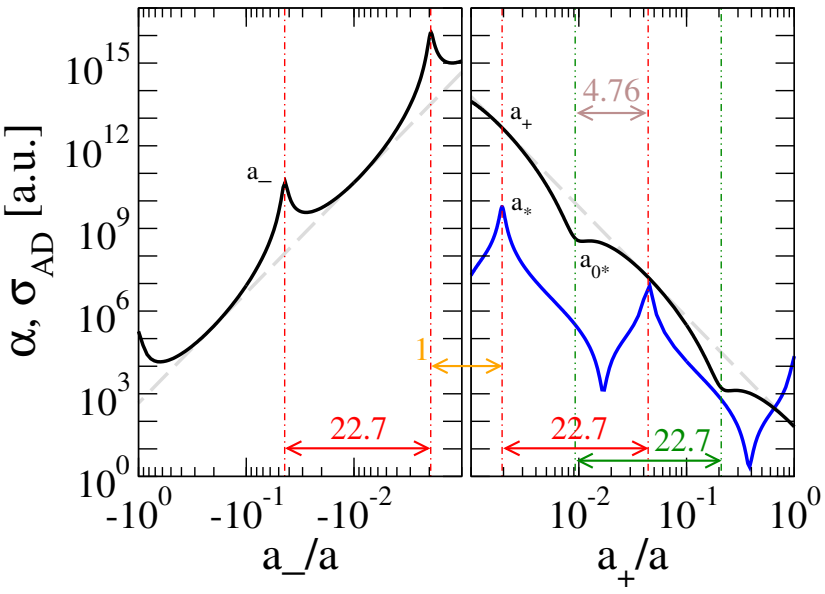

Figure 2.7: Relation between the different structures due to Efimov states. More details are explained in the text.

true for general systems, see Chapters 5 and 6. However, all ratios are universal and do not depend on the three-body parameter. It is also important to note that α and σ are given for different three-body energy E. The recombination rate is measured for vanishing energy, $E = 0$. However, σ is given for $E = -E_\mathrm{D}$, i.e., along the atom-dimer scattering threshold. This should not be confused with the dimer breakup threshold at $E = 0$. It is also possible to derive the scattering cross section at $E = 0$ and for intermediate energies, this is done in the subsequent chapters. The peak position depends on the energy, and, interestingly, the atom-dimer cross section at the breakup threshold also peaks at a_+.

The inelastic atom-dimer scattering cross section in the presence of deep dimers is directly related to the dimer relaxation rate. It describes the scattering of a shallow dimer and an atom into a deep dimer and the atom. Again, due to released binding energy, the scattering partners are lost from the system. The event rate is defined via

$$\frac{d}{dt} n_\mathrm{A} = \frac{d}{dt} n_\mathrm{D} = -\beta \, n_\mathrm{A} \, n_\mathrm{D} \,, \tag{2.27}$$

where $n_{\mathrm{A/D}}$ denotes the atomic/molecular density, respectively. The dimer relaxation rate also peaks at $a = a_*$, further details can be found in Chapter 4.

2.4.2 Experimental Realization

In this subsection, we give a short review of the experiments that have been conducted in the last five years and that have seen signatures of the Efimov effect. For another review, see, e.g., [FG10]. Due to the presence of the deep dimers, the signatures mostly were detected in recombination processes.

The first experimental evidence of the existence of the Efimov effect in ultracold atoms was seen in Innsbruck in 2006 [Kr$^+$06]. In a sample of ultracold ^{133}Cs, a resonance in the three-body recombination rate for negative scattering length was detected. This could be attributed to an Efimov state hitting the scattering threshold and thus enhancing the process of three atoms recombining to form a deep dimer and a third atom. Because of the large scaling factor of 22.7, only one resonance could be seen experimentally.
The same ^{133}Cs system was subsequently used to prepare a mixture of atoms and shallow dimers [Kn$^+$09]. With this, the atom-dimer scattering for $a > 0$ could be monitored and another resonance feature was seen. The process of a shallow dimer and a third atom scattering into a deep dimer and an atom is described by the relaxation rate. It gets enhanced close to a_*, where the Efimov trimer hits the atom-dimer threshold. This experiment is investigated in Chapter 4. Unfortunately, the two experiments in Innsbruck were not conducted in the same universal regime across the divergence of the scattering length. The regions were rather connected by a zero of a such that a comparison is not practically meaningful [DGE09].

In Florence, ^{39}K atoms were investigated and three Efimov features were detected [Za$^+$09]. One of them is a recombination maximum for $a < 0$ as in Innsbruck, whereas the other two are recombination minima for $a > 0$. The ratio of the two measured minima was close to the expected 22.7 within 10% and thus gave the first unambiguous evidence of Efimov scaling in an atomic system. Tuning across the Feshbach resonance, this experiment stayed in the same universal regime. However, the experimentally found ratios differ by 50% from the universal prediction of $a_+/|a_-| = 1.0$. For $a > 0$, two more maxima were detected to be superimposed on the (very broad) maxima of the three-body recombination. They might be due to enhanced atom-dimer scattering as dimers can form spontaneously in the trap. This would mean that each of those dimers had to expel approximately ten atoms via secondary scattering processes. We come back to this issue in Chapter 5.

Using bosonic lithium, signs of the Efimov effect were also seen in two subsequent experiments. The first one, conducted in Israel, detected one maximum for negative and one minimum for positive scattering length [GSKK09]. They are connected via a universal region and the ratio of the positions deviates only by 4% from the universal value. The second experiment in Houston used a different hyperfine state of ^{7}Li and obtained different results [PDH09]. In total, they measured eleven features, six of which are connected to four-body processes not of interest here. From the others, two are maxima for $a < 0$, two are minima for $a > 0$, and one is again a resonance which could be due to secondary atom-dimer processes. On each side of the unitarity limit, the ratios agree within a few percent with the prediction. However, across the resonance, a systematic deviation of again 50% is observed. This finding was not confirmed by a follow-up experiment of the Israel group with the second hyperfine state of lithium [GSKK10, Gro$^+$11]. They attribute this discrepancy to the fact that the Feshbach resonance has to be measured very precisely to determine the correct connection between magnetic field and scattering length as given in Eq. (2.2). This measurement may not have been carried out precisely enough in the Houston experiment.

A first signature of the heteronuclear Efimov effect was seen in Florence in a mixture of ^{87}Rb and ^{41}K [Ba$^+$09]. Two recombination maxima, which could be attributed to the two Efimov channels present in the system, Rb-Rb-K and Rb-K-K, were measured by monitoring the numbers of the atomic species separately. They also found a resonance for positive scattering length which might be the sign of residual atom-dimer scattering once again. This experiment is discussed and investigated in more detail in Chapter 5.

The case of fermionic lithium in three hyperfine states was investigated in Japan, Heidelberg, and Pennsylvania. In this system, there are three scattering lengths with Feshbach resonances close enough to each other such that regions exist where all three are large. Two recombination maxima for two different universal regions with large negative scattering length were observed [Ot$^+$08, Wen$^+$09, Hu$^+$09, Wi$^+$09]. Four features in atom-dimer scattering were also seen. Two of those are loss resonances connected to the crossing of an Efimov trimer with the atom-dimer threshold at $a = a_*$ [Lo$^+$10a, Na$^+$10]. The others are interference minima attributed to suppressed exchange reactions. Furthermore, in Heidelberg the first direct association of Efimov trimers was achieved [Lo$^+$10b]. Starting from a gas of dimers and atoms similar to one of the species inside the dimer, these atoms could be transformed into the third species required for the formation of trimers by shining an rf pulse of frequency ν_0 on the sample. If this pulse was tuned to transmit the energy not only for transforming the atom but also dissociating the dimer and allowing for the association of the trimer, i.e., $\hbar\nu = \hbar\nu_0 + E_D - E_T$, a resonant signal could be measured. Shortly afterwards, this experiment was confirmed by the Japanese group [Na$^+$11]. These promising experiments set the stage for a more direct investigation of the Efimov trimers and their properties.

The next interesting step would be to measure the heteronuclear Efimov effect more precisely. In a mixture with heavy bosons, a lot more Efimov features could be seen on each side of the Feshbach resonance as the scaling factor can be as small as 5.5 for ^{7}Li-^{133}Cs. In a system with heavy fermions, the P-wave Efimov effect still remains to be measured. These aspects are described in more detail and observables are calculated in Chapters 5 and 6.

Chapter 3

Effective Field Theory

Effective field theories (EFTs) have proven to be very useful in many areas of physics. We therefore want to give a short introduction along the lines of an example in the first section. More general remarks about the concept of EFTs follow in Section 3.2. In Section 3.3, two-body scattering in EFT is described and is complemented by Section 3.4 about three-body scattering.

3.1 An Example

The example of Fermi's theory of the beta decay helps to illustrate the concept of EFTs. For simplicity, we only consider the decay of a neutron via the process

$$n \quad \longrightarrow \quad p + e^- + \bar{\nu}_e \,.$$

In 1934, Fermi postulated a pointlike interaction with the coupling strength G_F between the four involved fermions: neutron, proton, electron, and antineutrino. With this assumption, a lot of the phenomenological findings could be explained and the theory hence was very successful. Only about 30 years later was it realized that Fermi's theory was in fact an effective theory valid for small energies. It is the low-energy limit of the underlying theory of electroweak interactions mediated by the W and Z gauge bosons. The beta decay can then be pictured as in Fig. 3.1, where the quark content of the nucleons is also shown. The gauge bosons were finally discovered in 1983, their large masses of 80 and 91 GeV, respectively, prohibiting an earlier discovery. Besides, the *separation of scales* typical for EFTs is visible in the difference between the mass of the gauge bosons and the mass of the four involved fermions ($\lesssim$ 1 GeV) as well as the energy used for probing the process, less than 10 MeV. The propagator of the W bosons can then be expanded,

$$\frac{1}{p^2 - M_\mathrm{W}^2 + i\epsilon} = -\frac{1}{M_\mathrm{W}^2}\left(1 + \frac{p^2}{M_\mathrm{W}^2} + \mathcal{O}\Big(\frac{p^4}{M_\mathrm{W}^4}\Big)\right) \quad \text{for} \quad p \ll M_\mathrm{W}\,, \tag{3.1}$$

where p is the four-momentum and M_W the mass of the W boson. Thinking in terms of Feynman diagrams, the two weak vertices at the endpoints of the propagator (proportional

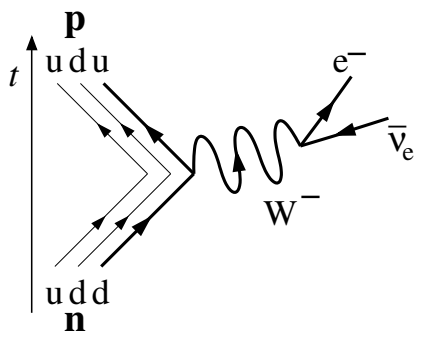

Figure 3.1: Feynman diagram for the beta decay of the neutron.

to g, the weak coupling constant) and the propagator all contract into one single interaction point for small enough energies. The coupling of this vertex now fulfils

$$G_{\mathrm{F}} \propto \frac{g^2}{M_{\mathrm{W}}^2} \,. \tag{3.2}$$

Hence, Fermi's original theory can be reconstructed from the more general theory of electroweak interaction as its low-momentum approximation. However, in the beginning, it was not necessary to know the detailed structure of the interaction. Furthermore, there are also EFTs that have been constructed to simplify calculations (or make them possible at all) after the more general theory had already been established. Both ways are possible and have been used, a few examples are given in the next subsection.

3.2 General Remarks

In the above example, the main characteristics of an EFT can already be seen. First, there is the *separation of scales* realized by large differences of the masses of the involved particles. This separation could also be given by different length scales in a system, as we show below for the case of cold atoms. The scales allow directly for the construction of a small parameter, necessary for an expansion and the *power counting*. In the case of the beta decay, the expansion parameter is given by p^2/M_{W}^2. Power counting in general quantifies how important a term is for a specific calculation. There possibly can be more than one small parameter contributing to an expansion. The knowledge of the involved parameters leads to a clear ordering of terms according to their relative importance into leading order, next-to-leading order, etc. and allows for an error estimate. Secondly, in an EFT, there are usually degrees of freedom (dofs) which are *integrated out*. The W bosons in the example above do not occur in Fermi's theory. Due to their large mass, even when starting with the full electroweak theory, they basically do not contribute to the observables and can, in the field theory approach, be integrated out. Their effect is then incorporated in an effective coupling, also called a *low-energy constant* (LEC). If the underlying theory is known, the LECs can be calculated from it. Otherwise, they have to be fitted to the experiment. The outcome of this process is that only the dofs of interest have to be built into an EFT and all other physical aspects

do not play an explicit role. This is in close relation to a third characteristic of EFTs, *universality*. As long as the long-range (or equivalently low-energy) physics stays the same, it does not matter what the underlying dofs of the short-range regime are. The obtained results are *universal*, i.e., valid for many different systems. We come back to this issue below in connection to cold atoms. The last aspect of EFTs important to mention is the question of the region of validity. As can be seen in Eq. (3.1), the expansion in the beta decay only holds for momenta $p \ll M_{\mathrm{W}}$. There always is a region where the used expansion breaks down and where thus the EFT approach is not valid any more. This is often incorporated by a momentum or energy cutoff mostly chosen to be at the same order of magnitude as the high-energy scale, in our example this would be M_{W}. *Dimensional regularization* is also used as a gauge-invariant way to obtain finite result for loop integrals. Renormalization in EFTs is fulfilled order by order.

A few other examples for successful EFTs are also worth mentioning. There is chiral perturbation theory describing low-energy quantum chromodynamics (QCD). It makes use of the approximately realized chiral symmetry and has hadrons such as pions and nucleons as dofs instead of quarks and gluons which become important only at high energies. General relativity is often thought of as the effective theory for a quantum theory of gravity. This is an example for the case where the more fundamental, underlying theory is still unknown but sought after. Besides, even though they are mostly not referred to as such, many theories in condensed matter physics are basically EFTs.

Now we discuss a few facts concerning EFTs for ultracold atoms. The main focus of this work is on atoms with resonant interactions. This strongly interacting regime is generally achieved with the help of Feshbach resonances, which are described in more detail in Subsection 2.1.4. In the vicinity of a Feshbach resonance, the atomic scattering length can be tuned to values $a \gg \ell_{\mathrm{vdW}}$, where the van der Waals length is the typical underlying length scale for atoms. Hence, a momentum cutoff Λ should be chosen to satisfy $\Lambda \gtrsim 1/\ell_{\mathrm{vdW}}$. Another length scale that has to be considered for next-to-leading order (NLO) calculations is the range of the potential r. This is discussed in more detail in Chapter 7, where NLO calculations are performed. Also, physical systems exist in which the scattering length is naturally large compared to the typical length scale, for example, nucleons. The neutron-neutron scattering length is $a_{\mathrm{nn}} = -18.7 \pm 0.6$ fm [Go^{+}99], whereas the range of the potential is an order of magnitude smaller, $r_{\mathrm{nn}} = 2.75 \pm 0.11$ fm [MNS90]. Now, due to universality, a lot of the results obtained for cold atoms can be applied to nucleons (when Coulomb effects can be neglected) and vice versa. Originally, the Efimov effect was predicted in nuclear physics but proves to be of tremendous interest nowadays in the cold atom community (see Section 2.4).

3.3 Two-Body Scattering in EFT

The descriptions in this and the follwing section closely follow Ref. [BH06]. Therein, more details and further references can be found. Here, we focus on the case of identical particles. To consider two-body scattering of two identical particles in an EFT, we start with an adequate Lagrangian which respects Galilean invariance,

$$\mathcal{L}_2 = \psi^\dagger \left(i\frac{\partial}{\partial t} + \frac{\nabla^2}{2m} \right) \psi - \frac{g_2}{4} \left(\psi^\dagger \psi \right)^2 , \tag{3.3}$$

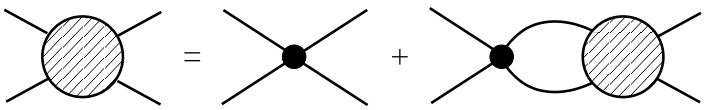

Figure 3.2: Two-body scattering integral equation.

where g_2 denotes the bare two-body coupling constant. From this Lagrangian, we can derive the Feynman rules. The particle propagator is given by $i/(k_0 - \vec{k}^2/(2m) + i\epsilon)$ and the vertex factor is ig_2. For the calculation of the two-body scattering amplitude, we have to take into account an infinite series of bubble diagrams as they all contribute to the same order. Therefore, we have to solve the integral equation shown in Fig. 3.2. Imposing an ultraviolet cutoff Λ to regulate the loops, the scattering amplitude $\mathcal{A}_2$ is determined by the integral equation

$$\mathcal{A}_2(E) = -g_2 - \frac{i}{2} g_2 \int \frac{d^3q}{(2\pi)^3} \int \frac{dq_0}{2\pi} \frac{1}{q_0 - q^2/(2m) + i\epsilon} \frac{1}{E - q_0 - q^2/(2m) + i\epsilon} \mathcal{A}_2(E)\,. \quad (3.4)$$

This can be solved to yield the amplitude

$$\mathcal{A}_2(E) = -g_2 \left[1 + \frac{mg_2}{4\pi^2} \left(\Lambda - \frac{\pi}{2}\sqrt{-mE - i\epsilon}\right)\right]^{-1} . \quad (3.5)$$

As $f_k = \frac{m}{8\pi}\mathcal{A}_2(E = k^2/m)$, we impose the following constraint on $\mathcal{A}_2$,

$$a = -\frac{m}{8\pi}\mathcal{A}_2(0)\,. \quad (3.6)$$

Therefore, the amplitude can be *renormalized* with the relation

$$a = \frac{mg_2}{8\pi}\left[1 + \frac{mg_2}{4\pi^2}\Lambda\right]^{-1} \quad \Leftrightarrow \quad g_2 = \frac{8\pi a}{m}\left[1 - \frac{2a}{\pi}\Lambda\right]^{-1} . \quad (3.7)$$

This finally leads to the renormalized amplitude, independent of the ultraviolett cutoff

$$\mathcal{A}_2(E) = \frac{8\pi/m}{-1/a + \sqrt{-mE - i\epsilon}}\,. \quad (3.8)$$

For $a > 0$, the amplitude has a pole for

$$E = -E_\mathrm{D} = -\frac{\hbar^2}{2\mu a^2} = -\frac{\hbar^2}{ma^2}\,, \quad (3.9)$$

where powers of $\hbar$ were reinserted. The pole indicates the existence of a two-body bound state whose binding momentum is given by $\kappa = \hbar/a$. This dimer state is always present in systems with large positive scattering length. A prominent example already mentioned is the deuteron. With a proton-neutron triplet scattering length of $a_\mathrm{t} = 5.42$ fm [BP07], Eq. (3.9) yields $E_\mathrm{D} \approx 1.4$ MeV. This is a good first approximation to the measured value of $E_\mathrm{deuteron} = 2.225$ MeV [BH06]. The discrepancy of approximately 37% is partly due to the size of the effective range, $r_\mathrm{t} = 1.8$ fm [BP07]. It does not fulfil the condition $r_\mathrm{t} \ll a_\mathrm{t}$. These dimer states become virtual states for $a < 0$. Note that instead of solving the integral equation (3.4), one could have used an analogous approach where the infinite sum of bubbles corresponds to a geometric series which can be summed. This method is shown in Appendix A.1. Furthermore, the two-body scattering amplitude is closely connected to the dimer propagator, which plays an important role in the following section.

3.4 Three-Body Scattering in EFT

We now want to investigate three-body scattering in the framework of EFT. Again, we closely follow the description given in [BH06], where further references can be found. To incorporate three-body effects in the EFT described in the previous section, one can quite generally include a three-body interaction,

$$\mathcal{L}'_3 = \mathcal{L}_2 - \frac{g_3}{36}\left(\psi^\dagger\psi\right)^3 , \tag{3.10}$$

where g_3 denotes the three-body coupling constant. This leads, however, to diagrams and equations that are too complicated to be solved analytically or even numerically. Therefore, it is convenient to introduce an auxiliary dimer field d. It is a local operator that annihilates two atoms. It can hence be thought of as a dimer consisting of two atoms, having the mass $2m$. The corresponding three-body Lagrangian can then be written as

$$\mathcal{L}_3 = \psi^\dagger\left(i\frac{\partial}{\partial t} + \frac{\nabla^2}{2m}\right)\psi + \frac{g_2}{4}d^\dagger d - \frac{g_2}{4}\left(d^\dagger\psi^2 + \psi^{\dagger 2}d\right) - \frac{g_3}{36}d^\dagger d\psi^\dagger\psi\,. \tag{3.11}$$

Deriving an equation for d with the help of the Euler-Lagrange equations and reinserting it into Eq. (3.11), we can recover the Lagrangian of Eq. (3.10) up to higher-order corrections. We derive the Feynman rules and present them in Table 3.1.

Description	Feynman rule
Atom propagator	$i/(k_0 - \frac{k^2}{2m} + i\epsilon)$
Bare dimer propagator	$4i/g_2$
(A-A $\to$ D)–vertex, (D $\to$ A-A)–vertex	$-ig_2/2$
(A-D $\to$ A-D)–vertex	$-ig_3/36$

Table 3.1: Feynman rules for $\mathcal{L}_3$.

Note that as the dimer field is not dynamical, its bare propagator is simply a constant. However, we have to take into account that a dimer field can split up into two atoms which subsequently recombine. This amounts again to a resummation of an infinite sum of bubble terms. The result can be derived directly from Eq. (3.8) with the replacement $E \to P_0 - P^2/(4m)$ with P_0 the energy and $\vec{P}$ the momentum of the dimer. One, furthermore, has to multiply by the inverse vertex factor squared, $(-ig_2/2)^{-2}$, to account for the outer dimer legs. This yields

$$iD(P_0, P) = i\frac{32\pi}{mg_2^2}\left[\frac{1}{a} - \sqrt{-mP_0 + P^2/4 - i\epsilon}\right]^{-1} . \tag{3.12}$$

The wave function renormalization is given by

$$Z_{\mathrm{D}}^{-1} = i\frac{\partial}{\partial P_0}\big(iD(P_0, P)\big)^{-1}\Big|_{P_0=-1/(ma^2),\,P=0} = \frac{m^2 g_2^2\, a}{64\pi}\,. \tag{3.13}$$

For the description of a three-body system, it is now necessary to derive the atom-dimer scattering amplitude $\mathcal{A}_3$. The corresponding integral equation is depicted in Fig. 3.3 and is

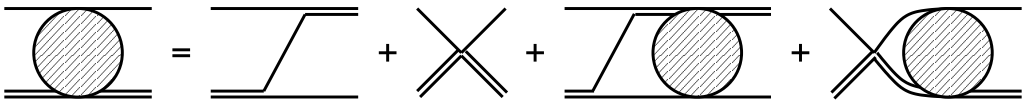

Figure 3.3: Integral equation for the atom-dimer scattering amplitude, known as the STM equation. Single (double) lines denote the atom (dimer) propagators, respectively.

known as the STM equation, because it was derived by Skorniakov and Ter-Martirosian for the first time [STM57].

Using the above Feynman rules, setting the outer atom legs on-shell, making use of the residue theorem, and projecting onto S-waves, the STM equation can be deduced. The details of the derivation can be found in Appendix A.1 for the heteronuclear case. The STM equation can be written as

$$\begin{aligned}\mathcal{A}_3(p,k;E) &= \frac{16\pi}{am}\left[\frac{1}{2pk}\ln\left(\frac{p^2+pk+k^2-mE-i\epsilon}{p^2-pk+k^2-mE-i\epsilon}\right)+\frac{H(\Lambda)}{\Lambda^2}\right] \\ &\quad +\frac{4}{\pi}\int_0^\Lambda dq\, q^2\left[\frac{1}{2pk}\ln\left(\frac{p^2+pq+q^2-mE-i\epsilon}{p^2-pq+q^2-mE-i\epsilon}\right)+\frac{H(\Lambda)}{\Lambda^2}\right] \\ &\quad \times\frac{\mathcal{A}_3(q,k;E)}{-1/a+\sqrt{3q^2/4-mE-i\epsilon}}\,,\end{aligned} \tag{3.14}$$

where the incoming (outgoing) momenta are denoted by p (k) and E is the total energy. The occurring loop integrals have to be regulated as for two-particle scattering. To compensate for the resulting cutoff dependence, the function $H(\Lambda)/\Lambda^2 = -g_3/(9g_2^2 m)$ is introduced. It corresponds to a cutoff dependent three-body coupling and ensures renormalization. It is related to the occurrence of a UV renormalization group limit cycle and obeys

$$H(\Lambda) \approx \frac{\cos\left[s_0\ln(\Lambda/\Lambda_*)+\arctan s_0\right]}{\cos\left[s_0\ln(\Lambda/\Lambda_*)-\arctan s_0\right]}\,, \tag{3.15}$$

where s_0 is exactly the transcendental number occurring in the Efimov effect and Λ_* corresponds to a three-body parameter. It is only defined up to factors of e^{π/s_0} and is related to the binding momentum κ_* by $s_0\ln\kappa_* \approx s_0\ln(0.381\Lambda_*)$ mod π. Without the cutoff and the regulating function, the STM equation would not have a unique solution. By fixing the three-body parameter (fixing Λ_*, κ_*, a_*, or a_-), we effectively fix one branch of Efimov trimers (see also Section 2.4). We can obtain the other branches by multiplication with the appropriate powers of the scaling factor. The Efimov effect therefore emerges quite naturally in this EFT treatment for three resonantly interacting particles.

It is now possible to use appropriate kinematics to derive binding energies of three-body bound states or recombination rates from the STM equation (3.14). Note that in the practical calculations, we can set the function $H(\Lambda)/\Lambda^2$ to zero and directly use the cutoff as the three-body parameter to deduce the log-periodic behavior of the solutions numerically.

3.5 Further Applications

So far, we have only shown how to treat identical particles in an EFT framework. It is, however, straightforward to derive generalizations of this method. The easiest extension consists in the study of two different atomic species that interact resonantly whereas the interaction between the like particles is neglected. By adjusting symmetry factors and introducing the two different masses, a very similar equation can be derived. This is a central part of this work. Therefore, all calculations shown in Sections 3.3 and 3.4 are carried over to heteronuclear systems in Chapters 5 and 6. More detailed derivations can be found in Appendix A.1.

If three different particles with three independent two-body scattering lengths are of interest, a coupled-channels STM equation has to be investigated. This was done for ^{6}Li [BHKP09, BHKP10] and in the context of hadronic molecules [HHH11].

Another type of generalization that can be made is the dimensionality of the considered system. The Lagrangian stays the same and only the subsequently derived equations have to be adapted to the new number of spatial dimensions. For two dimensions, this was carried out and can be found in Chapter 7.

Note that the following four chapters are adapted from previous publications in [HH09, HHP10, HH11a, HH11b].

Chapter 4

Atom-Dimer Scattering at Finite Temperatures

After having established the preliminaries in the previous chapters, we can now start to investigate aspects of few-body physics in quantum gases in detail. The first topic we cover is finite temperature atom-dimer scattering. This chapter has been published previously in Ref. [HH09].

We consider identical bosons in a single spin state and for positive scattering length. We especially focus on the Efimov resonance in atom-dimer scattering found in ^{133}Cs [Kn$^+$09]. This process was previously considered in [BH04, BH07a]. We go beyond these earlier studies in several respects: we use the full effective field theory results for the atom-dimer phase shifts instead of the effective range expansion and perform a thermal average using the Bose-Einstein instead of the Boltzmann distribution. Moreover, we correct an error in the calculation of [BH07a].

The structure of the chapter is as follows: we start by giving a few details on atom-dimer scattering and on atom-dimer relaxation. Then, the results are shown and discussed. We end with a short summary and conclusion section.

4.1 Atom-Dimer Scattering

We consider the scattering of an atom with mass $m_\mathrm{A} = m$ and dimer with mass $m_\mathrm{D} = 2m$. The wave numbers $\vec{p}_\mathrm{A}$ and $\vec{p}_\mathrm{D}$ of the incoming atom and dimer, respectively, can be decomposed into the total wave number $\vec{p}_\mathrm{tot} = \vec{p}_\mathrm{A} + \vec{p}_\mathrm{D}$ and the relative wave number $\vec{k} = \frac{2}{3}\vec{p}_\mathrm{A} - \frac{1}{3}\vec{p}_\mathrm{D}$. Because of Galilean invariance, the scattering observables depend on the relative wave numbers and the collision energy E in the center-of-mass system only, $E = 3\hbar^2k^2/(4m)$. The differential cross section for elastic atom-dimer scattering is

$$\frac{d\sigma_\mathrm{AD}^\mathrm{(el)}}{d\Omega} = |f_\mathrm{AD}(k,\theta)|^2 \ , \tag{4.1}$$

where $f_{\rm AD}(k,\theta)$ is the scattering amplitude. The elastic cross section $\sigma_{\rm AD}^{\rm (el)}$ is obtained by integrating Eq. (4.1) over the full solid angle. The total cross section (including elastic and inelastic contributions) can be calculated using the optical theorem:

$$\sigma_{\rm AD}^{\rm (tot)} = \frac{4\pi}{k}{\rm Im} f_{\rm AD}(k,\theta=0)\,, \tag{4.2}$$

such that the inelastic cross section is given by the difference of the total and elastic cross sections. At low energies, higher partial waves with $L>0$ are suppressed and the scattering amplitude is dominated by S-waves ($L=0$):

$$f_{\rm AD}(k) = \left[k\cot\delta_0^{\rm AD}(k) - ik\right]^{-1}\,. \tag{4.3}$$

For the S-wave atom-dimer phase shift $k\cot\delta_0^{\rm AD}(k)$, we will use the results from a calculation using the effective field theory of Ref. [BHvK99a]. A convenient parametrization of these results was given in [BH03, BH06]:

$$ka\cot\delta_0^{\rm AD}(k) = c_1(ka) + c_2(ka)\cot\left[s_0\ln\left(0.19\,a/a_*\right) + \phi(ka)\right]\,, \tag{4.4}$$

where

$$\begin{aligned} c_1(ka) &= -0.22 + 0.39\,k^2a^2 - 0.17\,k^4a^4\,,\\ c_2(ka) &= 0.32 + 0.82\,k^2a^2 - 0.14\,k^4a^4\,,\\ \phi(ka) &= 2.64 - 0.83\,k^2a^2 + 0.23\,k^4a^4\,. \end{aligned} \tag{4.5}$$

This parametrization is valid up to the dimer breakup wave number of $k_{\rm br} = 2/(\sqrt{3}a)$. A parametrization for higher wave numbers beyond the dimer breakup exists [BHKP08] but will not be required for our purposes as we will demonstrate below.

To leading order in the large scattering length, atom-dimer relaxation can only proceed via S-waves. For the relaxation into deep dimers to take place, the atom and the dimer have to approach each other to very short distances. However, because of the angular momentum barrier this can only happen in the relative S-wave channel. The parametrization of the S-wave phase shift in Eqs. (4.4, 4.5) is therefore sufficient to calculate atom-dimer relaxation.

4.2 Atom-Dimer Relaxation

To incorporate the effects of deep dimers, we make the simple replacement in the amplitude [BH04]

$$\ln a_* \to \ln a_* - i\eta_*/s_0\,, \tag{4.6}$$

where η_* determines the probability for an atom and a dimer to scatter into an energetic atom and deep dimer pair at short distances. This inelastic process generates the width of the Efimov resonances. The phase shift becomes imaginary even below the dimer breakup threshold and the released binding energy is converted to the kinetic energy of the recoiling atom and dimer. Thus, they are lost to the system. The event rate β for this dimer relaxation process in an ultracold gas of atoms and dimers can be written as

$$\frac{d}{dt}n_{\rm A} = \frac{d}{dt}n_{\rm D} = -\beta\,n_{\rm A}\,n_{\rm D}\,, \tag{4.7}$$

where n_{A} and n_{D} denote the number density of the atoms and dimers, respectively.

For an ensemble of atoms and dimers at nonzero temperature that are held in a trap, temperature and trap geometry have to be included in the calculation of the observed dimer losses. The dimer loss rate can be expressed as

$$\frac{d}{dt}N_{\mathrm{D}} = -\int d^3r \prod_{i=\mathrm{A,D}} \left[\int \frac{d^3p_i}{(2\pi)^3} n_i(p_i,r)\right] g(k), \tag{4.8}$$

where N_{D} is the number of dimers and we use the generalized Bose-Einstein distribution function

$$n_i(p_i,r) = \left[\exp\Big\{\Big(\frac{\hbar^2 p_i^2}{2m_i} + \frac{m_i\overline{\omega}^2 r^2}{2} - \mu_i\Big)/k_{\mathrm{B}}T\Big\} - 1\right]^{-1}, \tag{4.9}$$

with $i = \mathrm{A,D}$ denoting an atom or dimer, respectively. The properties of the trap enter via the average trap frequency $\overline{\omega}$, while the function $g(k)$ to be averaged is given by

$$g(k) = \frac{3\hbar k}{2m}\,\sigma_{\mathrm{AD}}^{(\mathrm{inel})}(k) = \frac{3\hbar k}{2m}\left(\sigma_{\mathrm{AD}}^{(\mathrm{tot})}(k) - \sigma_{\mathrm{AD}}^{(\mathrm{el})}(k)\right). \tag{4.10}$$

In the limit $k \to 0$, $g(k)$ reduces to the relaxation rate constant at zero temperature. Note that the function $g(k)$ introduces an implicit dependence on the angle between $\vec{p}_{\mathrm{A}}$ and $\vec{p}_{\mathrm{D}}$. The chemical potentials μ_i are fixed via the equation

$$\int d^3r \int \frac{d^3p_i}{(2\pi)^3}\, n_i(p_i,r) = N_i\,, \tag{4.11}$$

with N_i being the particle number and $i = \mathrm{A,D}$.

All angular integrations except for one can be carried out immediately and the expression (4.8) can be rewritten as:

$$\frac{d}{dt}N_{\mathrm{D}} = -\frac{1}{2\pi^3}\int_0^\infty r^2\,dr \int_0^\infty p_{\mathrm{tot}}^2\,dp_{\mathrm{tot}} \int_0^\infty k^2\,dk \int_{-1}^1 dx\, n_{\mathrm{A}}(p_{\mathrm{A}},r)\, n_{\mathrm{D}}(p_{\mathrm{D}},r)\, g(k)\,, \tag{4.12}$$

where x is the cosine of the angle between $\vec{p}_{\mathrm{tot}}$ and $\vec{k}$.

In evaluating Eq. (4.12), we will cut off the integral over k at the breakup wave number $k_{\mathrm{br}} = 2/(\sqrt{3}a)$ since the parametrization in Eqs. (4.4, 4.5) is only valid up to k_{br}. We have estimated the error from this simplification by using the unitary bound i/k for the S-wave scattering amplitude $f_{\mathrm{AD}}(k)$. For the data of Ref. [Kn$^+$09], the error involved is greatest for the largest scattering length considered, but even there only adds up to 0.2% for the largest temperature $T = 170\,\mathrm{nK}$. As a consequence, we can simply neglect the contribution from $k > k_{\mathrm{br}}$ in the analysis of the data.

4.3 Results and Discussion

We now apply our formalism to the experimental data for the atom-dimer relaxation rate of ultracold Cs atoms as a function of the scattering length obtained by Knoop et al. [Kn$^+$09].

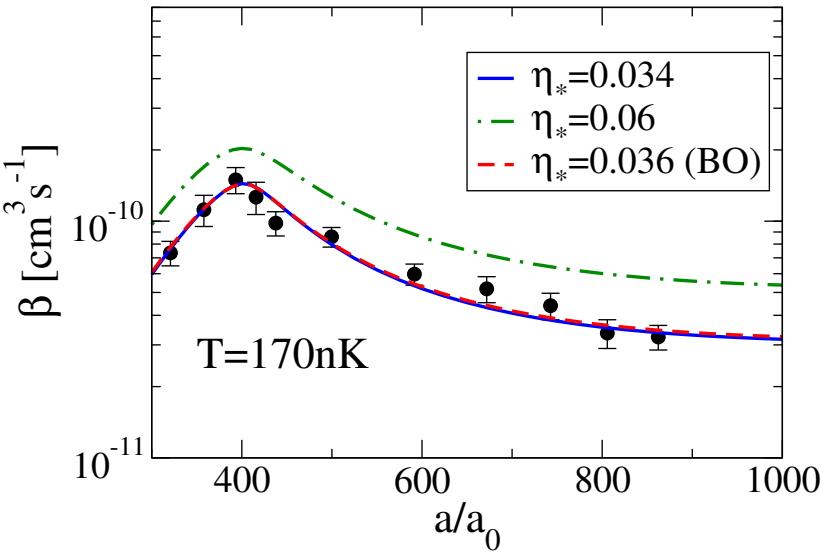

Figure 4.1: The dimer relaxation coefficient β as a function of a/a_0 for $T = 170\,\mathrm{nK}$, $a_* = 397\,a_0$, and different values of η_*. The data points are from [Kn+09]. BO indicates a Boltzmann average.

Our free parameters are a_*, which determines the position of the resonance, and η_*, which determines its width. These parameters cannot be calculated in our approach and must be taken from experiment. We will determine a_* and η_* from the data of Knoop et al. and compare our results with what is known from other experiments. In Ref. [Kn+09], the dimer relaxation coefficient was extracted from the dimer loss data using a loss model resulting in the rate equation

$$\frac{d}{dt}N_\mathrm{D} = -\frac{8}{\sqrt{27}}\,\beta\,\bar{n}_\mathrm{A}\,N_\mathrm{D} - \xi\,\bar{n}_\mathrm{D}\,N_\mathrm{D}\,, \tag{4.13}$$

with $\bar{n}_\mathrm{A} = [m\overline{\omega}^2/(4\pi k_\mathrm{B}T)]^{3/2}N_\mathrm{A}$ the mean atomic density, $\bar{n}_\mathrm{D} = [m\overline{\omega}^2/(2\pi k_\mathrm{B}T)]^{3/2}N_\mathrm{D}$ the mean molecular density, and ξ the dimer-dimer relaxation rate coefficient. As $\beta\,N_\mathrm{A} \gg \xi\,N_\mathrm{D}$ was fulfilled for the range of the scattering length that we are interested in, the dimer loss term can be neglected. In order to compare our calculation with the experiment of Knoop et al., we extract a value for β from our result for dN_D/dt (cf. Eq. (4.12)) using

$$\beta \equiv -\frac{\sqrt{27}}{8\,\bar{n}_\mathrm{A}\,N_\mathrm{D}}\frac{d}{dt}N_\mathrm{D}\,. \tag{4.14}$$

We start with the data at $T = 170\,\mathrm{nK}$ and fix the chemical potentials as described above. For atom number $N_\mathrm{A} = 10^5$, dimer number $N_\mathrm{D} = 4\times10^3$, and an average trap frequency of $\overline{\omega} = 45\,\mathrm{Hz}$ [Kn], we obtain the chemical potentials $\mu_\mathrm{A} = -2.74\times10^{-7}\,k_\mathrm{B}\mathrm{K}$ and $\mu_\mathrm{D} = -8.17\times10^{-7}\,k_\mathrm{B}\mathrm{K}$. In Fig. 4.1 the data for the recombination constant β is shown together with our best fit as the solid blue line. We only take into account data points for $a > 300\,a_0$. This fit yields $\chi^2/\mathrm{dof} = 1.2$. We obtain for the peak position $a_* = 397\,a_0$ and for the resonance width parameter $\eta_* = 0.034$. Also shown as a dashed-dotted green line is the resulting curve for the same resonance position but with $\eta_* = 0.06$. This value of η_* was obtained from fitting the three-body recombination resonance in Cs for negative scattering

length in [Kr$^+$06]. It is also compatible with the three-body recombination data for positive scattering length presented in the same paper.[1] However, the data for $a > 0$ are not very sensitive to the precise value of η_* and values of η_* as small as 0.01 would also be compatible. The width parameter η_* should only be weakly dependent on the magnetic field in a universal region [BH06]. In a first approximation, it can be assumed to remain constant. A more serious puzzle is that the resonance position $a_* = 397\,a_0$ extracted from the dimer relaxation data is not compatible with the value $a_* \approx 1200\,a_0$ found in [Kr$^+$06]. The three-body recombination data cannot be satisfactorily described using $a_* = 397\,a_0$. This disagreement requires further study. However, one has to keep in mind that the atom-dimer resonance is at the border of the universal region since the van der Waals length scale is $\ell_{\rm vdW} \approx 200\,a_0$ for Cs atoms.

For temperatures much larger than the Bose-Einstein-condensation temperature, the thermal average can be replaced by a Boltzmann average.

The critical temperatures are estimated by setting the chemical potential to zero and solving Eq. (4.11) for the critical temperature. This yields $T_{\rm c,A} \approx 94\,{\rm nK}$ for the atoms and $T_{\rm c,D} \approx 32\,{\rm nK}$ for the dimers. Therefore, it seems justified to use Boltzmann distributions instead of the Bose-Einstein distribution functions n_i. The resulting calculation for β is analogous to the method of Ref. [BH07a] but uses the parametrization of the scattering phase (4.4) instead of an effective range expansion. The resulting curve is also shown in Fig. 4.1 as the dashed red line. We remark that in the numerical evaluation of Eq. (8) in Ref. [BH07a] a factor of k^2 in the thermal average was omitted. This led to a wrong normalization of the curves in Figs. 1 and 2 of this reference. The dashed line also obviously describes the data quite well but yields $\eta_* = 0.036$. This shows how temperature dependence and averaging methods can partly be compensated by adjusting the width parameter η_*. Thus, for an accurate determination of η_*, reliable temperature and particle number measurements are crucial.

Using the effective range expansion for the atom-dimer scattering amplitude as in Ref. [BH07a] instead of the phase shift parametrization of Eqs. (4.4, 4.5) does not alter the overall shape or normalization of the dimer relaxation coefficient β. However, the extracted value of a_* is shifted by about 3% to a higher value, whereas η_* remains unchanged. The scattering length approximation with the atom-dimer scattering length given by $a_{\rm AD}/a = 1.46 + 2.15\cot[s_0\ln(a/a_*) + i\eta_*]$ does not lead to an equally good fit. The obtained values for β are smaller especially for higher values of a. Besides a change in peak position, width and height, we can only obtain a $\chi^2/{\rm dof}$ of 3–4.

We now turn to the data for $T = 40\,{\rm nK}$ [Kn$^+$09] and compare them to our theoretical results for different values of η_*. Here, the atom and dimer numbers are $N_{\rm A} = 3\times10^4$ and $N_{\rm D} = 4\times10^3$, and the trap frequency is $\overline{\omega} = 25.2\,{\rm Hz}$ [Kn$^+$09] leading to the chemical potentials $\mu_{\rm A} = -1.21\times10^{-8}\,k_{\rm B}{\rm K}$ and $\mu_{\rm D} = -8.87\times10^{-8}\,k_{\rm B}{\rm K}$. The critical temperatures are estimated as $T_{\rm c,A} \approx 35\,{\rm nK}$ for the atoms and $T_{\rm c,D} \approx 18\,{\rm nK}$ for the dimers such that the temperature is only slightly larger than the critical temperature for the atoms. In Fig. 4.2 we show the data for the relaxation coefficient β at $T = 40\,{\rm nK}$ together with our fit results. The dashed red line gives our prediction for the relaxation coefficient β using the parameters obtained by fitting the 170 nK data. The prediction is about a factor 2 too large compared to the data. The dip in the data at the peak position represented by the third and fourth data

[1] Note that in the Cs experiment of [Kr$^+$06] the regions $a > 0$ and $a < 0$ are not required to have the same parameters since they are separated by a zero in the scattering length rather than a pole. See also the discussion in [Kn$^+$09].

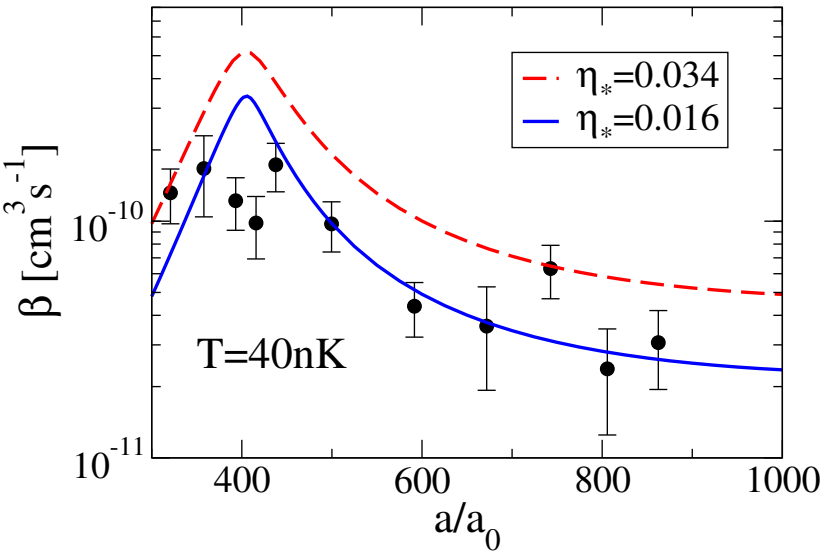

Figure 4.2: The dimer relaxation coefficient β as a function of a/a_0 for $T = 40\,\mathrm{nK}$, $a_* = 397\,a_0$, and different values of η_*. The data points are from [Kn+09].

points cannot be reproduced within our theory. If it is not simply a statistical fluctuation, it must be due to physics not captured in our theory, such as non-universal effects or four-body physics [PHM04, HP07, vSDG09]. If we keep the resonance position at $a_* = 397\,a_0$ but fit the parameter η_* to the 40 nK data excluding the third and fourth data points, we obtain the solid blue line. Still excluding the third and fourth data points this gives $\eta_* = 0.016$ with $\chi^2/\mathrm{dof} = 1.5$ and describes the data satisfactorily.

4.4 Summary and Conclusions

In summary, we have calculated the atom-dimer relaxation rate for large positive scattering length in a universal zero-range approach. We have improved on previous studies [BH04, BH07a] by using a Bose-Einstein distribution for the thermal average and calculations of the atom-dimer scattering phase shifts from effective field theory. Our results were then applied to the atom-dimer relaxation data for Cs obtained by Knoop et al. [Kn+09]. Fitting the resonance position and width parameters a_* and η_*, we could get a good description of the 170 nK data. Using these parameters, we overpredict the relaxation data at 40 nK by a factor of two. Moreover, our theory is not able to reproduce the dip in the 40 nK data directly at the resonance position and the corresponding physics appears to be missing in our theory. We demonstrated that this discrepancy is neither due to the thermal averaging procedure nor due to the phase shift parametrization used. The resonance position at the border of the universal region and the mismatch in the extracted resonance position from atom-dimer relaxation and the three-body recombination data [Kr+06] suggest that non-universal physics could be responsible. However, it is also conceivable that four-body losses become important at the lower temperature. This question deserves further study but lies outside the range of this thesis.

Chapter 5

Heteronuclear Systems – Bosons in the S-Wave Channel

In this and in the following chapter, heteronuclear systems involving two species of atoms with resonant interspecies interaction are investigated. We start in this chapter by considering bosons as the majority species. For total angular momentum $L = 0$, the Efimov effect is always present and can be seen in the observables. This chapter has been published as part of Ref. [HHP10].

For the considered systems, only the interspecies scattering length is large. Therefore, we now have only two resonant interactions out of three leading to different scaling factors. For comparable masses, the scaling factor is quite large (for equal masses $e^{\pi/s_0} \approx 1986.1$). However, in the case of two heavy atoms and one light atom, this factor can become significantly smaller, even smaller than the value 22.7 for identical bosons with three resonant interactions [AN72, Ef72, Ef73, BH06]. This should stimulate experimental investigation of the discrete scaling invariance. Relaxation and recombination losses near an interspecies resonance have recently been investigated in mixtures of rubidium and potassium. The Bose-Fermi combination ^{87}Rb-^{40}K has been studied at JILA [Zi$^+$08] and measurements on the Bose-Bose mixture ^{41}K-^{87}Rb have been carried out in Florence [Ba$^+$09]. We apply our theory to these and other mixtures of interest for ongoing and planned experiments.

The method used for the calculations is presented first of all. Then the numerical results are given and we compare them subsequently to existing and future experiments. We end with a summary.

5.1 Method

First, we set up the effective field theory method which provides a convenient implementation of the universal theory for large scattering length. We consider a system of one boson or fermion of mass m_1 (species 1) and two identical bosons of mass m_2 (species 2). We assume the interspecies interaction to be resonant and characterized by the S-wave scattering length

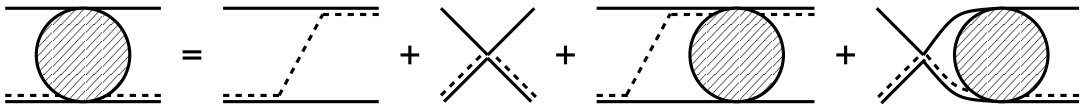

Figure 5.1: Integral equation for the atom-dimer scattering amplitude $\mathcal{A}$. Solid (dashed) lines denote atom species 2 (1). Mixed double lines denote the full dimer propagator.

$a \gg \ell_{\rm vdW}$, where $\ell_{\rm vdW}$ is the van der Waals range of the potential. Nonresonant intraspecies interaction will be neglected. If species 1 is also bosonic and weakly interacting, all the forthcoming results directly apply to the other possible (interacting) triple by simply exchanging the labels 1 and 2. We therefore include only the interaction between the atoms of species 2 and the dimers. Hence, our effective Lagrangian reads

$$\begin{aligned}\mathcal{L} &= \psi_1^\dagger\left(i\partial_t + \frac{\nabla^2}{2m_1}\right)\psi_1 + \psi_2^\dagger\left(i\partial_t + \frac{\nabla^2}{2m_2}\right)\psi_2 + g_2 d^\dagger d \\ &\quad - g_2\left(d^\dagger\psi_1\psi_2 + \psi_1^\dagger\psi_2^\dagger d\right) - \frac{g_3}{4}d^\dagger d\psi_2^\dagger\psi_2 + \cdots ,\end{aligned} \tag{5.1}$$

where the dots represent higher-order derivative interactions, and g_2 and g_3 are the bare two- and three-body coupling constants.

From the Lagrangian (5.1), we can deduce Feynman rules and obtain the full dimer propagator and the three-body integral equation (see Appendix A.1 for details on the derivation). For the full dimer propagator we find

$$D(P_0,\vec{P}) = \frac{2\pi}{\mu g_2^2}\left[\frac{1}{a} - \sqrt{-2\mu\Big(P_0 - \frac{P^2}{2M}\Big) - i\epsilon}\right]^{-1} , \tag{5.2}$$

where $P = |\vec{P}|$, $\mu = m_1 m_2/(m_1+m_2)$ is the reduced mass, and $M = m_1 + m_2$ is the mass of the dimer. The dimer wave function renormalization is given by $Z_{\rm D}^{-1} = g_2^2 a\mu^2/(2\pi)$.

The scattering between a dimer and an atom is described by the integral equation shown in Fig. 5.1. Using the Feynman rules derived from Eq. (5.1) and given in Appendix A.1 and projecting onto relative S-waves, we have

$$\begin{aligned}\mathcal{A}(p,k;E) &= \frac{2\pi m_1}{a\mu^2}\left[K(p,k) - \frac{g_3}{4m_1 g_2^2}\right] \\ &\quad + \frac{m_1}{\pi\mu}\int_0^\Lambda dq\, q^2\left[K(p,q) - \frac{g_3}{4m_1 g_2^2}\right]\frac{\mathcal{A}(q,k;E)}{-\frac{1}{a} + \sqrt{-2\mu\left(E - \frac{q^2}{2\mu_{\rm AD}}\right) - i\epsilon}} ,\end{aligned} \tag{5.3}$$

where $\mu_{\rm AD} = m_2(m_1+m_2)/(2m_2+m_1)$ is the reduced mass of an atom and a dimer, the relative momenta of the incoming and outgoing atom-dimer pair are denoted by p and k, respectively; and E is the total energy. The contribution of the S-wave projected one-atom exchange is given by

$$K(p,q) = \frac{1}{2pq}\ln\left[\frac{p^2+q^2+2pq\frac{\mu}{m_1} - 2\mu E - i\epsilon}{p^2+q^2-2pq\frac{\mu}{m_1} - 2\mu E - i\epsilon}\right] , \tag{5.4}$$

and the contribution of the three-body coupling g_3 can be written as

$$\frac{g_3}{4m_1 g_2^2} = -\frac{H(\Lambda)}{\Lambda^2}\,, \tag{5.5}$$

where $H(\Lambda)$ is a dimensionless log-periodic function of the cutoff Λ, which depends on a three-body parameter Λ_* [BHvK99a, BHvK99b]. The mass-ratio dependence of the discrete scaling factor $\exp(\pi/s_0)$ follows from the equation for s_0 (see Appendix A.3 for the derivation):

$$s_0 \cosh(\pi s_0/2) - 2\sinh(\phi s_0)/\sin(2\phi) = 0\,, \tag{5.6}$$

where we introduce the parameter

$$\phi = \arcsin\left[1/(1+\delta)\right] \tag{5.7}$$

and the notation $\delta = m_1/m_2$. For particles of equal mass, the solution of Eq. (5.6) is $s_0 \approx 0.4137$ leading to the scaling factor $\exp(\pi/s_0) \approx 1986.1$. Because of the log-periodicity of $H(\Lambda)$ one can always find a value of the cutoff Λ with $H = 0$. In practice, one can therefore simply omit the three-body coupling in the leading-order calculations and use the cutoff Λ as a three-body parameter [HM01]. We use this strategy in the following. For fixed δ, the values of Λ and Λ_* are related by a multiplicative constant.

The scattering amplitude $\mathcal{A}$ has simple poles at the three-body bound-state energies $E = -E_\mathrm{T} < 0$. The energies can be obtained from the solution of the following homogeneous integral equation for the bound-state amplitude $\mathcal{B}$:

$$\mathcal{B}(p; E_\mathrm{T}) = \frac{m_1}{\pi\mu}\int_0^\Lambda \frac{dq\, q^2\, K(p,q)\, \mathcal{B}(q; E_\mathrm{T})}{-\frac{1}{a} + \sqrt{2\mu\left(E_\mathrm{T} + \frac{q^2}{2\mu_\mathrm{AD}}\right)}}\,, \tag{5.8}$$

which has nontrivial solutions only for three-body binding energies $E_\mathrm{T} > 0$. In the following, we use Eqs. (5.3) and (5.8) to describe three-body properties of heteronuclear mixtures.

5.2 Numerical Results

Few-body loss phenomena offer a unique view on scattering processes in ultracold quantum gases. In particular, an enhancement of the loss rate can be an evidence of a few-body resonance. The universal theory predicts the relative positions of such resonances as a function of the scattering length. The universality can thus be tested experimentally by measuring the lifetime of a cold atomic gas as a function of a. Ideally, in order to see the universal scaling, one needs to detect more than one resonance in a single universal region, that is, a region where the three-body parameter can be assumed constant. This is believed to happen in a narrow vicinity of a Feshbach resonance, where large variations of a are accompanied by (assumed) much weaker variations of the three-body parameter. We now discuss three-body loss resonances in a heteronuclear mixture as predicted by the universal theory.

5.2.1 Resonance Positions

The mechanism of three-body losses and its relation to the positions of Efimov levels in the heteronuclear case are qualitatively the same as for three identical bosons given in Subsection 2.4.1. Nevertheless, we here describe it again in some detail to facilitate the reading of this chapter. The scattering-length dependence of the energy of a generic trimer is illustrated in Fig. 2.6. On the negative side of a Feshbach resonance, the trimer hits the three-body scattering threshold at $a = a_- < 0$, which leads to an enhanced probability of finding three atoms at distances of the order of $|a|$. Such atoms can then approach each other to distances of the order of $\ell_{\rm vdW}$ and recombine into a deeply bound dimer and a residual atom. The released binding energy (of order $\hbar^2/(2\mu\ell_{\rm vdW}^2)$) transforms into the kinetic energy of the recombination products, which hence leave the trap. On the positive side of the Feshbach resonance, there exists a weakly bound (shallow) dimer state with binding energy $E_{\rm D} = \hbar^2/(2\mu a^2)$. This formula, taken with a minus sign, determines the atom-dimer threshold (parabola in Fig. 2.6). By following the upper blue line in Fig. 2.6 from negative to positive values of a, one can see that the trimer crosses the atom-dimer threshold at $a = a_* > 0$, where one predicts an elastic atom-dimer resonance. At this point, formation of deep dimer states (in this case called relaxation) in atom-dimer collisions is also enhanced for the same reason as above. According to [Za$^+$09], the atom-dimer scattering resonance should be noticeable even in a purely atomic sample due to rescattering processes. Indeed, before leaving the trap, shallow dimers formed in the process of three-body recombination can collide with other atoms. The recombination rate itself is featureless around $a = a_*$, but the atom-dimer cross section in the vicinity of this point is highly a dependent. Thus, at $a = a_*$ the three-body recombination can be enhanced in the sense that many more than three atoms are expelled from the trap leading to a measurable trap loss. We come back to this issue in Subsection 5.3.2.

The ratio of the two resonance positions, $a_*/|a_-|$, is of fundamental importance for studies of the universal three-body physics because in the universal limit, it does not depend on the three-body parameter. In order to calculate this ratio we solve the bound-state Eq. (5.8) for $E_{\rm T} = 0$, $a < 0$, and for $E_{\rm T} = E_{\rm D}$, $a > 0$, with the same (arbitrary) cutoff Λ. The solid red line in Fig. 5.2 shows $a_*^{(n)}/|a_-^{(n)}|$ as a function of the mass ratio δ. Here we use the index n introduced in Eq. (2.18) in order to emphasize that the values of a_* and a_- are taken for one and the same Efimov state (connected by the blue lines in Fig. 2.6). The dashed black line in Fig. 5.2 differs from the solid one by the scaling factor $\exp(\pi/s_0)$ and shows the ratio $a_*^{(n+1)}/|a_-^{(n)}|$. Note that the scaling factor rapidly increases with δ for $\delta \gtrsim 1$ and one can conclude that a sequence of Efimov resonances is more likely to be seen in systems with smaller mass ratios.

5.2.2 Three-Body Recombination for $a > 0$

Let us now discuss the shapes of the inelastic loss resonances and calculate the three-body rate constants in a heteronuclear system. We first consider the case of positive scattering length, $a > 0$, where the atoms can recombine into the shallow dimer and into deep dimers. The recombination into the shallow dimer can be related to the T-matrix element shown in Fig. 5.3 a). The event rate constant for inelastic scattering α is defined by the rate equation

$$\frac{d}{dt}n_2 = 2\frac{d}{dt}n_1 = -2\,\alpha\,n_1\,n_2^2\,, \tag{5.9}$$

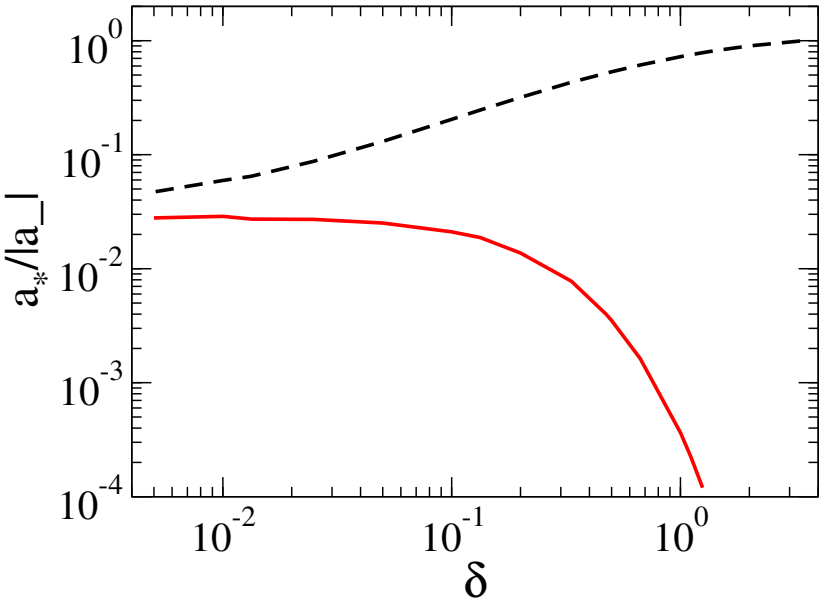

Figure 5.2: Solid red line: $a_*^{(n)}/|a_-^{(n)}|$ as a function of δ, where n is the index of the Efimov state. Dashed black line: $a_*^{(n+1)}/|a_-^{(n)}| = \exp(\pi/s_0)a_*^{(n)}/|a_-^{(n)}|$.

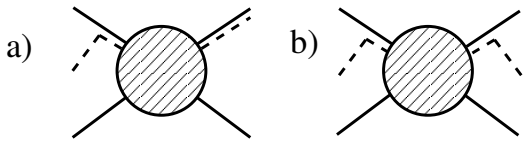

Figure 5.3: Diagrammatic representation of a) the three-body recombination amplitude and b) the elastic three-body scattering. Line patterns are the same as in Fig. 5.1.

where n_i denotes the atomic number densities of the corresponding species.

The rate constant α_s for recombination into the shallow dimer is given by

$$\alpha_\mathrm{s} = 4\,\mu_\mathrm{AD}\sqrt{\frac{\mu_\mathrm{AD}}{\mu}}a^2\,|\mathcal{A}\,(0,k_\mathrm{br};0)|^2\ , \tag{5.10}$$

with the dimer breakup momentum $k_\mathrm{br} = \sqrt{\mu_\mathrm{AD}/\mu}\,a^{-1}$. If deep dimers are present, their effect on the recombination into the shallow dimer can be incorporated by analytically continuing the three-body parameter into the complex plane [BHKP09]. We thus make the substitution

$$\Lambda \ \rightarrow \ \Lambda_\mathrm{c} = \Lambda e^{i\eta_*/s_0} \tag{5.11}$$

in Eq. (5.3), where η_* accounts for the effect of the deep dimers. A nonzero value of η_* also generates the width of the Efimov trimers. By evaluating Eq. (5.10) numerically, we find that the known analytical formula for the three-boson case [BHKP10] simply acquires a new mass-dependent overall coefficient. The modified analytical formula is hence

$$\alpha_\mathrm{s} = C(\delta)\,\frac{B\,(\sin^2[s_0\ln(a/a_{0*})] + \sinh^2\eta_*)}{\sinh^2(\pi s_0+\eta_*) + \cos^2[s_0\ln(a/a_{0*})]}\,\frac{\hbar a^4}{m_1}\,, \tag{5.12}$$

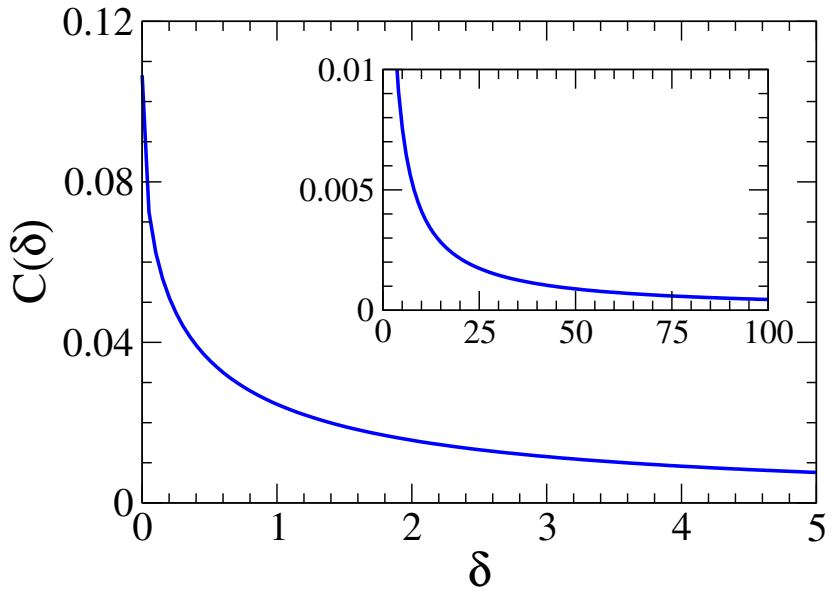

Figure 5.4: The coefficient C for the different three-body recombination rates as a function of the mass ratio $\delta = m_1/m_2$. The inset shows C for larger values of δ.

where $B = 128\pi^2(4\pi - 3\sqrt{3})$ and the mass-dependent coefficient is denoted by $C(\delta)$. The parameter a_{0*} gives the position of the minimum in the three-body recombination. The coefficient $C(\delta)$ is shown in Fig. 5.4. The error in the extraction of $C(\delta)$ from fitting Eq. (5.12) to our numerical results for α_s is of order 10^{-3} for $\delta \leq 2$. For larger values of δ the numerical extraction of C becomes difficult because of a very large value of the scaling factor. To depict $C(\delta)$ for $\delta \geq 2$ we use the analytical formula derived in detail in Section IV of Ref. [HHP10],

$$C(\delta) = \frac{(1+\delta)^2 \arcsin\left[1/(1+\delta)\right] - \sqrt{\delta(2+\delta)}}{2(4\pi - 3\sqrt{3})} \,. \tag{5.13}$$

Although our calculations in this section are conducted by varying the complex three-body parameter Λ_c, we present the results in terms of the practically relevant length parameters $a_- < 0$, $a_* > 0$, and $a_{0*} > 0$, and the dimensionless elasticity parameter η_*. The universal theory predicts that the ratios $a_*/|a_-|$ and $|a_-|/a_{0*}$ depend only on the mass ratio δ. The former is shown in Fig. 5.2 and the latter is $|a_-|/a_{0*} = \exp(\pi/2s_0)$ as derived in [HHP10]. This fixes the relative positions of all the three-body loss features on both sides of the Feshbach resonance.

The total rate of three-body recombination into all dimers (shallow and deep) for $a > 0$ can be obtained from the optical theorem. It relates the imaginary part of the forward T-matrix element (shown in part b) of Fig. 5.3) for vanishing momenta to the event rate constant of inelastic scattering, α. This leads to the total recombination rate constant

$$\alpha_s + \alpha_d = \mathrm{Im} T_{122\to122} = 8\,\pi\,a^3\,\mathrm{Im}\bar{\mathcal{A}}(0,0;0)\,, \tag{5.14}$$

where $\bar{\mathcal{A}}$ denotes the appropriately infrared subtracted amplitude [BHKP10]:

$$\bar{\mathcal{A}}(p,k;E) = \mathcal{A}(p,k;E) - \frac{4\pi(1+\delta)}{m_1 a p^2} + \frac{4\pi(1+\delta)^2}{m_1 p}\arcsin\left[1/(1+\delta)\right] + \frac{8a}{m_1}\left[(1+\delta)^2\arcsin\left[1/(1+\delta)\right] - \sqrt{\delta(2+\delta)}\right]\ln p\,. \tag{5.15}$$

More details on the derivation of $\bar{\mathcal{A}}$ can be found in Appendix A.2. By subtracting Eq. (5.12) from Eq. (5.14) we find the rate constant for the recombination into deep dimers:

$$\alpha_{\rm d} = C(\delta)\,\frac{B\,\coth(\pi s_0)\cosh(\eta_*)\sinh(\eta_*)}{\sinh^2(\pi s_0+\eta_*)+\cos^2[s_0\ln(a/a_{0*})]}\,\frac{\hbar a^4}{m_1}\,, \tag{5.16}$$

where the coefficients $C(\delta)$ and B are the same as in Eq. (5.12).

When s_0 is not too small, such that $\exp(2\pi s_0) \gg 1$, the denominators in Eqs. (5.12) and (5.16) are practically independent of a. In this case the a dependence of $\alpha_{\rm s}$ and $\alpha_{\rm d}$ is simplified, and the corresponding expressions are known in the case of three identical bosons (see, for example, Ref. [BH06]).

5.2.3 Atom-Dimer Scattering

On the positive side of the Feshbach resonance ($a > 0$) it is also possible to prepare an ultracold mixture of atoms and weakly bound dimers (see, for example, Refs. [Zi$^+$08, Kn$^+$09]). An important observable in this case is the atom-dimer scattering length. Within our theory, it is given by

$$a_{\rm AD} = -\frac{\mu_{\rm AD}}{2\pi}\mathcal{A}\left(0,0;-\frac{1}{2\mu a^2}\right)\,, \tag{5.17}$$

and its universal dependence on a is parametrized by

$$a_{\rm AD} = \Big(C_1(\delta) + C_2(\delta)\cot[s_0\ln(a/a_*)]\Big)a\,, \tag{5.18}$$

where the coefficients $C_1(\delta)$ and $C_2(\delta)$, calculated numerically, are shown in Fig. 5.5. Here, we estimate the numerical error in the determination of $C_1(\delta)$ and $C_2(\delta)$ to be of order 10^{-3}.

Efremov and collaborators have recently derived Eq. (5.18) for the atom-dimer scattering length in the Born-Oppenheimer approximation valid in the limit $\delta \to 0$ [Ef$^+$09]. For $\delta = 0.081$, corresponding to the ^{7}Li-^{87}Rb-^{87}Rb system, our values for the coefficients C_1 and C_2 agree with the ones given in Ref. [Ef$^+$09] to within 2-3% (see Table 5.1). However, we observe a stronger discrepancy in between our value, $s_0 = 1.523$, and the Born-Oppenheimer result, $s_0 = 1.322$, for this system [Ef$^+$09].

The effect of deep dimers on the atom-dimer scattering process can be incorporated by replacing $a_* \to a_*\exp(-i\eta_*/s_0)$, equivalent to Eq. (5.11). At the scattering threshold, the atom-dimer relaxation rate constant β, defined by the rate equation

$$\frac{d}{dt}n_{\rm A} = \frac{d}{dt}n_{\rm D} = -\beta\, n_{\rm A}\, n_{\rm D}\,, \tag{5.19}$$

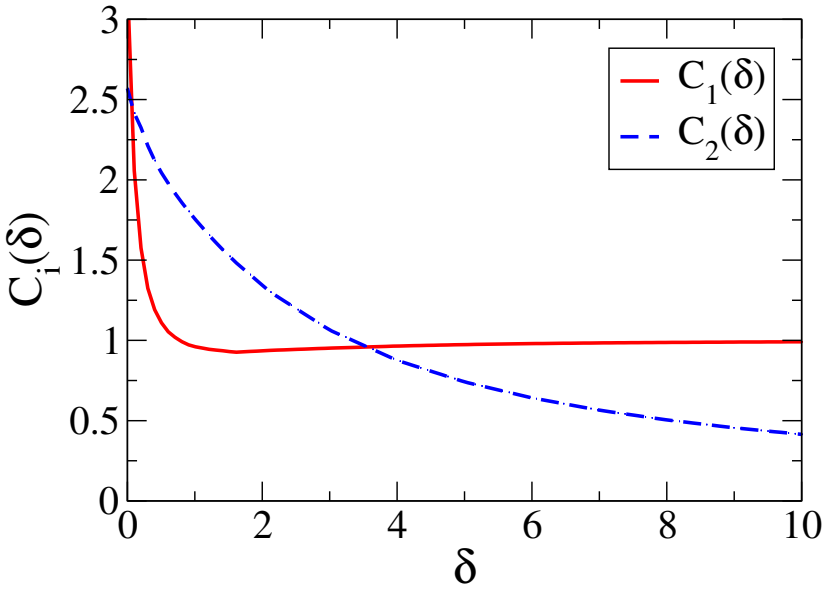

Figure 5.5: The parameters $C_1(\delta)$ and $C_2(\delta)$ in the expression for the atom-dimer scattering length, Eq. (5.18).

is given by [BH04]

$$\begin{aligned}\beta(E=-E_{\rm D}) &= -(4\pi\hbar/\mu_{\rm AD})\,{\rm Im}a_{\rm AD} \\ &= 2\pi\,C_2(\delta)\,\frac{\delta(\delta+2)}{\delta+1}\,\frac{\sinh(2\eta_*)}{\sin^2[s_0\ln(a/a_*)]+\sinh^2\eta_*}\,\frac{\hbar a}{m_1}\,. \end{aligned} \tag{5.20}$$

Furthermore, we can calculate the atom-dimer relaxation rate constant above threshold. It is related to the inelastic atom-dimer scattering cross section by

$$\beta(E) = \frac{k}{\mu_{\rm AD}}\sigma_{\rm AD}^{\rm (inel)}(E)\,, \tag{5.21}$$

where $k=\sqrt{2\mu_{\rm AD}(E+E_{\rm D})}$. The energy dependent inelastic cross section is given by the difference of the total and the elastic cross sections,

$$\sigma_{\rm AD}^{\rm (inel)}(E) = \frac{2\mu_{\rm AD}}{k}{\rm Im}\mathcal{A}(k,k;E) - \frac{\mu_{\rm AD}^2}{\pi}\,|\mathcal{A}(k,k;E)|^2\,. \tag{5.22}$$

We can use this formula up to the dimer breakup threshold at $k=k_{\rm br}$ and thus map out the trajectory of the resonance peak. It moves from a_* at the scattering threshold, $E=-E_{\rm D}$, to $|a_-|$ at the dimer breakup threshold, $E=0$. For $\delta<3.475$ the resonance peak moves to values $a>a_*$. Starting at $\delta=3.475$, where we have exactly $a_*/|a_-|=1$, it reverses this behavior and moves to values $a<a_*$. The peak height diminishes considerably with the energy. This effect is very large, especially for small values of δ. For example, for $\eta_*=0.1$ and $\delta=0.1$, the peak at $E=0$ is smaller by a factor of 706 than the peak at $E=-E_{\rm D}$. For $\delta=10$, this factor still is 19.1. At $E=0$, we find excellent agreement with the analytical formula

$$\beta(E=0) = \pi\,\frac{[\delta(\delta+2)]^{3/2}}{(\delta+1)^2}\,\frac{\sinh(2\pi s_0)\sinh(2\eta_*)}{\sinh^2(\pi s_0+\eta_*)+\cos^2[s_0\ln(a/a_{0*})]}\,\frac{\hbar a}{m_1}\,, \tag{5.23}$$

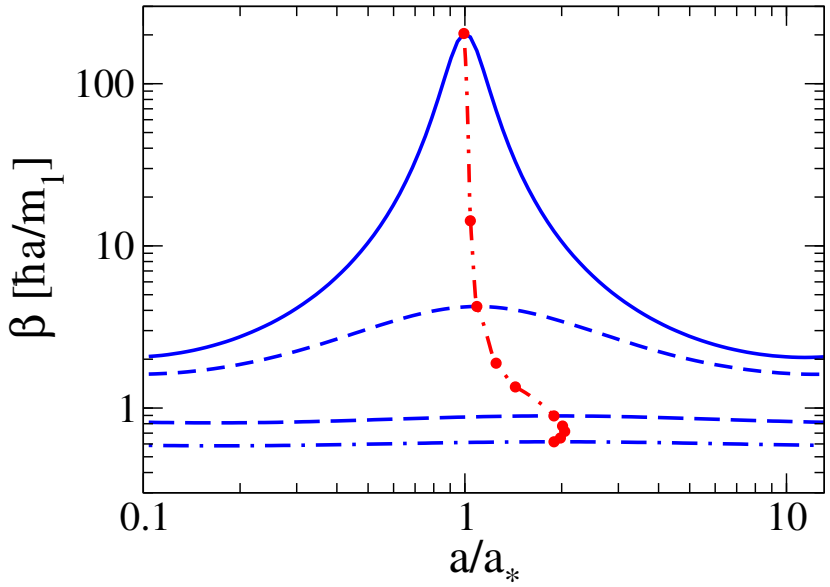

Figure 5.6: The dimer relaxation rate constant β in units of $\hbar a/m_1$ for $\eta_* = 0.1$ and $\delta = 0.471$ as function of a/a_*. The solid, short-dashed, long-dashed, and dot-dashed blue lines show β for $E/E_\mathrm{D} = -1$, -0.95, -0.5, and 0, respectively. The double-dot-dashed red line indicates the trajectory of the resonance maximum as the energy is increased from $-E_\mathrm{D}$ to zero.

which is derived in [HHP10]. The peak position of $\beta\,(E = 0)$ coincides exactly with the position of the maximum of the three-body recombination rate at threshold.

In Fig. 5.6, we show numerical results for β for $\eta_* = 0.1$ and $\delta = 0.471$ corresponding to the K-Rb-Rb system observed in the Florence experiment [Ba$^+$09]. The solid, short-dashed, long-dashed, and dot-dashed blue lines show β for $E/E_\mathrm{D} = -1$, -0.95, -0.5, and 0, respectively. As the energy is increased toward the breakup threshold, the resonance height decreases strongly and the resonance becomes less pronounced. The double-dot-dashed red line shows the trajectory of the resonance maximum as the energy is increased from $-E_\mathrm{D}$ to zero. As the energy is increased, the resonance position is shifted from a_* toward larger values of a until it reaches its maximum value of $2.04\,a_*$ for $E/E_\mathrm{D} \approx -0.25$. For larger energies, the resonance position moves back to smaller values of a and reaches $|a_-| = 1.89\,a_*$ at the dimer breakup threshold.

5.2.4 Three-Body Recombination for $a < 0$

On the negative side of the Feshbach resonance, shallow dimers are absent and atoms can only recombine into deep dimers. The corresponding rate constant is again determined by using the optical theorem

$$\alpha_\mathrm{d} = \mathrm{Im}T_{122\to122} = 8\,\pi\,a^3\,\mathrm{Im}\bar{\mathcal{A}}(0,0;0)\,. \tag{5.24}$$

	δ	s_0	$\exp(\pi/s_0)$	$a_*/\lvert a_-\rvert$	$C(\delta)$	$C_1(\delta)$	$C_2(\delta)$
^{6}Li-^{174}Yb-^{174}Yb	0.034	2.249	4.043	0.10	0.077	2.89	2.56
^{7}Li-^{133}Cs-^{133}Cs	0.053	1.850	5.465	0.13	0.072	2.54	2.52
^{6}Li-^{87}Rb-^{87}Rb	0.069	1.635	6.835	0.16	0.068	2.33	2.5
^{7}Li-^{87}Rb-^{87}Rb	0.081	1.523	7.864	0.18	0.066	2.22	2.47
^{40}K-^{87}Rb-^{87}Rb	0.460	0.6536	122.7	0.51	0.037	1.14	2.08
^{41}K-^{87}Rb-^{87}Rb	0.471	0.6444	131.0	0.52	0.037	1.13	2.07
^{87}Rb-^{174}Yb-^{174}Yb	0.5	0.6238	153.8	0.53	0.036	1.11	2.05
^{87}Rb-^{41}K-^{41}K	2.21	0.2462	348000	0.91	0.015	0.94	1.30

Table 5.1: Universal parameters for various heteronuclear mixtures.

We have performed numerical calculations of $\alpha_{\rm d}$ for mass ratios $\delta \leq 2$, where the numerical accuracy is better than 0.1%. Our results agree with the formula

$$\alpha_{\rm d} = \frac{C(\delta)}{2} \frac{B \coth(\pi s_0) \sinh(2\eta_*)}{\sin^2[s_0 \ln(a/a_-)] + \sinh^2(\eta_*)} \frac{\hbar a^4}{m_1}, \tag{5.25}$$

where the coefficients $C(\delta)$ and B are the same as in Eqs. (5.12) and (5.16). Equation (5.25) is derived in Ref. [HHP10].

5.3 Comparison to Experiments

There are several experiments on heteronuclear Bose-Bose and Bose-Fermi mixtures, to which our results are directly applicable (in the universal limit). In Table 5.1, we present the universal predictions for some combinations of alkali isotopes being investigated at the moment and interesting from the viewpoint of Efimov few-body physics. We sort them by the value of the scaling factor.

5.3.1 The ^{40}K-^{87}Rb Mixture

Zirbel et al. at JILA recently studied weakly bound fermionic ^{40}K-^{87}Rb molecules and their stability in collisions with atoms near a wide (open-channel-dominated) heteronuclear Feshbach resonance at $B_0 = 546.7\,\mathrm{G}$ [Zi$^+$08]. In particular, they measured the atom-dimer relaxation rate for collisions of these dimers with Rb atoms as a function of a. The corresponding data can be fit very well with our Eq. (5.20), where the fitting parameters are $a_* = 200 \pm 50\, a_0$ and $\eta_* = 0.05 \pm 0.02$, see Fig. 5.7. In the same work, the authors also measured the three-body recombination rate constant on both sides of this Feshbach resonance (i.e., in the same universal region). We fit their results with Eq. (5.25) on the negative side of the resonance and with the sum $\alpha_{\rm s} + \alpha_{\rm d}$ given by Eqs. (5.12) and (5.16) on the positive side[1]. A good

[1]Note that our rate constant α is half the three-body loss coefficient K_3 defined in [Zi$^+$08].

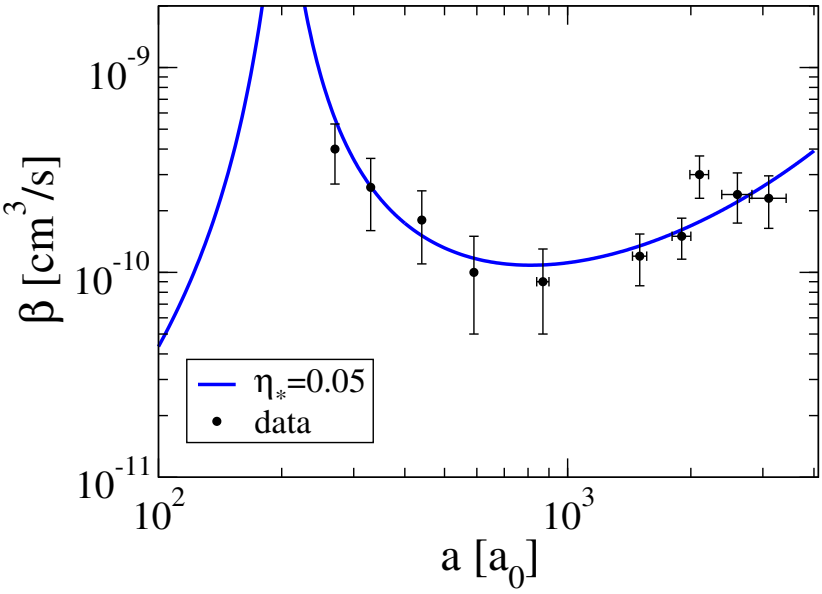

Figure 5.7: The relaxation rate β as a function of a in units of a_0 for the ^{40}K^{87}Rb–^{87}Rb system assuming $a_* = 200\,a_0$ and $\eta_* = 0.05$. The data points and errors are read off from Ref. [Zi$^+$08].

agreement is achieved if we choose $a_* = 300 \pm 100\,a_0$ (for this mass ratio $a_- = -1.96\,a_*$, see Table 5.1) and the same η_* as above. This is shown in Fig. 5.8. These parameter values lead to a peak of the three-body recombination at $a = a_- \approx -600\,a_0$. As the interspecies van der Waals length in the K-Rb system is $\ell_{\rm vdW} \approx 70\,a_0$ [Ju09], this resonance should be within the range of validity of the universal theory. In Fig. 5.8, we show the region $a \lesssim 3\ell_{\rm vdW}$ as grey shaded area. Although in Ref. [Zi$^+$08] the peak has not been identified, the overall shapes of β and α measured for this particular Feshbach resonance indicate that it is worth performing a more detailed measurement of the three-body loss rate around this value of a.

5.3.2 The ^{41}K-^{87}Rb Mixture

The group of Inguscio and Minardi in Florence investigated a Bose-Bose mixture of ^{87}Rb and ^{41}K [Ba$^+$09]. They observed three loss resonances by scanning the scattering length and monitoring the population dynamics of the species in the vicinity of each of the resonances. For negative scattering length, they identified a K-Rb-Rb resonance at $a = -246\,a_0$ and a K-K-Rb resonance at $a = -22000\,a_0$. The third resonance is observed at the positive scattering length $a = 667\,a_0$ and attributed to enhanced atom-dimer scattering in the K-Rb-Rb three-body system. This process is assumed to contribute to three-body losses through multiple rescattering processes (see also Ref. [Za$^+$09]). An independent confirmation of this resonance in a system prepared directly out of K-Rb dimers and Rb atoms would be desirable. Unfortunately, in contrast to the JILA experiment, the dimers are bosonic and their short lifetime can make such a confirmation difficult [Mi].

With an interspecies van der Waals length of $\ell_{\rm vdW} \approx 70\,a_0$ [Ju09], these resonances should be within the range of validity of the universal theory. Assuming that the observed K-Rb-Rb

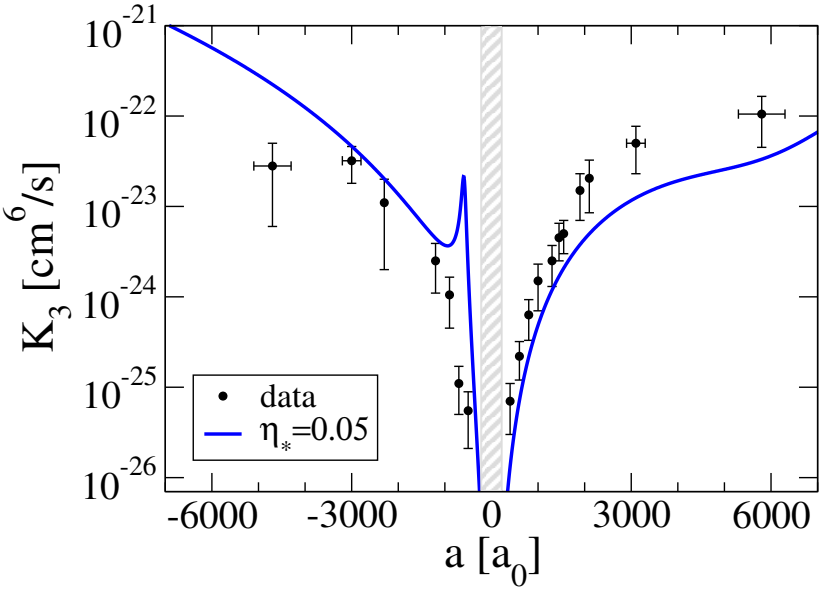

Figure 5.8: The recombination rate $K_3 = 2\alpha$ as function of a for the ^{40}K-^{87}Rb-^{87}Rb system assuming $a_* = 300\,a_0$ and $\eta_* = 0.05$. The shaded grey area indicates the region that lies outside the range of validity of the universal theory. More details are given in the text. The data points and errors are read off from Ref. [Zi$^+$08].

features are due to Efimov resonances, one can extract the ratio $a_*/|a_-| = 2.7$ from the Florence experiment, whereas our theory predicts $a_*/|a_-| = 0.52$. The discrepancy can be attributed to the effective range corrections. In particular, one should be careful with the feature at $a = -246\,a_0$, which is not too large compared to the van der Waals length. Besides, if we believe in the "rescattering" nature of the positive-a resonance, one should take into account a finite-energy shift of the position of the atom-dimer scattering resonance. Indeed, even at zero temperature, dimers formed by three-body recombination collide with stationary Rb atoms at the finite collision energy $[m_{\rm Rb}^2/(m_{\rm K} + 2m_{\rm Rb})^2]\,E_{\rm D} \approx 0.16\,E_{\rm D}$. In Fig. 5.6, we have shown numerical results for β for energies from the scattering threshold, $E = -E_{\rm D}$, up to the breakup threshold, $E = 0$, using $\eta_* = 0.1$ and $\delta = 0.471$ corresponding to the K-Rb-Rb resonance at $a = 667\,a_0$. At $E = 0$, the resonance peak is only 7% higher than the minimum value of β and the resonance is almost completely washed out. Moreover, the peak value of β at $E = 0$ is a factor of 300 smaller than at $E = -E_{\rm D}$. Of course, the explicit numbers depend on the value of η_*, but one should not exclude the possibility of other explanations of this positive-a feature.

Aside from detecting the positions of the resonances, it is desirable to compare the actual shapes of the a-dependence of the loss rate with the theoretical predictions, especially on the positive side of the resonance, where $\alpha_{\rm s} + \alpha_{\rm d}$ is rather smooth. So far, the three-body recombination rate in the ^{87}Rb-^{41}K mixture has been measured for two values of $a < 0$ [Ba$^+$09, Mi], and the comparison with our calculation is rather inconclusive. Figure 5.9 shows $\alpha_{\rm d}$ for the K-Rb-Rb resonance at $a = -246\,a_0$ where only the recombination into deep dimers can occur. The dashed blue curve is calculated using the value $\eta_* = 0.12$ suggested in Ref. [Ba$^+$09]. The data point close to the resonance is taken from Ref. [Ba$^+$09], whereas the one farther away from the resonance gives an upper limit of the recombination rate [Mi]. In order to illustrate

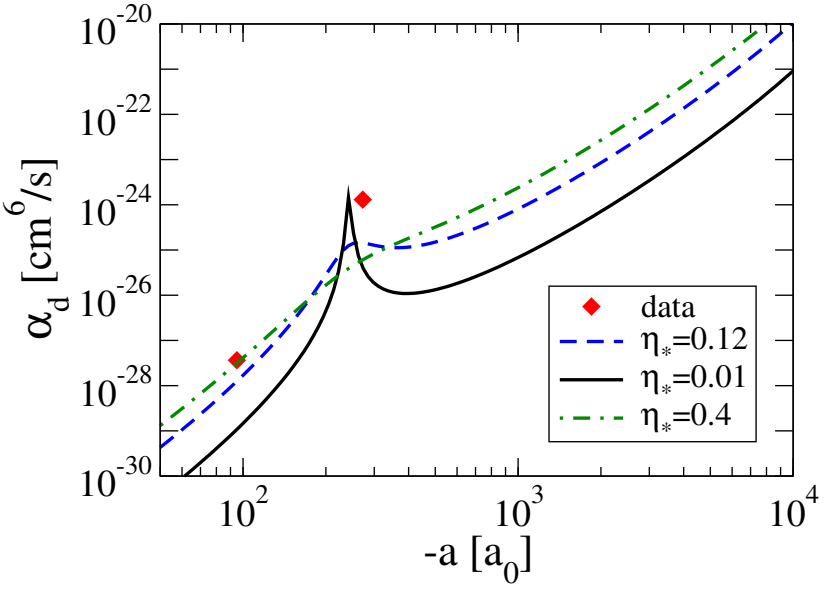

Figure 5.9: The recombination rate α_d as a function of a for the ^{41}K-^{87}Rb-^{87}Rb system assuming $a_- = -246\,a_0$ and three values of η_*: $\eta_* = 0.12$ (dashed blue line), $\eta_* = 0.01$ (solid black line), and $\eta_* = 0.4$ (dash-dotted green line). Data points indicated by diamonds are taken from Refs. [Ba$^+$09, Mi]; see text.

the sensitivity of the result to η_*, we also show curves for $\eta_* = 0.01$ (solid black line) and $\eta_* = 0.4$ (dash-dotted green line). The discrepancy between the measured recombination rate at the resonance and our result for $\eta_* = 0.12$ is about one order of magnitude. In order to understand its origin, more measurements around the resonance position are required. Such data would allow for a more precise determination of the width parameter η_* and of the resonance shape predicted by the universal theory.

5.3.3 Future Experiments

A mixture with nearly the same mass ratio as the two already mentioned experiments is currently investigated in Düsseldorf: ^{87}Rb-$^{174/176}$Yb. They already succeeded in creating heteronuclear molecules [Ne$^+$09] and ultracold mixtures of the two species [Ta$^+$10]. However, further cooling seems to be necessary for measuring the Efimov effect. The Tübingen group of Zimmermann recently studied the ^{7}Li-^{87}Rb and ^{6}Li-^{87}Rb mixtures. They identified and quantified several interspecies Feshbach resonances in both of them [Ma$^+$09, DMZC08] and have reached quantum degeneracy [Si$^+$05]. These mixtures are characterized by rather small mass ratios and, therefore, small scaling factors, which is favorable for observing the discrete scaling invariance. Another very good candidate for studying the Efimov effect with even smaller scaling factors is a mixture of ^{133}Cs with either isotope of lithium (the ^{7}Li-^{133}Cs mixture was created in Heidelberg [De$^+$08]). The smallest mass ratio within reach is $\delta = 0.034$ for ^{6}Li-$^{174/176}$Yb. This heteronuclear system is investigated in Japan [Har$^+$11] and Seattle [Iv$^+$11, Han$^+$11] at the moment and both groups have already reached quantum degeneracy. As soon as the interspecies Feshbach resonances are mapped out, a search for Efimov features can begin. The universal parameters for all of the mentioned mixtures can be

found in Table 5.1. Predictions for the three-body recombination and atom-dimer relaxation rates can be obtained from Eqs. (5.12), (5.16), (5.20), (5.23), and (5.25).

5.4 Summary and Conclusions

In this chapter, we have calculated the three-body loss rates in heteronuclear mixtures of atoms for the case of large scattering length between the unlike atoms. We have analyzed this problem using an effective field theory framework.

We have formulated a universal EFT for this system and derived momentum-space integral equations for the trimer energies and the atom-dimer scattering amplitude. From an analysis of the bound-state equation we have calculated the ratio of the resonance positions $a_*/|a_-|$ as a function of the mass ratio δ. Moreover, we have calculated the three-body recombination and atom-dimer relaxation rates numerically. We have provided semianalytical expressions for the rate constants of three-body recombination into shallow and deep dimers as a function of the interspecies scattering length a and the Efimov width parameter η_*. Furthermore, we have calculated the atom-dimer relaxation constant from the scattering threshold at $E = -E_\mathrm{D}$ up to the dimer breakup threshold at $E = 0$. We find excellent agreement of our numerical results from the momentum-space integral equations with the expressions derived analytically from configuration space in [HHP10].

The expressions in Eqs. (5.12), (5.13), (5.16), and (5.25) fully determine the three-body recombination rates for heteronuclear bosonic mixtures with resonant scattering between the unlike atoms in the universal zero-range theory. The atom-dimer relaxation rates at $E = -E_\mathrm{D}$ and $E = 0$ are given by Eqs. (5.18), (5.20), and (5.23). These equations are universal and can be used to analyze experimental data for any combination of atoms within the range of applicability of the universal theory.

In Ref. [DE06a], D'Incao and Esry give a general functional dependence of the recombination rates on the scattering length for all possible combinations of bosons and fermions. This includes the case of two identical bosons and a third atom with $L = 0$ which we address here. We agree with their expressions for α_d in the case $a < 0$ and for β. For α_s, our general form (5.12) does not agree with their result. The proportionality of α_s to $\sin^2(s_0 \ln a + \phi_3)$ where ϕ_3 is a short-range phase [DE06a, DE06b] emerges only if $\exp(2\pi s_0) \gg 1$ and the expression (5.12) can be simplified (cf. Ref. [BH06]). This is the case for small mass ratios δ. Moreover, our prediction for the dependence of α_s on δ (see Eqs. (5.12) and (5.13)) differs from the result $\alpha_s \propto [\delta(2+\delta)]^{3/2} a^4/(1+\delta)^2/m_1$ obtained in Ref. [DE06a].

We have applied our results to some heteronuclear mixtures in ongoing and planned experiments. We find good agreement between theory and the JILA experiment [Zi$^+$08] that investigated ^{40}K-^{87}Rb molecules and their stability in collisions with atoms near a wide heteronuclear Feshbach resonance at $B_0 = 546.7\,\mathrm{G}$. For the recent experiment by the Florence group which uses a mixture of ^{41}K and ^{87}Rb atoms [Ba$^+$09], we observe moderate discrepancies between theory and experiment. We obtain $a_*/|a_-| = 0.52$ for the resonance positions while the experimental ratio is $a_*/|a_-| = 2.7$. Because neither the effective range corrections nor the experimental errors of the ratio are known accurately, no definite conclusion can be

drawn at the moment. In particular, our analysis of atom-dimer relaxation suggests that explanations should be considered other than an Efimov resonance for the feature at $a = 667\,a_0$ that was used to extract the value of a_*.

Using the value $\eta_* = 0.12$ extracted in Ref. [Ba$^+$09], we find that the calculated recombination rate at the resonance is about one order of magnitude too small. Using smaller values of η_*, the size of the experimental rate can be reproduced. In order to resolve this discrepancy, more measurements around the resonance position are required. Currently, there are only two data points and η_* cannot be determined accurately. Additional data would allow for a more precise determination of η_* and allow for a test of the resonance shape predicted by the universal theory.

Finally, we have calculated the universal parameters determining the three-body loss rates for various other mixtures and have summarized them in Table 5.1. Extending earlier work by D'Incao and Esry [DE06a, DE06b], our predictions lay the theoretical groundwork for the experimental observation of Efimov physics in heteronuclear mixtures. They should be useful for planning and analyzing future experiments.

Chapter 6

Heteronuclear Systems – Fermions and Higher Angular Momenta

The most prominent case of heteronuclear systems has been demonstrated in the previous chapter and we now turn to the other possibilities. This includes bosons in higher angular momentum channels and all systems where fermions are the majority species. The presented results were previously published in [HH11b].

If the heavy species in a heteronuclear mixture is fermionic, the Efimov effect is only present in a P-wave channel and only if the masses differ by at least a factor of 13.61 [Ef73]. This behavior can be generalized to higher partial waves. The parameters s_L, determining the scaling factor for total angular momentum L, can be estimated by [Ef73]

$$s_L^2 \approx s_0^2 - L(L+1)\,, \tag{6.1}$$

where s_0 characterizes the corresponding scaling factor for zero angular momentum. $s_L^2 \geq 0$ must be fulfilled for the occurrence of the Efimov effect (also see more detailed discussion in section 6.1). The necessary mass ratios for the P-wave case ($L = 1$) could be realized, for example, with ^{6}Li-^{87}Sr, $^{6/7}$Li-^{137}Ba, $^{6/7}$Li-^{167}Er, or $^{6/7}$Li-$^{171/173}$Yb. Higher partial waves would only become accessible if hydrogen or helium atoms can be used. Dimer-dimer scattering in heteronuclear mixtures showing a P-wave Efimov effect was investigated in [MKSP08].

The main focus of this chapter is also on such mixtures prepared as atom-dimer systems. We study in detail how the Efimov effect in higher partial waves affects observables such as atom-dimer scattering and atom-dimer relaxation. We briefly introduce our effective field theory framework and derive analytical expressions for the elastic and inelastic atom-dimer scattering cross sections at the dimer breakup threshold. For the P-wave case, we numerically calculate the atom-dimer scattering cross sections and relaxation rates as a function of the scattering length, three-body parameter, and mass ratio away from threshold. Finally, some quantities for systems without the Efimov effect are also computed.

	^{87}Sr	^{137}Ba	^{167}Er	^{171}Yb	^{173}Yb
^{6}Li	14.5	22.8	27.8	28.5	28.8
^{7}Li	-	19.6	23.9	24.4	24.7

Table 6.1: Mass ratios δ^{-1} for possible experimental mixtures showing the P-wave Efimov effect.

6.1 Framework

In the following, we investigate various heteronuclear atomic systems in detail and closely follow the formalism and conventions already used in Chapter 5.

We consider systems consisting of two different atomic species, where the occurring trimers, Efimov or non-Efimov, are built of one atom of type 1 and two atoms of type 2. The unlike particles have a resonant S-wave interaction which can be tuned using a Feshbach resonance, whereas the interaction between identical particles can be neglected. The corresponding Lagrangian is given as in Chapter 5 by

$$\begin{aligned}\mathcal{L} &= \Psi_1^\dagger \left(i\partial_t + \frac{\nabla^2}{2m_1} \right) \Psi_1 + \Psi_2^\dagger \left(i\partial_t + \frac{\nabla^2}{2m_2} \right) \Psi_2 \\ &\quad + g_2 d^\dagger d - g_2 \left(d^\dagger \Psi_1 \Psi_2 + \Psi_1^\dagger \Psi_2^\dagger d \right) - \frac{g_3}{4} d^\dagger d \Psi_2^\dagger \Psi_2 + \cdots , \end{aligned} \tag{6.2}$$

where $m_{1/2}$ denotes the mass of particles of species 1 or 2, $g_{2/3}$ are the bare two-body and three-body coupling constants, and d is an auxiliary field for a dimer consisting of particle species 1 and 2. The ellipses represent higher-order terms containing more fields and/or derivatives. As in Chapter 5, we denote the ratio of the masses of particle species 1 and 2 by $\delta \equiv m_1/m_2$. In this study, however, we explicitly focus on higher partial waves with total angular momentum $L > 0$.

Because of symmetry, the Efimov effect can only occur in even angular momentum channels if the two like particles are bosons and in odd angular momentum channels if they are fermions [NFJG01]. In the following, we will refer to the first case as *bosonic* and the second case as *fermionic* for simplicity. The nature of the third particle is not relevant for our purpose. For inverse mass ratios δ^{-1} larger than a critical ratio $\delta_{\mathrm{c},L}^{-1}$, Efimov physics can be observed [Ef73]. At $\delta_{\mathrm{c},L}^{-1}$ and beyond, the angular momentum barrier is overcome by the attractive interaction between unlike particles (cf. Eq. (6.1)). The light particle can be thought of as an exchange particle between the two heavy atoms. In this case, the "fall to the center" phenomenon typical for the Efimov effect can occur. A (hybrid) Born-Oppenheimer description has been used in the limit of a very light particle of species 1 [MKSP08, Ef$^+$09]. In the case of $L = 1$, the mass ratio must satisfy $\delta^{-1} \gtrsim 13.61 = \delta_{\mathrm{c},1}^{-1}$ [Ef73, Pe03]. The D-wave Efimov effect starts at $\delta^{-1} \gtrsim 38.63 = \delta_{\mathrm{c},2}^{-1}$ [Ef73, KM07b] and its observation would always be obscured by the already present S-wave effect. Consequently, the fermionic P-wave case is the only relevant one in cold atom experiments besides the S-wave bosonic case. The mass ratios δ^{-1} for some possible mixtures showing the P-wave Efimov effect are given in Table 6.1.

It is straightforward to derive Feynman rules and to obtain the full dimer propagator from the Lagrangian in Eq. (6.2) (for more details, see Chapter 6 or Appendix A.1). In the three-body system, we obtain an integral equation for the off-shell atom-dimer scattering amplitude $\mathcal{A}_L(p,k;E)$ known as the STM equation [STM57]. The amplitude depends on the relative momenta of the atom and the dimer in the initial state k and in the final state p as well as on the total energy E. All three-body observables can be obtained from this amplitude evaluated in appropriate kinematics. Projecting on total angular momentum L, the equation becomes

$$\begin{aligned}\mathcal{A}_L(p,k;E) &= (\pm 1)\frac{2\pi m_1}{a\mu^2}\frac{1}{pk}(-1)^L Q_L\left(\frac{p^2+k^2-2\mu E}{2pk\mu/m_1}\right)\\ &\quad +(\pm 1)\frac{m_1}{\pi\mu}\int_0^{\Lambda_c} dq\,\frac{q}{p}(-1)^L Q_L\left(\frac{p^2+q^2-2\mu E}{2pq\mu/m_1}\right)\\ &\quad \times\frac{\mathcal{A}_L(q,k;E)}{-1/a+\sqrt{-2\mu(E-q^2/(2\mu_{AD}))}}\,,\end{aligned} \tag{6.3}$$

where the prefactor $+1$ corresponds to the atoms of species 2 being bosons and -1 to fermions. Moreover, $\mu = m_1m_2/(m_1+m_2)$ is the reduced mass of two unlike atoms, $\mu_{AD} = m_2(m_1+m_2)/(m_1+2m_2)$ is the reduced mass of an atom and a dimer, and

$$Q_L(z) = \frac{1}{2}\int_{-1}^{1} dx\,\frac{P_L(x)}{z-x} \tag{6.4}$$

is a Legendre function of the second kind. The log-periodic dependence of the three-body interaction g_3 on the cutoff has been used to absorb the complex three-body parameter into the momentum cutoff Λ_c in Eq. (6.3) [BH04]. The absolute value of the cutoff Λ_c is proportional to the binding momentum of the deepest Efimov state, whereas the complex phase determines the lifetime of the Efimov trimers, $\Lambda_c \propto e^{i\eta_*/s_L}\kappa_*$. Physically, the parameter η_* takes into account the effects of deeply bound dimers which provide decay channels for the Efimov trimers [BH04]. In the channels without the Efimov effect (odd angular momenta for bosons, even angular momenta for fermions, or for $\delta^{-1} < \delta_{c,L}^{-1}$), the absolute value of the momentum cutoff Λ_c can be taken to infinity. The three-body interaction in Eq. (6.2) is higher order in these channels and all observables are to leading order determined by the scattering length alone.

6.2 Scaling Factor and Resonance Positions

If more than one Efimov resonance feature can be measured in an experiment, the scaling factor $\exp(\pi/s_L)$ can be deduced. The quantity s_L can be computed analytically by considering the large momentum behavior of Eq. (6.3) [Da61, BHvK99a, Gr05]. In this limit the energies and inverse scattering lengths can be neglected compared to the momenta p and q, the inhomogeneous term as well as purely polynomial terms in the integral kernel are suppressed, and the momentum integration can be extended to infinity. This leads to the equation

$$\tilde{\mathcal{A}}_L(p) = (\pm 1)(-1)^L\frac{m_1}{\pi\mu}\sqrt{\frac{\mu_{AD}}{\mu}}\int_0^\infty\frac{dq}{q}\,P_L\left(\frac{p^2+q^2}{2pq\mu/m_1}\right)Q_0\left(\frac{p^2+q^2}{2pq\mu/m_1}\right)\tilde{\mathcal{A}}_L(q)\,, \tag{6.5}$$

where we have defined $\tilde{\mathcal{A}}_L(p) \equiv p\mathcal{A}_L(p,k;E)$. Since the equation is scale invariant, it has power law solutions. If the Efimov effect is present, the exponent is complex: $\tilde{\mathcal{A}}_L(p) \propto p^{\pm i s_L}$. Identifying the right hand side of Eq. (6.5) as a Mellin transform, we then obtain a transcendental equation for s_L:

$$\begin{aligned} 1 &= \pm \frac{(-1)^L}{\sin(2\phi)} \sum_{k=0}^{k_{max}} \frac{(2L-2k)!}{(L-k)!\,k!} \frac{(-1)^k}{2^{2L-2k}(\sin\phi)^{L-2k}} \\ &\quad \times \sum_{m=0}^{L-2k} \frac{1}{m!\,(L-2k-m)!} \frac{2}{is_L+2m-L+2k} \frac{\sin\left[(is_L+2m-L+2k)\phi\right]}{\cos\left[(is_L+2m-L+2k)\frac{\pi}{2}\right]}\,, \end{aligned} \tag{6.6}$$

where we defined

$$\phi = \arcsin\frac{1}{\delta+1}\,, \tag{6.7}$$

and

$$k_{max} = \begin{cases} L/2 & \text{if } L \text{ is even} \\ (L-1)/2 & \text{if } L \text{ is odd} \end{cases}\,. \tag{6.8}$$

A few more details on this derivation can be found in Appendix A.3. In the case $L = 1$, Eq. (6.6) reduces to

$$1 = \frac{1}{2\sin^2\phi\cos\phi}\left[\frac{1}{is_1-1}\frac{\sin[(is_1-1)\phi]}{\cos[(is_1-1)\pi/2]} + \frac{1}{is_1+1}\frac{\sin[(is_1+1)\phi]}{\cos[(is_1+1)\pi/2]}\right]. \tag{6.9}$$

The corresponding equation for $L = 2$ is given by

$$\begin{aligned} 1 &= \frac{3}{8\sin^3\phi\cos\phi}\left[\frac{1}{is_2-2}\frac{\sin[(is_2-2)\phi]}{\cos[(is_2-2)\pi/2]} + \frac{1}{is_2+2}\frac{\sin[(is_2+2)\phi]}{\cos[(is_2+2)\pi/2]}\right. \\ &\quad \left. + \frac{2-4/3\sin^2\phi}{is_2}\frac{\sin[is_2\phi]}{\cos[is_2\pi/2]}\right]. \end{aligned} \tag{6.10}$$

An equivalent equation for general L using hypergeometric functions was derived by Nielsen and coworkers [NFJG01]. The results of Eqs. (6.9) and (6.10) coincide with the ones obtained by making use of Eq. (117) in [NFJG01]. The critical mass ratios $\delta_{c,L}$ are obtained by considering the case, when s_L tends to zero. We find $\delta_{c,1}^{-1} = 13.61$ and $\delta_{c,2}^{-1} = 38.63$ in agreement with previous determinations [Pe03, KM07b]. The resulting scaling factors $\exp(\pi/s_L)$ are shown in Fig. 6.1 as a function of the mass ratio $\delta = m_1/m_2$. The critical mass ratios $\delta_{c,1}$ and $\delta_{c,2}$ for $L = 1, 2$ can be read off from the positions where the scaling factor diverges (indicated by the vertical dotted lines). For $L \to \infty$, the critical mass ratio approaches zero. For $\delta \to 0$, all scaling factors approach unity corresponding to the limit $s_L \to \infty$.

Another important observable is the ratio $a_*/|a_-|$, that compares the values of the scattering length a_* and a_- at which Efimov trimers cross the atom-dimer and three-particle thresholds, respectively. This ratio can be measured experimentally if at least one resonance feature is seen for negative scattering length and one in the atom-dimer system. The calculated ratios for $L = 1$ are shown in Fig. 6.2 for following one Efimov state and for comparing neighboring states, both as a function of the mass ratio $\delta = m_1/m_2$.

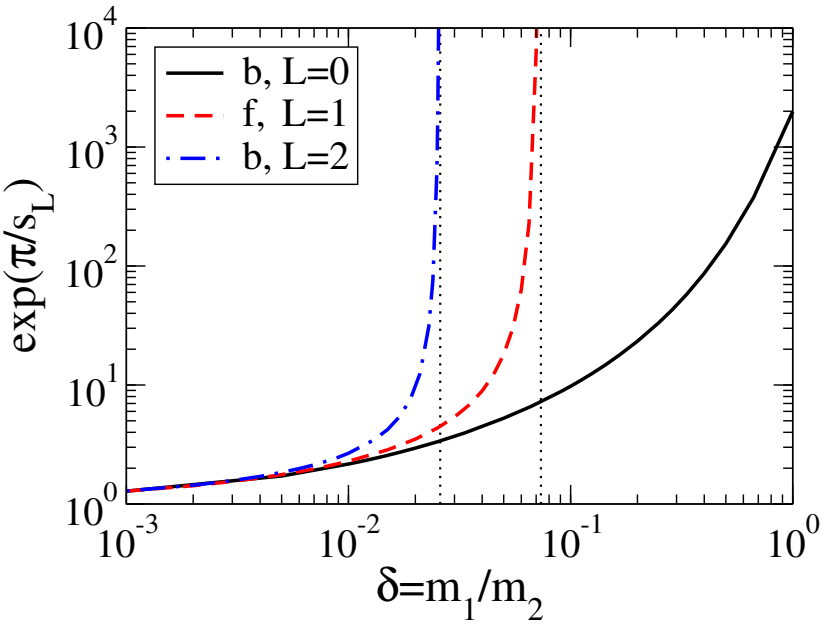

Figure 6.1: Scaling factors $\exp(\pi/s_L)$ for bosons (b) and fermions (f) as a function of the mass ratio $\delta = m_1/m_2$ for $L = 0, 1, 2$, respectively. The vertical dotted lines indicate the critical mass ratios $\delta_{\mathrm{c},1}$ and $\delta_{\mathrm{c},2}$ for the Efimov effect with $L = 1, 2$.

6.3 Analytical Results for Atom-Dimer Scattering

The scattering of atoms and dimers can be directly related to the STM equation (6.3) with equal incoming and outgoing momenta. The scattering amplitude is given by

$$f_L(k) = \frac{k^{2L}}{k^{2L+1}\cot\delta_{\mathrm{AD},L}(k) - ik^{2L+1}} = \frac{\mu_{\mathrm{AD}}}{2\pi}\mathcal{A}_L(k,k;E)\,, \tag{6.11}$$

where the energy E and center-of-mass momentum k are related by $E = k^2/(2\mu_{\mathrm{AD}}) - E_{\mathrm{D}}$. The dimers are built of two unlike particles and their binding energy is given by $E_{\mathrm{D}} = 1/(2\mu a^2)$. The dimer breakup threshold at $E = 0$ corresponds to $k = \sqrt{\mu_{\mathrm{AD}}/\mu}\,/a \equiv k_{\mathrm{br}}$. It is useful to define an energy dependent *scattering length*,

$$\tilde{a}_{\mathrm{AD},L}(k) = \frac{-1}{k^{2L+1}\cot\delta_{\mathrm{AD},L}(k)}\,. \tag{6.12}$$

Note that this quantity does not have the dimension of length for $L > 0$. We can now calculate the elastic atom-dimer scattering cross section in the Lth partial wave

$$\sigma^{(\mathrm{el})}_{\mathrm{AD},L}(k) = (2L+1)\,4\pi\,|f_L(k)|^2\,. \tag{6.13}$$

The total cross section can be obtained with the help of the optical theorem

$$\sigma^{(\mathrm{tot})}_{\mathrm{AD},L}(k) = (2L+1)\,\frac{4\pi}{k}\,\mathrm{Im}f_L(k)\,, \tag{6.14}$$

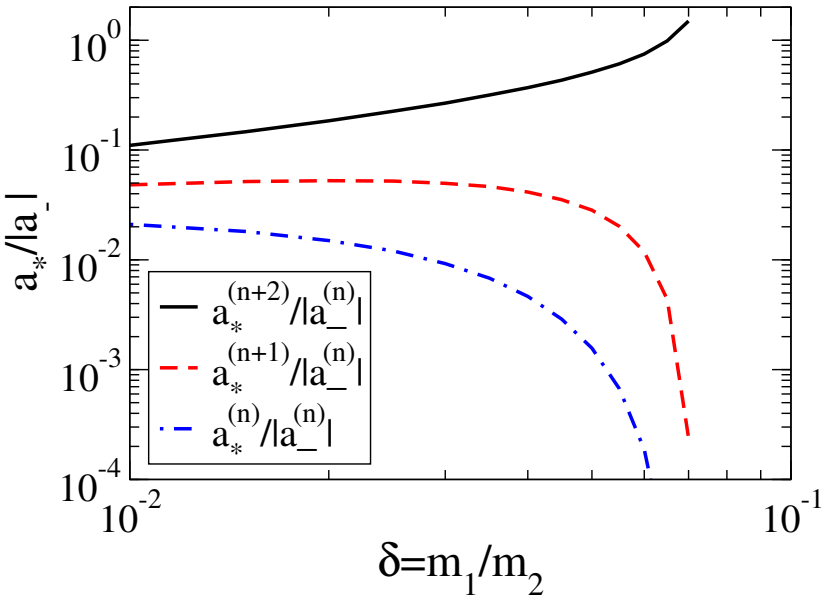

Figure 6.2: The ratio $a_*/|a_-|$ for following one Efimov state and for comparing neighboring states as a function of the mass ratio $\delta = m_1/m_2$ in the case $L = 1$.

and the inelastic cross section $\sigma^{(\mathrm{inel})}_{\mathrm{AD},L}(k)$ by subtracting Eq. (6.13) from Eq. (6.14).

At $E = 0$, it is also possible to deduce these quantities analytically using the methods of Section IV of Ref. [HHP10]. If the Efimov effect is present, the S-matrix element for elastic atom-dimer scattering can be written as

$$S_L = -e^{2i\sigma_L} \cosh(\pi s_L + i s_L \ln(a/a_{0*}) - \eta_*)/\cosh(\pi s_L - i s_L \ln(a/a_{0*}) + \eta_*)\,, \tag{6.15}$$

where σ_L is a real number and a_{0*} determines the position of the minima in the elastic atom-dimer cross section and in the three-body recombination rate for positive scattering length. Hence, the elastic cross section can be expressed as

$$\begin{aligned}\sigma^{(\mathrm{el})}_{\mathrm{AD},L}(E=0) &= (2L+1)\,\frac{\pi}{k_{\mathrm{br}}^2}\,|S_L - 1|^2 \\ &= (2L+1)\,4\pi a^2\,\frac{\delta(\delta+2)}{(\delta+1)^2}\,\frac{\sinh^2(\pi s_L)\left\{\sinh^2(\eta_*) + \sin^2[s_L \ln(a/a_{0*})]\right\}}{\sinh^2(\pi s_L + \eta_*) + \cos^2[s_L \ln(a/a_{0*})]}\,,\end{aligned} \tag{6.16}$$

where $k_{\mathrm{br}} a = (\delta+1)/\sqrt{\delta(\delta+2)}$ was used. The inelastic cross section is given by

$$\begin{aligned}\sigma^{(\mathrm{inel})}_{\mathrm{AD},L}(E=0) &= (2L+1)\,\frac{\pi}{k_{\mathrm{br}}^2}\left(1 - |S_L|^2\right) \\ &= (2L+1)\,\pi a^2\,\frac{\delta(\delta+2)}{(\delta+1)^2}\,\frac{\sinh(2\pi s_L)\sinh(2\eta_*)}{\sinh^2(\pi s_L + \eta_*) + \cos^2[s_L \ln(a/a_{0*})]}\,.\end{aligned} \tag{6.17}$$

Atom-dimer relaxation is the process where an atom and a shallow dimer collide and an energetic deep dimer and atom are ejected. It is one of the main loss processes in mixtures of

atoms and dimers. The atom-dimer relaxation rate constant β is defined by the rate equation

$$\frac{d}{dt}n_{\rm D} = \frac{d}{dt}n_{\rm A} = -\beta\, n_{\rm D}\, n_{\rm A}\,, \tag{6.18}$$

where $n_{\rm A/D}$ denotes the number densities of atoms and dimers, respectively. The relaxation rate is directly related to the inelastic scattering cross section,

$$\beta_L(E) = \frac{k}{\mu_{\rm AD}}\,\sigma^{\rm (inel)}_{{\rm AD},L}(E)\,. \tag{6.19}$$

At $E = 0$, we therefore obtain

$$\beta_L(E=0) = (2L+1)\,\pi\,\frac{\sqrt{\delta(\delta+2)}^3}{(\delta+1)^2}\,\frac{\sinh(2\pi s_L)\sinh(2\eta_*)}{\sinh^2(\pi s_L+\eta_*)+\cos^2[s_L\ln(a/a_{0*})]}\,\frac{\hbar a}{m_1}\,. \tag{6.20}$$

At the atom-dimer threshold, $E = -E_{\rm D}$, only the S-wave contribution survives. This case was studied in detail in the previous chapter. For all other angular momenta $L > 0$, the atom-dimer scattering amplitude, Eq. (6.11), vanishes for $k \to 0$.

Another important process in cold atom experiments is three-body recombination. This process can happen in a mixture, as long as some atoms of species 1 are not bound in dimers. The atom of species 1 and an atom of species 2 form a dimer, shallow or deep, and another atom of species 2 balances energy and momentum. Typically, all three atoms are lost if this process occurs in a trap. For angular momenta $L > 0$, however, the three-body recombination rate vanishes at $E = 0$.

In the following, we present numerical results for the atom-dimer observables discussed above focusing on the experimentally most relevant case $L = 1$.

6.4 Numerical Results

6.4.1 Atom-Dimer Observables Without Efimov Effect

In this subsection, we only consider the case $\eta_* = 0$ which corresponds to no deeply bound dimers. As a consequence, the inelastic cross section vanishes below the dimer breakup threshold. In the P-wave channel, there is no Efimov effect for bosons. The total (=elastic) atom-dimer scattering cross section for $E = 0$ (at dimer breakup) is shown as the solid black line in Fig. 6.3. Note that for increasing δ^{-1}, the cross section does not tend monotonically to zero but rather oscillates with diminishing amplitude. This oscillation is not due to the crossing of bound three-body states with the atom-dimer threshold as three-body bound states are not present in this system (see below for the fermionic case). Using Eq. (6.13), the elastic cross section at threshold can be written as

$$\sigma^{\rm (el)}_{{\rm AD},L}(k_{\rm br}) = (2L+1)\,4\pi\,a^2\,\frac{(1+2\delta^{-1})}{(1+\delta^{-1})^2}\,\sin^2\delta_{{\rm AD},L}(k_{\rm br})\,. \tag{6.21}$$

The observed oscillation then implies a monotonic dependence of the elastic phase shift at threshold on δ^{-1} [KM07a] with $\delta_{{\rm AD},L}(k_{\rm br}) = 0$ for $\delta^{-1} = 0$. For decreasing energy, the

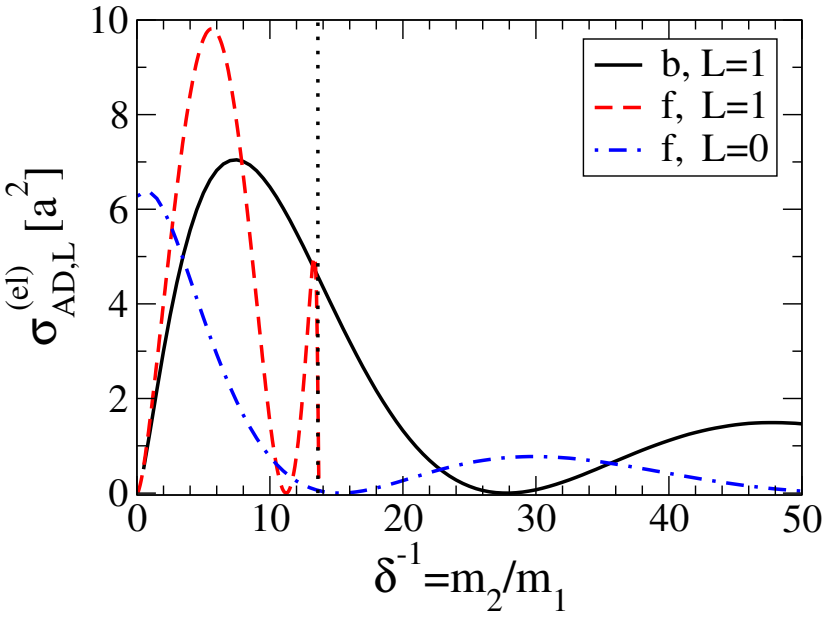

Figure 6.3: The elastic atom-dimer scattering cross sections for bosons (b) and fermions (f) in the P-wave channel and for fermions in the S-wave channel at $E = 0$ as a function of the mass ratio δ^{-1}. The vertical dotted line indicates the critical mass ratio for fermions in the P-wave channel, $\delta^{-1}_{c,1} = 13.61$.

amplitude of the cross section gets larger and the peaks move toward larger mass ratios δ^{-1}.

A similar behavior is observed for fermions in the S-wave channel. The atom-dimer scattering length can be determined according to the formula $a_{AD,0} = -\mathcal{A}_0(0,0;-E_D)\mu_{AD}/(2\pi)$. This reproduces the results for the mass dependence found by Petrov [Pe03] that were confirmed in Refs. [IS08, Is10]. The corresponding total cross section is shown in Fig. 6.3 as the dash-dotted blue line. Again, the oscillation is not due to bound states and Eq. (6.21) implies a monotonic dependence of the threshold phase shift on δ^{-1}. However, in this case $\delta_{AD,L}(k_{br})$ approaches a value slightly below $\pi/2$ for $\delta^{-1} = 0$. As in the case of bosons with $L = 1$, we find that the amplitude of the cross section gets larger for decreasing energy and the peaks move toward larger mass ratios δ^{-1}.

For fermions in the P-wave channel, the Efimov effect only comes into play for mass ratios $\delta^{-1} \gtrsim 13.61$. For the region without the Efimov effect, many observables have already been calculated [PSS04, PSS05, KM07a, LTWP09, LP11, ENU11]. Kartavtsev and Malykh found one three-body bound state for the range $8.17260 < \delta^{-1} < 12.91743$ and two three-body bound states for $12.91743 < \delta^{-1} < 13.6069657$ [KM07a]. They call these states *universal*, as their binding energies only depend on the dimer binding energy, or equivalently, the scattering length. The occurrence of these states was recently confirmed by Endo et al. [ENU11]. They also demonstrated the divergence of the atom-dimer scattering length at the mass ratios where the universal trimer states appear and how similar behavior occurs for higher angular momenta. We have confirmed these results. Kartavtsev and Malykh also found

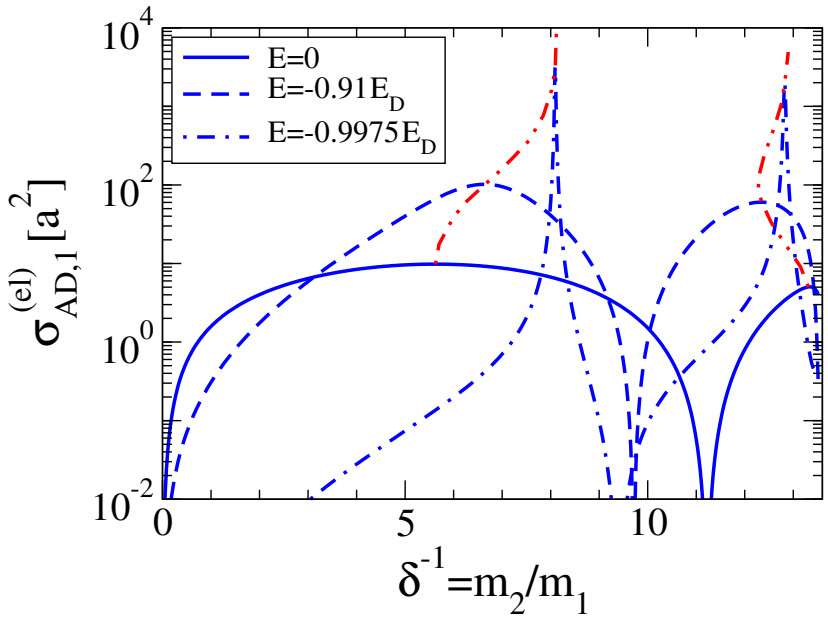

Figure 6.4: The elastic cross section $\sigma^{(\mathrm{el})}_{\mathrm{AD},1}$ in units of a^2 vs. the mass ratio δ^{-1} at the energies $E = 0, -0.91\,E_{\mathrm{D}},$ and $-0.9975\,E_{\mathrm{D}}$ (blue solid, dashed, dash-dotted lines). The red dash-double-dotted lines indicate the position of the two peaks for varying energy.

that close to the critical mass ratio, the energies of the universal states follow a square-root dependence [KM07a], $E - E_{\mathrm{c}} \propto \sqrt{\delta_{\mathrm{c},1}^{-1} - \delta^{-1}}$. An investigation of the behavior of Efimov states for δ^{-1} slightly above $\delta_{\mathrm{c},1}^{-1}$ would be interesting. The behavior of the energies must be non-analytic in $\delta^{-1} - \delta_{\mathrm{c},1}^{-1}$, since Efimov states can be shifted to any desired energy by adjusting the three-body parameter. However, such a study is beyond the scope of the present investigation as our numerical calculations converge only slowly close to the critical mass ratio.

In Ref. [KM07a], atom-dimer elastic scattering at the dimer breakup threshold was also calculated. We show this process as the dashed red line in Fig. 6.3 in comparison to the results for bosons with $L = 1$ and for fermions with $L = 0$. In order to elucidate the physics of the two peaks in the elastic cross section, we show our results for $\sigma^{(\mathrm{el})}_{\mathrm{AD},1}$ in Fig. 6.4 as a function of δ^{-1} for three energies, $E = 0, -0.91\,E_{\mathrm{D}},$ and $-0.9975\,E_{\mathrm{D}}$, i.e., at and below the dimer breakup threshold. The dash-double-dotted red lines show how the peak positions move with varying energy. While the first peak moves monotonically to larger values of δ^{-1} as the energy is decreased, the second peak shows a more complicated behavior. Initially, it moves to smaller values and reaches a minimum $\delta_{\mathrm{min}}^{-1} \approx 12.3$ for $E/E_{\mathrm{D}} \approx -0.938$, before it moves back to larger values of δ^{-1} as the atom-dimer threshold is approached. Our results demonstrate that the two-peak structure is indeed due to the presence of the two universal three-body bound states. The positions of the two peaks move from $\delta^{-1} = 5.63$ and 13.31 at $E = 0$ to two sharp, δ-function like peaks at $\delta^{-1} = 8.17$ and 12.9 for $E = -0.9999\,E_{\mathrm{D}}$, which are the critical values for the occurrence of the three-body bound states.

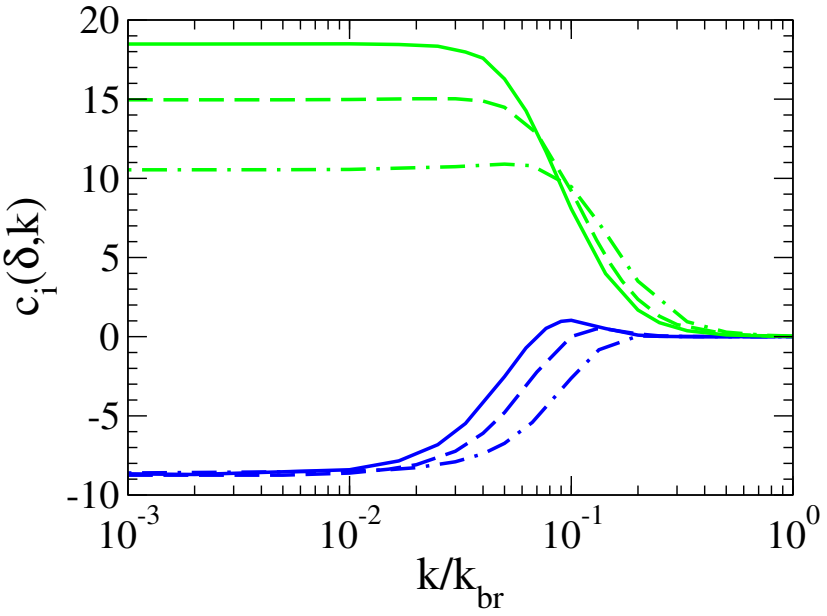

Figure 6.5: Coefficients $c_1(\delta, k)$ (blue) and $c_2(\delta, k)$ (green) as a function of $k/k_{\rm br}$ for mass ratios $\delta = 0.03,\ 0.04,$ and 0.06 indicated by the solid, dashed, and dash-dotted lines, respectively.

6.4.2 Atom-Dimer Observables With Efimov Effect

In the presence of the Efimov effect, the observables do not only depend on the mass ratio and the energy, but they also depend log-periodically on the scattering length. From now on, we focus on the case of fermions with $L = 1$. We omit the additional subscript 1 indicating the P-wave channel for notational simplicity. We find the energy-dependent atom-dimer scattering length for $\delta^{-1} > 13.61$ calculated with Eq. (6.12) to be very well approximated by the formula

$$\tilde{a}_{\rm AD}(\delta, k, a) \equiv \frac{-1}{k^3 \cot \delta_{\rm AD}(\delta, k, a)} = \Big\{ c_1(\delta, k) + c_2(\delta, k) \cot\big[s_1 \ln(a/a_*) + i\eta_* \big] \Big\} a^3 \,. \qquad (6.22)$$

We show $c_{1/2}(\delta, k)$ in Fig. 6.5 for the mass ratios $\delta = 0.03, 0.04,$ and 0.06 as functions of the momentum in units of the breakup momentum $k_{\rm br}$ from $0.001\, k_{\rm br}$ up to the dimer breakup threshold. Interestingly, for all considered mass ratios, $c_1(\delta, k) = -8.7 \pm 0.2$ for $k \to 0$. The coefficient $c_2(\delta, k)$ also approaches constant values in this limit but this value depends on the mass ratio: the smaller δ, the larger this approached value.

At the dimer breakup threshold, we find

$$c_2(\delta, k_{\rm br}) \approx k_{\rm br}^{-3} \qquad \text{and} \qquad c_1(\delta, k_{\rm br}) \approx 0 \qquad (6.23)$$

to be very good approximations for $\delta \lesssim 0.06$. This behavior is similar to the case of spinless bosons [BH06]. From Eq. (6.15), we can deduce the atom-dimer scattering phase shift $\delta_{\rm AD}$ at $E = 0$. For $\exp(2\pi s_1) \gg \exp(\pm 2\eta_*)$, the expression simplifies to

$$\delta_{\rm AD} = \sigma_1 + s_1 \ln(a/a_{0*}) + i\eta_* \,, \qquad (6.24)$$

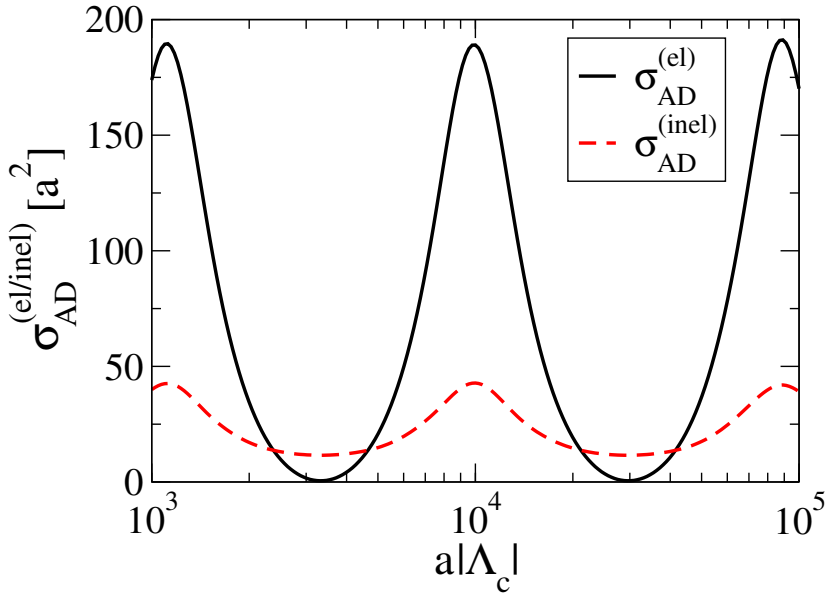

Figure 6.6: Elastic (solid black line) and inelastic (dashed red line) atom-dimer scattering cross sections in units of a^2 for $\delta = 0.04$, $\eta_* = 0.1$, and $E = -0.99\,E_\mathrm{D}$ vs. $a|\Lambda_\mathrm{c}|$.

and the constraints (6.23) follow from Eq. (6.22). Since s_1 approaches 0 as $\delta \to \delta_{\mathrm{c},1} = 0.07349$ from below, this approximation is invalid at larger mass ratios. In this case, we find that $c_1(\delta, k_\mathrm{br})$ tends to slightly larger and $c_2(\delta, k_\mathrm{br})$ to slightly smaller values.

The elastic and inelastic atom-dimer scattering cross sections show the typical log-periodic dependence on the scattering length. For general momenta, they can be approximated with Eqs. (6.11)–(6.14), (6.22), and the appropriate coefficients from Fig. 6.5. At $E = 0$, we can compare our numerical calculation to the analytical formulae in Eqs. (6.16) and (6.17). For $\sigma_\mathrm{AD}^{(\mathrm{inel})}(k_\mathrm{br})$, which shows only a weak dependence on a, we find generally good agreement. For the elastic cross section $\sigma_\mathrm{AD}^{(\mathrm{el})}(k_\mathrm{br})$, we find very good agreement in the region $\delta \lesssim 0.06$. For larger δ, the numerical calculation becomes difficult, because of the large scaling factor.

As an example, we show the elastic and inelastic cross sections for $\delta = 0.04$, $\eta_* = 0.1$, and $E = -0.99\,E_\mathrm{D}$ in Fig. 6.6. This mass ratio δ roughly corresponds to the mixtures ^{7}Li-$^{171/173}$Yb. The cross sections show the typical log-periodic dependence on the scattering length. The values of the maximal and minimal cross section depend strongly on the energy and vary over several orders of magnitude. To demonstrate this dependence, we show the maximal and minimal values of $\sigma_\mathrm{AD}^{(\mathrm{el})}$ as a function of the center-of-mass momentum k/k_br for $\delta = 0.03$, 0.06 and $\eta_* = 0.2$ in Fig. 6.7.

The atom-dimer relaxation rate β which can be measured in cold atom experiments is determined by the inelastic cross section via Eq. (6.19). In the case of P-waves, β vanishes at the atom-dimer threshold $E = -E_\mathrm{D}$. In Fig. 6.8, we show β for $\delta = 0.04$, $\eta_* = 0.1$, above threshold for $E = -0.9999\,E_\mathrm{D}, -0.9984\,E_\mathrm{D}, -0.96\,E_\mathrm{D}$, and 0. We also give the positions of the peak in β for varying energy. The relaxation rate β shows a strong energy dependence as well. Starting from being zero at the atom-dimer threshold, it develops resonant log-periodic

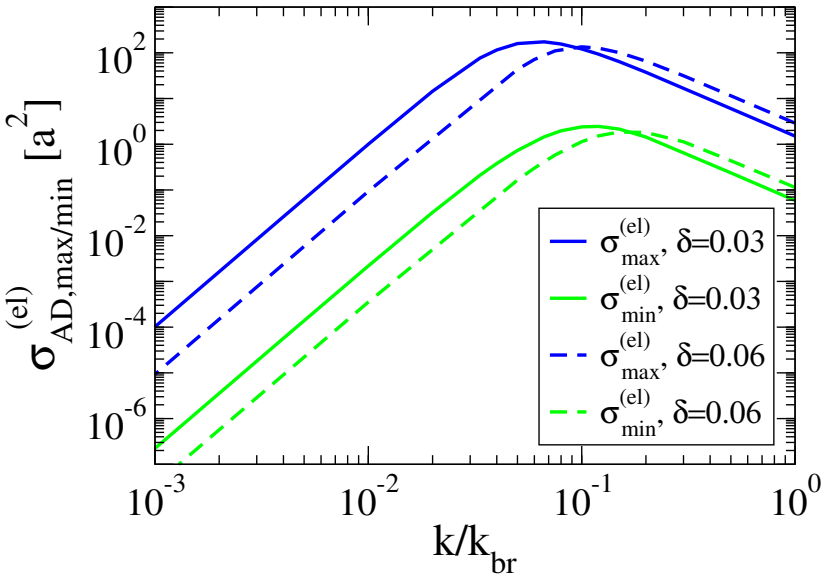

Figure 6.7: Maximal (blue) and minimal (green) values of $\sigma^{(\mathrm{el})}_{\mathrm{AD}}(k)$ as a function of k/k_{br} for $\delta = 0.03$ (solid lines), $\delta = 0.06$ (dashed lines) and $\eta_* = 0.2$.

structures for larger energies which become less pronounced as the dimer breakup threshold is approached. The peak position is also strongly energy dependent and varies by a factor of five.

6.5 Summary and Outlook

In this chapter, we have investigated the Efimov effect for heteronuclear systems of two identical particles and a third distinguishable particle in higher partial waves. The unlike particles were assumed to have resonant S-wave interactions while the interaction between like particles was neglected. For even (odd) angular momentum L, the two identical particles must be bosons (fermions) for the Efimov effect to occur [Ef73]. Using an effective field theory framework, we have derived a generalized STM equation which describes the off-shell atom-dimer scattering amplitude in the total angular momentum channel L. All three-body observables can be extracted from this amplitude, when taken in appropriate kinematics.

We have derived a transcendental equation for the preferred scaling factor $\exp(\pi/s_L)$ for arbitrary L as a function of the mass ratio δ. The numerical results agree well with a previously derived equation using hypergeometric functions derived by Nielsen and coworkers [NFJG01]. For the experimentally most relevant case of the P-wave Efimov effect, we have predicted the ratio of the scattering lengths where Efimov states cross the atom-dimer and three-atom thresholds $a_*/|a_-|$. This ratio is independent of the three-body parameter and can be measured in experiment. For the S-wave case, Barontini et al. [Ba$^+$09] have measured the value $a_*/|a_-| = 2.7$ in a K-Rb mixture. The universal prediction for this system is $a_*/|a_-| = 0.52$. The discrepancy between the two values is at least partly due to effective range corrections

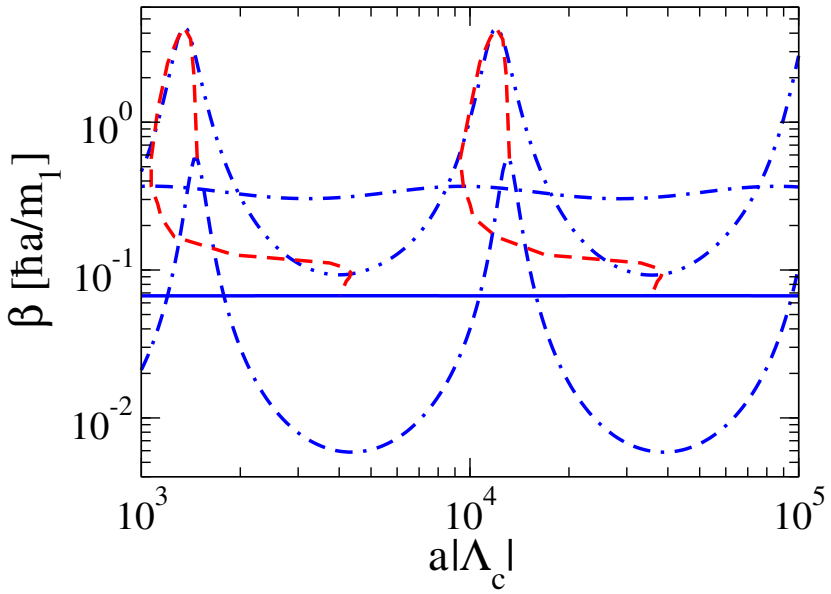

Figure 6.8: Dimer relaxation rate β in units of $\hbar a/m_1$ for $\delta = 0.04$ and $\eta_* = 0.1$ vs. $a|\Lambda_c|$. The blue double-dash-dotted, dash-double-dotted, dash-dotted, and solid lines correspond to the energies $E = -0.9999\,E_D$, $-0.9984\,E_D$, $-0.96\,E_D$, and 0, respectively. The dashed red lines show how the peak position shifts with the energy.

but there is also a finite energy shift of the rescattering resonance for negative scattering length that needs to be taken into account, see Chapter 5. For P-waves, no experiment has been carried out to date.

The measurement of atom loss rates has played a key role for the observation of the S-wave Efimov effect in cold atoms [FG10] and the P-wave Efimov effect in a Bose-Fermi mixture could be detected in an analogous way. We have derived analytical expressions for the elastic and inelastic atom-dimer cross sections as well as the atom-dimer relaxation rate for arbitrary angular momentum L at the dimer breakup threshold. For energies away from the threshold, we have laid out a framework to calculate these quantities numerically.

Using this framework, we have explicitly calculated the atom-dimer scattering cross sections for $E_D < E \leq 0$ in low angular momentum channels without the Efimov effect, i.e., bosons in the P-wave and fermions in the S-Wave channel. Furthermore, we have calculated the cross section for fermions in the P-wave channel below the critical mass ratio $\delta_{c,1}^{-1}$. The cross section shows two peaks due to the appearance of two non-Efimov three-body bound states [KM07a]. We have calculated the position of these peaks as a function of the collision energy E.

Focusing on the P-wave fermionic channel above the critical mass ratio, we have numerically calculated the atom-dimer cross section up to the dimer breakup threshold. The cross sections show the typical log-periodic dependence on the scattering length. The maximal and minimal cross section values depend strongly on the energy, varying over several orders of magnitude. At the atom-dimer threshold, we found good agreement with our analytical results. The atom-dimer cross section below the dimer breakup threshold can be parametrized by two universal

functions $c_1(\delta, k)$ and $c_2(\delta, k)$. We have calculated these functions for several mass ratios and derived simple analytical expressions for their values at the dimer breakup threshold as long as $\exp(2\pi s_1) \gg \exp(\pm 2\eta_*)$ is satisfied. Finally, we have numerically calculated the atom-dimer relaxation rate β as a function of the three-body parameter, mass ratio and energy. As for the bosonic case in the previous chapter, the position of the relaxation maxima is strongly energy dependent and not a monotonic function of energy.

In summary, our calculation provides a basis for interpreting experimental results on the Efimov effect in higher partial waves. Due to the fermionic nature of the dimers, the preparation of the required atom-dimer mixture for the P-wave case should be feasible. A few experimental groups already study heteronuclear mixtures of interest to this work, e.g., various Yb-Li mixtures in the groups of Takahashi [Har$^+$11] and Gupta [Han$^+$11]. Other groups are investigating heavy species that could be mixed with Li, e.g., fermionic Sr in Grimm's group [TSGS10]. A natural extension of this topic would be to calculate the three-body recombination rate for energies away from the dimer breakup threshold. This could, in principle, be done using the methods of Ref. [BHKP08] and Chapter 4.

Note that very recently a study was published considering heteronuclear trimers in fermionic systems close to a narrow Feshbach resonance [CT11]. Their results seem to agree with our findings where a comparison is possible.

Chapter 7

Two-Dimensional Systems

This chapter differs in two respects from the preceding ones. First, we consider a two-dimensional ($2D$) Bose system where the Efimov effect cannot occur [BT79, NFJ99]. Furthermore, effective range effects are included in the calculations, which are accordingly valid up to next-to-leading order. However, the bosons still interact resonantly and we can make use of effective field theory methods similar to those described earlier. This chapter has been published as [HH11a].

We start with a short introduction on $2D$ systems and then describe the EFT method in detail. It is subsequently used to derive three-body observables such as binding energies and atom-dimer scattering properties. We end with a summary and conclusion.

7.1 Introduction

We have already seen examples of how ultracold quantum gases have become a versatile tool to investigate few- and many-body phenomena in strongly interacting quantum systems. The possibility of using optical lattices also makes them interesting for the simulation of condensed matter problems such as the Hubbard model [Es10]. Special trap geometries allow for the creation of lower-dimensional systems. These systems can, for example, help to understand high-temperature superconductivity, which is a $2D$ problem. Moreover, $2D$ systems are interesting on their own, since their behavior can be qualitatively different $3D$ systems.

Here, we concentrate on the description of few-body phenomena in an expansion around the unitary limit. This limit refers to an idealized system where the range of the interaction is taken to zero and the scattering length a is infinite. To leading order in this expansion, the low-energy observables are universal. They are determined by the scattering length a of the particles alone. The leading non-universal corrections are due to the effective range of the interaction. We focus on these corrections. Since there is no Efimov effect [Ef70] in two dimensions [BT79, NFJ99], three-body interactions are suppressed and enter only at higher orders.

The definition of the scattering length a in $2D$ is ambiguous since $\cot\delta$ diverges logarithmically as the wave number k approaches zero and different conventions are used in the

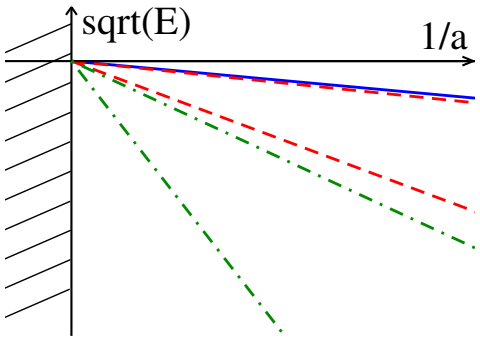

Figure 7.1: Spectrum of universal two-, three-, and four-body states in two spatial dimensions as a function of the inverse scattering length $1/a$.

literature. We follow the conventions of Verhaar et al. [VdGVvdE84], in which the effective range expansion of the scattering phase shift is given by

$$\cot\delta(k) = \frac{2}{\pi}\left\{\gamma_{\rm E} + \ln\left(\frac{ka}{2}\right)\right\} + \frac{r^2}{2\pi}k^2 + \mathcal{O}(k^4)\,, \tag{7.1}$$

where $\gamma_{\rm E} \simeq 0.577216$ is the Euler-Mascheroni constant. Note that the scattering length in two dimensions is always positive.

In the limit $a \gg |r|$, the binding energy of the shallow dimer is universal,

$$E_{\rm D} = 4e^{-2\gamma_{\rm E}}\,\frac{\hbar^2}{ma^2} + \mathcal{O}(r^2/a^2)\,. \tag{7.2}$$

The binding energies of three- and four-body states in this limit have been calculated by various groups and are also universal [BT79, NFJ99, HS04, PHM04, Br$^+$06, KM06]. Since there is no other parameter in the problem, the energies must be multiples of the dimer energy. There are two three-body bound states, which were first calculated by Bruch and Tjon [BT79]. Their binding energies are [HS04]

$$E_{\rm T}^{(1)} = 1.2704091(1)\,E_{\rm D} \quad \text{and} \quad E_{\rm T}^{(0)} = 16.522688(1)\,E_{\rm D}\,, \tag{7.3}$$

where the number in parentheses indicates the numerical error in the last quoted digit. The first calculation of four-body bound states in $2D$ was carried out by Platter et al. [PHM04]. They also found two universal bound states with binding energies

$$E_4^{(1)} = 25.5(1)\,E_{\rm D} \quad \text{and} \quad E_4^{(0)} = 197.3(1)\,E_{\rm D}\,. \tag{7.4}$$

These results were later confirmed in Ref. [Br$^+$06]. In Fig. 7.1, we illustrate the scattering length dependence of this spectrum. The universal few-body states do not cross the continuum threshold $E = 0$ for any finite value of the scattering length. In contrast to three dimensions, the $2D$ universal states can therefore not be observed as zero-energy resonances in few-body recombination.

For large values of $N \gg 1$, one can derive the universal properties of shallow N-boson ground states close to the unitary limit [HS04]. In particular, the binding energy E_N of the N-boson ground state increases geometrically with N:

$$\frac{E_{N+1}}{E_N} \approx 8.567, \qquad N \gg 1\,. \tag{7.5}$$

Thus, the separation energy for one particle is approximately 88% of the total binding energy. This is in contrast to most other physical systems, where the ratio of the single-particle separation energy to the total binding energy decreases to zero as the number of particles increases. The numbers $E_{\rm T}^{(0)}/E_{\rm D} = 16.5$ and $E_4^{(0)}/E_{\rm T}^{(0)} = 11.9$ obtained from the exact 3-body and 4-body results in Eqs. (7.3) and (7.4) appear to be converging toward the universal prediction for large N in Eq. (7.5). In Ref. [Le06], E_N was explicitly calculated up to $N = 10$ in lattice effective field theory and found to be consistent with Eq. (7.5). In any real physical system, however, the relation (7.5) can only be valid up to some maximum value of N determined by the range of the underlying interaction. When the states become compact enough that short-distance properties are probed, the binding energy will no longer be universal. In particular, for Lennard-Jones potentials and realistic Helium-Helium potentials, effective range effects can be quite large for three and more particles and the universal limit is approached only slowly [Bl05].

In experiments with cold atoms in a trap, the quasi-$2D$ limit can be reached by special trap geometries. The influence of a trapping potential on ultracold gases in this limit was extensively studied by Petrov and collaborators [PS01, PHS00, PBS03]. Although these works are mainly concerned with many-body effects in two-dimensional systems, they have applications for few-body aspects as well.

We concentrate on strictly two-dimensional systems of bosons neglecting any trapping effects. We calculate three-body observables close to unitarity in the framework of an effective field theory for large scattering length. We are especially interested in the leading non-universal corrections due to effective range effects. They enter at next-to-leading order in the effective field theory. Such effects must be under control for the experimental observation of universal phenomena in $2D$.

7.2 Method

In this section, we briefly review the derivation of the three-body equations for $D = 2$ in effective field theory. (See, e.g., Refs. [HS04, BH06] for more details.) We include a boson field Ψ and an auxiliary dimer field d in the Lagrangian. Since we include effective range effects, the dimer field is dynamical:

$$\mathcal{L} = \Psi^\dagger \left(i\partial_t + \frac{\nabla^2}{2m} \right) \Psi + d^\dagger \left(\eta \left(i\partial_t + \frac{\nabla^2}{4m} \right) + \Delta \right) d - \frac{g}{4}(d^\dagger \Psi^2 + \Psi^{\dagger 2} d) + \dots , \tag{7.6}$$

where the dots indicate higher order terms, m is the mass of the particles, $\eta = \pm 1$, and Δ and g denote the bare coupling constants. The sign η can be used to tune the sign of the effective range term. Negative η leads to positive values of the effective range r^2. In this case, the dimer kinetic term has a negative sign and the dimer field is a ghost. We will come back to this issue below. Note that three-body interactions enter only at higher orders and are not considered in this chapter.

The $2D$ effective range expansion, Eq. (7.1), can also be written in terms of the binding wave number $\kappa = \sqrt{m\, E_{\rm D}}$:

$$\cot \delta(k) = \frac{2}{\pi} \ln \left(\frac{k}{\kappa} \right) + \frac{r^2}{2\pi} (\kappa^2 + k^2) + \mathcal{O}(k^4) \, . \tag{7.7}$$

Figure 7.2: Integral equation for the full dimer propagator (thick solid line). The bare dimer propagator and the boson propagator are indicated by double and single lines, respectively.

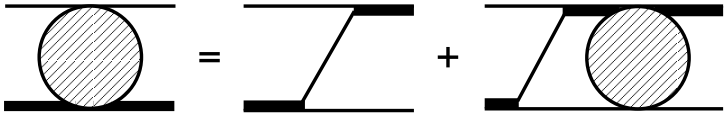

Figure 7.3: Integral equation for the boson-dimer scattering amplitude. The boson (full dimer) propagators are indicated by the solid (thick solid) lines. The external lines are amputated.

We can deduce the dependence of the binding wave number on the scattering length and the effective range from Eqs. (7.1) and (7.7),

$$\kappa = -\frac{i}{r}\sqrt{2\,W\left(-2e^{-2\gamma_{\rm E}}\,\frac{r^2}{a^2}\right)} \approx \frac{2e^{-\gamma_{\rm E}}}{a}\sqrt{1+2e^{-2\gamma_{\rm E}}\,\frac{r^2}{a^2}}\,, \tag{7.8}$$

where the signs are chosen such that $\kappa > 0$. The function W is the product logarithm or Lambert W-function. It is defined as the solution to $z = we^w$, namely $W(z) = w$. In the limit $r^2 \to 0$, the expression for E_D reduces to Eq. (7.2) and $\kappa \approx 1.1229/a$.

The Lagrangian in Eq. (7.6) implies the following Feynman rules: The propagator for a boson with energy k_0 and wave number $\vec{k}$ is given by $i\,[k_0 - k^2/(2m) - i\epsilon]^{-1}$, where $k = |\vec{k}|$. The bare dimer propagator is $i\,[\eta(k_0 - k^2/(4m)) + \Delta]^{-1}$ and the boson-dimer vertex coupling is given by $-ig/2$. Because the scattering length is large, boson loops are not suppressed and the bare propagator has to be dressed by boson bubbles to all orders. The full dimer propagator can be obtained by solving the integral equation in Fig. 7.2. This leads to the expression

$$iD(p_0,p) = -i\frac{32\pi}{mg^2}\left\{\ln\left[\frac{p^2/4 - mp_0 - i\epsilon}{\kappa^2}\right] + \frac{r^2}{2}\left(\kappa^2 + mp_0 - p^2/4\right)\right\}^{-1}\,, \tag{7.9}$$

where we have already matched g and Δ to the effective range expansion, Eq. (7.7). The wave function renormalization constant is given by the residue of the bound state pole in the propagator (7.9):

$$Z = \frac{32\pi}{m^2g^2}\,\frac{2\kappa^2}{2-\kappa^2 r^2}\,. \tag{7.10}$$

The boson-dimer scattering amplitude is given by the integral equation in Fig. 7.3, which iterates the one-boson exchange to all orders. Using the Feynman rules from above and

projecting onto S-waves, we obtain [BH06, HS04]:

$$\begin{aligned}\mathcal{A}(p,k;E) &= \frac{16\pi}{m}\frac{\kappa^2}{2-\kappa^2 r^2}\frac{1}{\sqrt{(p^2+k^2-mE)^2-p^2k^2}} \\ &\quad + 4\int_0^\infty \frac{dq\,q\,\mathcal{A}(q,k;E)}{\sqrt{(p^2+q^2-mE)^2-p^2q^2}} \\ &\quad \times\left(\ln\left[\frac{\frac{3}{4}q^2-mE-i\epsilon}{\kappa^2}\right]+\frac{r^2}{2}\left(\kappa^2+mE-\frac{3}{4}q^2\right)\right)^{-1}, \end{aligned} \tag{7.11}$$

where k (p) are the relative wave numbers of the incoming (outgoing) boson and dimer in the center-of-mass system and E is the total energy. The amplitude $\mathcal{A}(p,k;E)$ has simple poles at negative energies corresponding to three-body bound states. A more general discussion of the analytic properties of few-body scattering amplitudes in $2D$ is given in Ref. [AG92].

The three-body binding energies are most easily obtained from solving the homogeneous version of Eq. (7.11) for negative energies $E=-E_{\rm T}$:

$$\begin{aligned}\mathcal{B}(p;E_{\rm T}) &= 4\int_0^\infty \frac{dq\,q\,\mathcal{B}(q;E_{\rm T})}{\sqrt{(p^2+q^2+mE_{\rm T})^2-p^2q^2}} \\ &\quad \times\left(\ln\left[\frac{\frac{3}{4}q^2+mE_{\rm T}}{\kappa^2}\right]+\frac{r^2}{2}\left(\kappa^2-mE_{\rm T}-\frac{3}{4}q^2\right)\right)^{-1}. \end{aligned} \tag{7.12}$$

In Eqs. (7.11) and (7.12) the effective range r^2 is included nonperturbatively in the denominator of the dimer propagator (7.9). Therefore, both equations contain some higher-order effective range effects but still correspond to next-to-leading order in the effective field theory expansion. At the next higher order, where terms proportional to $(r^2)^2$ enter, there are also contributions from the k^4 term in the effective range expansion, Eqs. (7.1) and (7.7), which are not included here.[1]

The integral equations (7.11) and (7.12) can be solved in a straightforward way for negative effective range ($\eta=1$). For positive effective range ($\eta=-1$), an unphysical deep bound state pole appears in the dimer propagator (7.9). As the effective range is increased, this pole moves to lower energies. Its appearance is related to a violation of the Wigner causality bound, which constrains the value of the effective range r^2 for short-ranged, energy-independent interactions. For a detailed discussion of this bound in general dimension d, see Refs. [HL09, HL10]. This deep pole appears when we circumvent the Wigner bound by introducing a ghost dimer field ($\eta=-1$). It limits the energy range where our approach is applicable. Identifying the position space cutoff in [HL09] with $1/\Lambda$, the Wigner bound translates to

$$r^2 \le \frac{2}{\Lambda^2}\left\{[\ln(\Lambda a)+1/2]^2+1/4\right\}, \tag{7.13}$$

where Λ is an ultraviolet cutoff on the integration wave numbers in Eqs. (7.11) and (7.12). In the limit $\Lambda\to\infty$, the constraint becomes $r^2\le 0$. There are at least two strategies to deal with this problem:

[1] Note that in three dimensions the k^4 term enters one order higher and the corresponding equation would be valid to next-to-next-to-leading order. The difference is due to the form of the effective range expansion in two dimensions.

1. Expand the full dimer propagator (7.9) to linear order in r^2 and treat the range perturbatively. This removes the deep pole and includes all terms to next-to-leading order.

2. Keep an explicit wave number cutoff Λ in equations (7.11) and (7.12) such that Eq. (7.13) is satisfied. The unphysical pole then has no effect on low-energy observables.

Both strategies are applicable for wave numbers $|k^2 r^2| \ll 1$. In the following, we make use of Eqs. (7.11) and (7.12) and use strategy 2 to calculate three-body observables. A brief description of the perturbative treatment is given in the following paragraph.

In order to achieve a fully perturbative treatment, we expand the boson-dimer scattering amplitude into a leading order piece $\mathcal{A}^{(0)}(p,k;E)$ which satisfies Eq. (7.11) with $r^2 \equiv 0$ and a correction $\mathcal{A}^{(2)}(p,k;E)$ of order r^2:

$$\mathcal{A}(p,k;E) = \mathcal{A}^{(0)}(p,k;E) + \mathcal{A}^{(2)}(p,k;E) + \dots \,. \tag{7.14}$$

Next, we insert this expansion (7.14) into Eq. (7.11), expand the r^2 dependent terms, and collect all terms of order r^2 in order to obtain an equation for $\mathcal{A}^{(2)}(p,k;E)$. The on-shell scattering amplitude at next-to-leading order can then be written as an integral over the leading order amplitude and we finally obtain:

$$\begin{aligned} \mathcal{A}(k,k;E) &= \left(1 + \frac{r^2\kappa^2}{2}\right) \mathcal{A}^{(0)}(k,k;E) \\ &\quad - \frac{mr^2}{4\pi\kappa^2} \int_0^\infty dq\, q \left(\kappa^2 + mE - \frac{3}{4}q^2\right) \left[\frac{\mathcal{A}^{(0)}(k,q;E)}{\ln\left((\frac{3}{4}q^2 - mE - i\epsilon)/\kappa^2\right)}\right]^2 , \end{aligned} \tag{7.15}$$

where $E = 3k^2/(4m) - E_\mathrm{D}$. The scattering phase shift can be extracted in the same way as described in the following section.

7.3 Three-Body Observables

In this section, we present our results for the leading non-universal corrections to the three-boson binding energies, the boson-dimer scattering phase shifts and effective range parameters, and the three-boson recombination rate for finite energy. Since we are mainly interested in applications to cold atoms, we refer to the bosons as atoms in the remainder of this chapter.

7.3.1 Three-Body Binding Energies

We start with the effective range corrections to the three-body binding energies in Eq. (7.3). For $r^2\kappa^2 < 0$, the energies can straightforwardly be obtained by solving Eq. (7.12). This is similar to the three-dimensional case investigated in [Pe04]. For $r^2\kappa^2 > 0$, we have to keep track of the Wigner bound. We use an explicit wave number cutoff Λ and vary Λ from 1/5 to 4/5 of the maximum value determined by the position of the unphysical pole in Eq. (7.12). This value agrees within a factor of two with the maximum value given by Eq. (7.13). The dependence of the three-body energies on the cutoff is monotonic. The smallest cutoff results

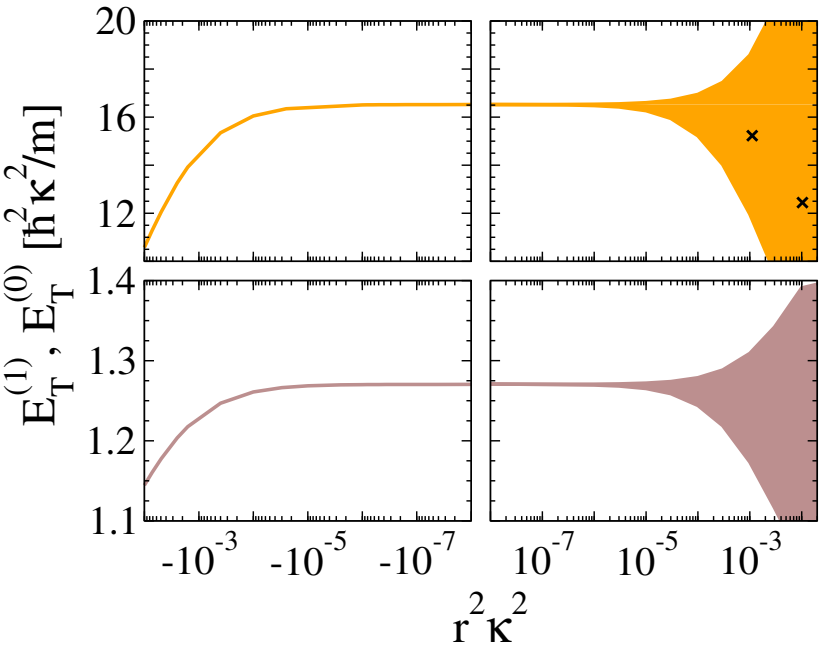

Figure 7.4: Three-body binding energies $E_{\rm T}^{(1)}$ and $E_{\rm T}^{(0)}$ in units of $\hbar^2\kappa^2/m$ vs. the two-body effective range $r^2\kappa^2$. The shaded bands are derived with the help of cutoff variation as described in the text and provide an error estimate. The crosses are Monte Carlo results for the modified KORONA potential from [Bl05, Bl].

in the smallest energy value whereas the largest cutoff results in the largest energy. This cutoff variation allows us to check whether the calculation is converged with respect to the cutoff and gives an error estimate for our results. We note that one still has to be careful about possible artefacts from the iteration of range terms. In the $3D$ case, it was shown that the ultraviolet behavior of the integral-equation kernel is already modified for momenta well below $1/r$ [PP06].

Our results for the three-body binding energies $E_{\rm T}^{(1)}$ and $E_{\rm T}^{(0)}$ as a function of the effective range, $r^2\kappa^2$, are summarized in Fig. 7.4. For negative effective range $r^2\kappa^2$, both three-body states become less bound as $|r^2\kappa^2|$ is increased. This behavior is quantitatively similar to the dimer state, cf. Eq. (7.8). The binding energies are very sensitive to the effective range. For $r^2\kappa^2 = -0.01$, we find the values $E_{\rm T}^{(1)} = 1.145(1)\,E_{\rm D}$ for the excited state and $E_{\rm T}^{(0)} = 10.578(1)\,E_{\rm D}$ for the ground state. For this rather small effective range, the ground state energy has already shifted by about 30%, while the excited state energy is shifted by about 10%. This sensitivity is partially related to the special nature of the effective range term in $2D$ which has units of [length]^2. Taking the square root, the leading range correction of $10-30\%$ for $|r\kappa| = 0.1$ looks more natural. Our calculation including the leading non-universal corrections suggests that the three-body states eventually cross the atom-dimer threshold as the effective range is made more negative. For the excited state this happens around $r^2\kappa^2 \approx -0.4$, but higher order corrections are expected to be important. If this behavior holds true and the effective range could be varied in experiment, the three-body states in $2D$ might be observable through zero energy scattering resonances similar to Efimov states in $3D$. For positive values of the effective range, the central value of our error band

also corresponds to a less strongly bound system but we can not make a definite prediction. Once the effective range effects become appreciable, the errors in our calculations become too large. Still, the Monte Carlo results for the modified KORONA potential from [Bl05, Bl] (see the crosses in Fig. 7.4) are in good agreement with our band. They also give a diminishing energy for larger positive effective range. Note that we only show the two points from [Bl05] closest to the unitary limit. All other data points are outside the range of $r^2\kappa^2$ displayed in Fig. 7.4.

For effective ranges close to zero, the binding energies depend linearly on $r^2\kappa^2$. We can determine the coefficient of the leading term numerically to about 15% accuracy. For $r^2\kappa^2 < 0$, we find:

$$\begin{aligned} E_{\rm T}^{(0)}/E_{\rm D} &= 16.522688(1) + 28000(5000)\, r^2\kappa^2 + \mathcal{O}(r^4\kappa^4)\,, \\ E_{\rm T}^{(1)}/E_{\rm D} &= 1.2704091(1) + 540(80)\, r^2\kappa^2 + \mathcal{O}(r^4\kappa^4)\,. \end{aligned} \tag{7.16}$$

For $r^2\kappa^2 > 0$, the coefficient of $r^2\kappa^2$ can not be extracted from our calculation. While the values of $E_{\rm T}^{(0)}$ and $E_{\rm T}^{(1)}$ are very insensitive to the cutoff variation at small positive $r^2\kappa^2$, even the sign of the slope is not well determined. We note that $r^2\kappa^2$ can be quite small in $2D$ systems even if the effective range is substantially larger than the range of the interaction (see, e.g., the explicit example of a circular well potential given in Section 6.1 of Ref. [HL10]). The large coefficients in Eq. (7.16), however, already cause significant effective range corrections for $|r^2\kappa^2|$ of order 10^{-4} to 10^{-3}.

7.3.2 Atom-Dimer Scattering

Next, we consider the effective range corrections to elastic atom-dimer scattering. We find scattering observables in general to be less sensitive to the unphysical deep poles. To obtain the scattering amplitude, we solve Eq. (7.11) for $E = \frac{3}{4m}k^2 - E_{\rm D}$ below the dimer breakup threshold and with the incoming particles on-shell. The elastic scattering phase shift $\delta_{\rm AD}(k)$ can then be obtained from the scattering amplitude for $p = k$ using

$$\mathcal{A}\left(k, k; \frac{3}{4m}k^2 - E_{\rm D}\right) = \frac{3}{m} f_k = \frac{3}{m}\, \frac{1}{\cot\delta_{\rm AD}(k) - i}\,. \tag{7.17}$$

In Fig. 7.5, we show $\cot\delta_{\rm AD}$ for different values of $r^2\kappa^2$ as a function of the wave number k up to the dimer breakup threshold $k \approx 1.15\kappa$. For small values of k, $\cot\delta_{\rm AD}$ is almost linear in $\ln k$ but at about half the breakup wave number the behavior becomes more complicated. For $r^2\kappa^2 < 0$, the non-universal corrections increase $\cot\delta_{\rm AD}$ compared to the universal result, while for $r^2\kappa^2 > 0$ the behaviour depends on the value of $r^2\kappa^2$.

The atom-dimer effective range parameters can be extracted from our results by fitting the effective range expansion, Eq. (7.1), to $\cot\delta_{\rm AD}$. We have performed fits with different orders in the expansion and different truncations of the data sets to estimate the error in this extraction. Our results for $\kappa a_{\rm AD}$ and $(\kappa r_{\rm AD})^2$ in dependence of $r^2\kappa^2$ are summarized in Fig. 7.6. The effective range $r_{\rm AD}^2$ comes out positive for all values of $r^2\kappa^2$ considered. For $|r^2\kappa^2| \lesssim 10^{-4}$ the curves are nearly symmetric around $r^2\kappa^2 = 0$ and can be approximated by

$$\kappa a_{\rm AD} = 2.614(1) - 4100(500)\, r^2\kappa^2 + \mathcal{O}(r^4\kappa^4)\,. \tag{7.18}$$

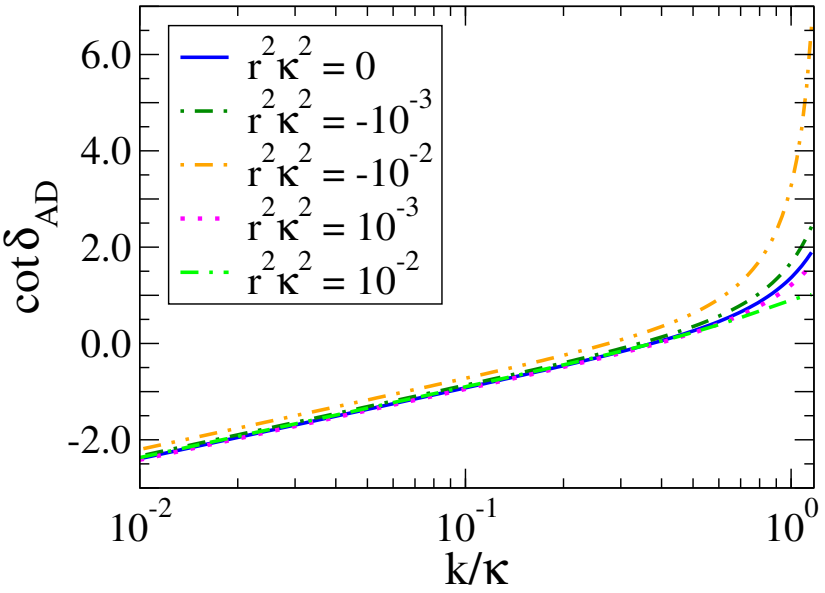

Figure 7.5: The elastic atom-dimer scattering phase shift $\cot \delta_{\rm AD}$ for $r^2\kappa^2 = 0, \pm 10^{-3}, \pm 10^{-2}$ as a function of the wave number k/κ.

Similar to the bound state case, we find large coefficients in the perturbative expansion in $r^2\kappa^2$. For larger values of $r^2\kappa^2$, the curves are not symmetric anymore. In the unitary limit, we find the effective range parameters $\kappa a_{\rm AD} = 2.614(1)$ and $(\kappa r_{\rm AD})^2 = 4.0(2)$. Converting to units of the scattering length a, our results correspond to $a_{\rm AD} = 2.328(1)\, a$ and $\ln(a_{\rm AD}/a) = 0.845(1)$. These numbers agree well with the value $\ln(a_{\rm AD}/a) = 0.8451$ obtained by Kartavtsev and Malykh [KM06] and are in qualitative agreement with the value $a_{\rm AD} = 2.95a$ found by Nielsen et al. [NFJ99]. For $r^2\kappa^2$ of order 0.01, there are again substantial effective range effects. In particular, we find the values $\kappa a_{\rm AD} = 3.540(1)$ and $(\kappa r_{\rm AD})^2 = 7.4(2)$ for $r^2\kappa^2 = -0.01$ and $\kappa a_{\rm AD} = 2.713(1)$ and $(\kappa r_{\rm AD})^2 = 2.9(2)$ for $r^2\kappa^2 = 0.01$.

We have also calculated the atom-dimer scattering phase shifts and effective range parameters using the fully perturbative treatment discussed at the end of Section 7.2. For sufficiently small effective range, the two methods agree.

7.3.3 Three-Body Recombination

Finally, we consider three-body recombination into the shallow dimer described by Eq. (7.2). Cold atoms typically also have a large number of deep dimer states. However, three-body recombination into the deep dimers is suppressed since the atoms have to approach distances comparable to the size of the deep dimers. This process enters at the same order as short-range three-body interactions. It could be calculated by introducing a complex three-body parameter [BH06].

The three-body recombination into the shallow dimer is strongly influenced by the behavior of the full dimer propagator, Eq. (7.9). There are three limits in which the propagator vanishes: (*i*) $a \to \infty$, (*ii*) $E \to 0$, and (*iii*) $E \to \infty$. In these three limits, the three-body

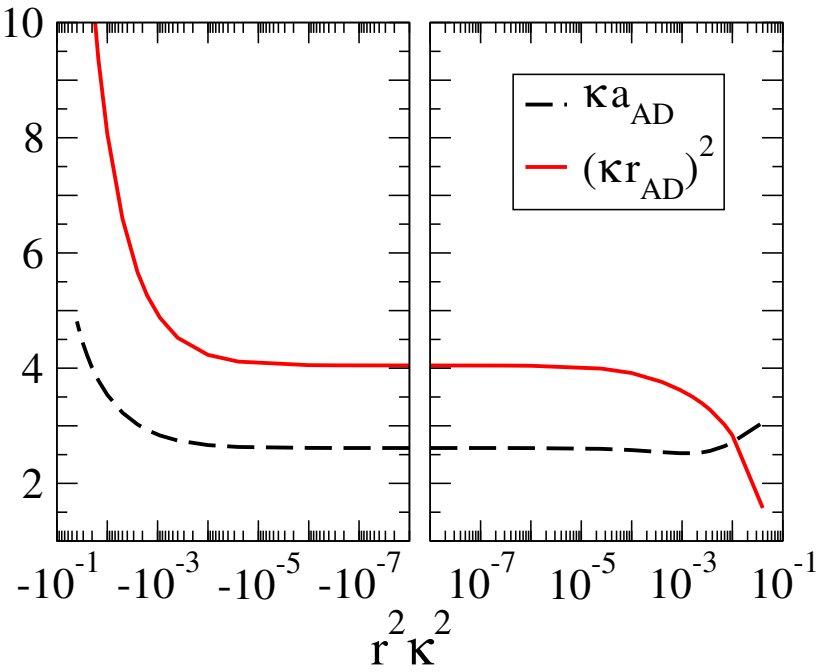

Figure 7.6: The atom-dimer scattering length $\kappa a_{\rm AD}$ and effective range $(\kappa r_{\rm AD})^2$ as a function of the two-body effective range $r^2\kappa^2$.

recombination rate also vanishes. For large but finite scattering length and finite energy, however, three-body recombination can occur.

The rate can be conveniently calculated using the inelastic atom-dimer scattering cross section [BHKP08] which has dimension of length in $2D$. The integration measure of the three-body phase space in two dimensions using hyperspherical variables is given by

$$d^2p_1\, d^2p_2\, d^2p_3 = m^2 E \sin(2\alpha_3)\, dE\, d\alpha_3\, d\varphi_{12}\, d\varphi_{3,12}\, d^2p_{\rm tot}\,. \tag{7.19}$$

More details on the derivation of this can be found in Appendix B.1. From this, the relation between the hyperangular average of the recombination rate at finite energy and the inelastic cross section in two dimensions is obtained as

$$K(E) = \frac{36\pi}{m^2 E}\, k\, \sigma_{\rm AD}^{\rm (inel)}(E)\,, \tag{7.20}$$

where $k = \sqrt{\frac{4m}{3}(E+E_{\rm D})}$. Intermediate steps of this computation can be found in Appendix B.2. The inelastic cross section in Eq. (7.20) can be obtained by subtracting the elastic cross section

$$\sigma_{\rm AD}^{\rm (el)}(E) = \frac{4}{k}\,|f_k|^2\,, \tag{7.21}$$

from the total cross section $\sigma_{\rm AD}^{\rm (tot)}(E)$. The latter can be obtained from the optical theorem which in $2D$ is given by [Ad86][2]

$$\sigma_{\rm AD}^{\rm (tot)}(E) = \frac{4}{k}\,{\rm Im} f_k(0)\,. \tag{7.22}$$

[2]Note the different normalization factor, our amplitude is $\sqrt{\pi/2}$ times their amplitude.

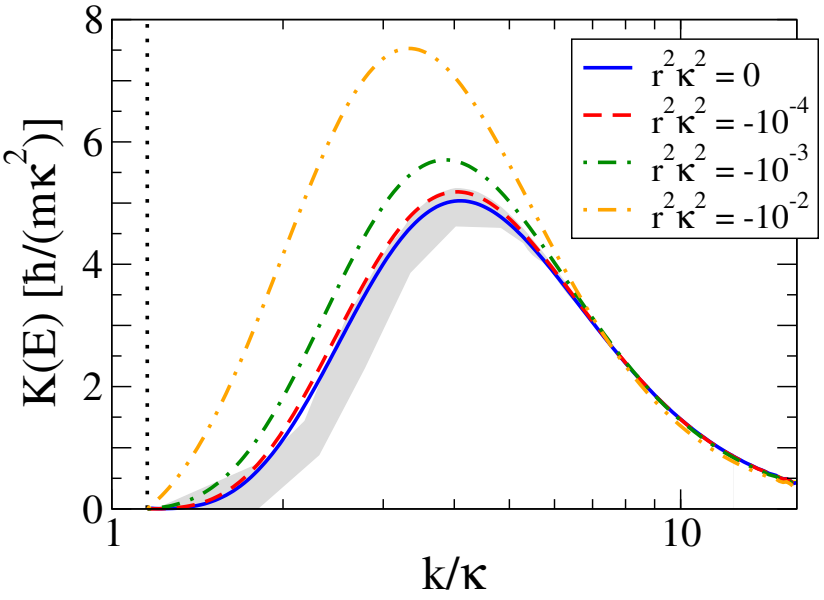

Figure 7.7: The energy-dependent three-body recombination rate $K(E)$ in units of $\hbar/(m\kappa^2)$ as a function of the wave number k/κ. The shaded band corresponds to $r^2\kappa^2 = 10^{-4}$ and is derived with the help of cutoff variation as described in the text.

Using the expression for the elastic scattering amplitude, Eq. (7.17), the three-body recombination rate $K(E)$ can be calculated from Eqs. (7.20), (7.21), and (7.22). Our results for $K(E)$ as a function of the wave number k are shown in Fig. 7.7. For positive $r^2\kappa^2$, we again make use of a cutoff variation in the range of 1/5 to 4/5 of the maximum allowed value. The grey band gives our result for $r^2\kappa^2 = 10^{-4}$. For larger values of $r^2\kappa^2$, the width of the band increases. As expected, the rate vanishes for large wave numbers and at threshold. Around $k \approx 3 - 4\kappa$, there is a maximum in the recombination rate. The position of the maximum is weakly dependent on the value of the effective range. It is governed by the behavior of the full dimer propagator as a function of the energy, Eq. (7.9). The maximum is not related in a simple way to the energy of the universal three-body states, Eq. (7.3), but our calculation establishes an implicit relation between the two.

In experiments with cold atoms, one typically uses ensembles of atoms in thermal equilibrium. The energy-dependent recombination rate $K(E)$ can be converted into an energy averaged rate by performing a Boltzmann average as described in Ref. [BHKP08]. Taking into account the energy dependence of the three-body phase space, Eq. (7.19), we have

$$\begin{aligned} \alpha(T) &= \frac{\int_0^\infty dE\, E\, e^{-E/(k_\mathrm{B}T)}\, K(E)}{3! \int_0^\infty dE\, E\, e^{-E/(k_\mathrm{B}T)}} \\ &= \frac{1}{6k_\mathrm{B}^2T^2} \int_0^\infty dE\, E\, e^{-E/(k_\mathrm{B}T)}\, K(E)\,. \end{aligned} \tag{7.23}$$

Our results for $\alpha(T)$ for different values of the effective range are shown in Fig. 7.8. We do not give results for $r^2\kappa^2 > 0$, but the shaded band for $r^2\kappa^2 = 10^{-4}$ in Fig. 7.7 translates into an error band around $r^2\kappa^2 = 0$ here as well. The temperature dependent rate also has a maximum at temperatures of the order of 5 to 7 times the dimer binding energy. The recombination rate at the maximum is very sensitive to the value of the effective range. If the

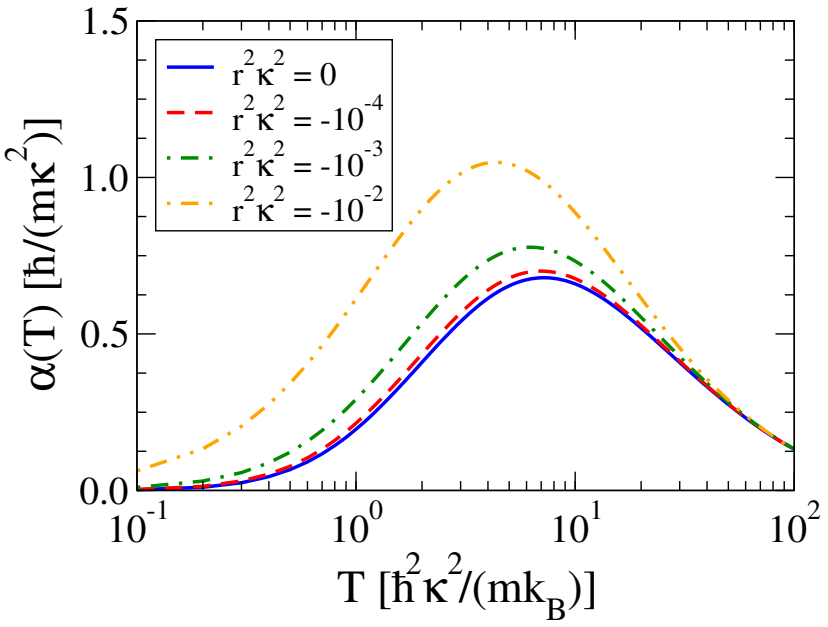

Figure 7.8: The three-body recombination rate α in units of $\hbar/(m\kappa^2)$ in dependence of the temperature T in units of $\hbar^2\kappa^2/(mk_\mathrm{B})$.

effective range is changed from zero to $r^2\kappa^2 = -0.01$, the rate at the maximum changes by a factor of two. For all values of the effective range considered, however, the recombination rate at the maximum remains of order one in natural units $\hbar/(m\kappa^2)$. This suggests that $2D$ Bose gases are stable enough to observe universal few-body phenomena experimentally. The lifetime of a $2D$ Bose gas with large scattering length was previously estimated by Pricoupenko and Olshanii [PO07]. The order of magnitude of our recombination rates is consistent with their results.

7.4 Summary and Conclusions

In this chapter, we have investigated the three-body properties of identical bosons close to the unitary limit in two spatial dimensions. Within an effective field theory for resonant interactions, we have calculated the leading non-universal corrections which are due to the two-body effective range. In particular, we have calculated the leading corrections to the three-body binding energies, the atom-dimer scattering phase shift and effective range parameters, and the three-body recombination rate at finite energy.

We have compared our results to previous calculations in the unitary limit, where available, and generally found good agreement. Our calculations show a large sensitivity of three-body observables to the effective range. Significant effective range effects can be observed already for $|r^2\kappa^2| \gtrsim 10^{-4} - 10^{-3}$. These corrections are due to large coefficients in the perturbative expansion of observables in $r^2\kappa^2$ (cf. Eqs. (7.16), (7.18)). It would be interesting to understand the physics behind these large coefficients. These coefficients could be reduced by an order of magnitude by renormalizing to the three-body ground state energy $E_\mathrm{T}^{(0)}$ instead of E_D [Bi], but they would still remain unnaturally large. Our results suggest that the convergence to

the unitary limit in $2D$ three-body observables is rather slow and effective range corrections play an important role even close to the unitary limit. This is in agreement with the results of Blume who investigated the universal properties of N-body droplets using Lennard-Jones potentials and realistic Helium potentials [Bl05].

Our calculation of the three-body energies including the leading non-universal corrections suggests that the bound states may eventually cross the atom-dimer threshold as the effective range is made more negative. If this behavior holds true when higher orders are included, it opens the possibility to observe three-body states in $2D$ through a variation of the $2D$ effective range. The states would then appear as zero energy scattering resonances similar to Efimov states in $3D$.

Our results are directly applicable to two-dimensional Bose gases with large scattering length and imply that effective range effects must be under control in experiments exploring universal properties of $2D$ Bose gases. Effective field theory provides a powerful tool to calculate these corrections and our study provides the first step towards accurate calculations of these effects.

On the experimental side, there has been some progress in the study of universal properties of $2D$ Bose gases. For example, Chin and coworkers have recently studied scale invariance and critical behavior near a BKT phase transition in $2D$ and observed universal behavior of the thermodynamic functions [HZGC11]. They have also attempted to show how the Efimov resonance in three-body recombination shifts when the system is tuned towards a dimensionality of two by increasing one of the trapping frequencies in a $3D$ experiment [Ch09].

Interesting few-body properties of $2D$ systems include universal N-body states and a geometric spectrum of N-body ground states [HS04]. Moreover, Nishida and Tan have shown that a two-species Fermi gas in which one species is confined in $2D$ or $1D$ while the other is free in the three-dimensional space is stable against the Efimov effect and has universal properties [NT08]. More complicated multispecies Fermi gases with similar properties are possible as well. They also showed that a purely S-wave resonance in $3D$ can induce higher partial wave resonances in mixed dimensions and pointed out that some of the resonances observed in a recent experiment by the Florence group [La$^+$10] can be interpreted as a P-wave resonance in mixed $2D$-$3D$ dimensions [NT10]. Thus, future experiments considering few-body phenomena in lower-dimensional ultracold gases will be very interesting. Our calculation of the leading non-universal corrections provides a basis for the interpretation of such experiments.

Chapter 8

Summary and Outlook

In this thesis, we have used the framework of effective field theory to study few-body physics in ultracold atomic gases. After an experimental and theoretical introduction to this topic in Chapters 2 and 3, we concentrated on four major aspects of few-body physics in the following four main chapters of this work. The first three are mainly concerned with the Efimov effect in various respects whereas the last chapter investigates three-body observables in two dimensions. All topics are again specified and summarized here.

Concerning atom-dimer scattering at finite temperatures, we calculated the atom-dimer relaxation rate β for large positive scattering length, i.e., in the presence of the Efimov effect. The atom-dimer phase shifts were taken from a parametrization derived previously in EFT. To include the temperature dependence of the process, the Bose-Einstein distribution function was used for thermal averaging. This is only possible with experimental input for atom and dimer numbers. We therefore used data from the experiment conducted by Knoop and coworkers [Kn$^+$09] to which our results were also applied.
The two free parameters of our theory, the resonance position a_* and the width η_*, were used to find a fit to the data taken at 170 nK. We found very good agreement for $a_* = 397\, a_0$ and $\eta_* = 0.034$ and subsequently used the same parameter values for the 40 nK data. With these values, we overpredicted the data by a factor of two. It should be noted, however, that the 40 nK data is much less precisely measured. Especially the dip in the curve that seems to be present in the data could be due to statistical fluctuations and is not reproduced in our theory. The fitted resonance position could not be used for a good description of the three-body recombination data obtained earlier [Kr$^+$06, BHKP08]. These discrepancies might be due to non-universal effects such as effective range corrections as the experiment was conducted at the very edge of the universal region. Also, the bigger importance of four-body effects at low temperatures could play a role. This question deserves further study.

For the study of heteronuclear systems for $L = 0$, we derived an STM equation for the atom-dimer scattering amplitude in a mixture of two atomic species where the majority atoms must be bosons. Only the interaction between unlike particles is taken into account; the intraspecies interaction is neglected. This is justified close to an interspecies Feshbach resonance. All results additionally depend on the mass ratio δ of the species under consideration. We calculated the ratio $a_*/|a_-|$ relating the three-body with the atom-dimer threshold crossing and derived semi-analytical formulae for three-body recombination and atom-dimer

relaxation rates at $E = 0$. They were found to be in excellent agreement with analytical formulae [HHP10]. Together with the semi-analytical result for the atom-dimer relaxation rate at $E = E_\mathrm{D}$, they can be used to analyze current and future experiments.
We applied our results to a mixture of ^{40}K-^{87}Rb that was investigated by Zirbel et al. [Zi$^+$08]. We found good overall agreement for the atom-dimer relaxation rate in a mixture of rubidium atoms with K-Rb molecules and for the three-body recombination rate. However, we predict an Efimov resonance in the three-body recombination rate at $a \approx -600\,a_0$ that has not yet been seen experimentally.
For the mixture of ^{41}K-^{87}Rb used by Barontini et al. [Ba$^+$09, Mi], only two data points for three-body recombination close to an Efimov resonance $a = -246\,a_0$ are available. The width parameter η_* can be adjusted to describe them adequately but no definitive conclusion can be drawn. One also has to be careful with the threshold ratio $a_*/|a_-|$ deduced from the experiment. The parameter a_* was taken from the three-body recombination that showed a peak at positive scattering length. This could be due to atom-dimer collisions from dimers formed spontaneously in the system and subsequently expelling a few atoms from the trap. However, we could show that the finite energy has a large influence on the height and position of the atom-dimer relaxation peak. Therefore, an independent check in a molecule-atom mixture is needed. However, this is hard to realize experimentally due to the bosonic nature and thus the short lifetime of the molecules.
Further experiments using heteronuclear mixtures with heavy bosons are under construction, for example, in Heidelberg [De$^+$08]. The results derived in Chapter 5 should give a tool to analyze the outcomes.

A natural extension to the description of heteronuclear systems in a total S-wave was the investigation of mainly fermionic systems in P-waves. The Efimov effect can only occur in even (odd) angular momentum channels for bosons (fermions) and the most relevant cases are the lowest possible angular momentum channels. Nevertheless, we generalized the formerly derived STM equation to general L and computed a transcendental equation for the parameters s_L yielding the scaling factor. They again depend on the mass ratio δ.
As three-body recombination vanishes at $E = 0$ for $L > 0$, we concentrated on atom-dimer scattering. We derived analytical expressions for the elastic and inelastic scattering cross sections and the atom-dimer relaxation rate.
We also calculated the elastic atom-dimer cross section for channels without the Efimov effect, namely bosons for $L = 1$ and fermions for $L = 0$. Besides, for fermions in a P-wave, the Efimov effect only sets in for $\delta^{-1} > 13.61$. Below this mass ratio, two non-Efimov three-body bound states were predicted to appear [KM07a]. We could confirm this by showing how the atom-dimer cross section behaves close to $E = -E_\mathrm{D}$. It develops two very sharp peaks at the critical mass ratios where the trimers appear.
Subsequently, we concentrated on the case of $L = 1$ for fermions in the presence of the Efimov effect. In this case, we calculated the threshold ratio $a_*/|a_-|$ and atom-dimer observables for $E < 0$. They can be parametrized by an energy-dependent atom-dimer scattering length with two universal functions $c_1(\delta, k)$ and $c_2(\delta, k)$. We found a strong energy dependence, that can also be seen in the observables, in addition to the log-periodic dependence on the scattering length typical for Efimov physics. For the example of $\delta = 0.04$ corresponding roughly to the mass ratio for $^{171/173}$Yb-^{7}Li, we explicitly show the atom-dimer cross sections and the energy dependence of the atom-dimer relaxation rate. The peak position varies non-linearly by a factor of 5 and the height by a factor of 70 when the energy is changed from $E = 0$ to $E = -0.9999\,E_\mathrm{D}$ for $\eta_* = 0.1$.

Up to now, this P-wave Efimov effect has not been seen in experiment but at least two groups are very likely to investigate it soon [Har$^+$11, Han$^+$11]. Therefore, our predictions can be used as reference and can hopefully also be validated in these experiments.

Chapter 7, discussing two-dimensional systems, differed from the preceding ones in two respects: Efimov physics does not play a role in $2D$ and we considered range effects leading to results that are valid up to next-to-leading order. To this purpose, we derived an integral equation describing atom-dimer scattering in $2D$ by including effects of the two-body effective range. From this, we could deduce three-body binding energies, the atom-dimer phase shift and effective range parameters, and three-body recombination at finite energy.
We found substantial range effects already for $|r^2\kappa^2| \gtrsim 10^{-4} - 10^{-3}$, showing that the unitary limit is approached only slowly in $2D$. Our result for the variation of the binding energies of the two trimers in the system suggest that, if it were possible to experimentally tune the effective range, the excited trimer could perhaps be seen as a scattering resonance. This would be similar to the variation of the scattering length in $3D$, which allows for a detection of the Efimov states.
There has been a lot of progress on $2D$ systems experimentally (see, e.g., [HZGC11]) and our findings should be of use in the understanding of future investigations of few-body effects in two-dimensional quantum gases.

As mentioned several times above, further comparisons to future experiments will be very interesting. They might help to solve current disagreement in the 40 nK data for β that is overpredicted theoretically or for the ^{40}K-^{87}Rb three-body recombination rate where an Efimov resonance is predicted to lie in the range accessible to experiments. New data on (other) heteronuclear mixtures should be able to show the scaling factors differing from 22.7 and validate our predictions for observable recombination rates. Specifically, a signature of the P-wave Efimov effect in atom-dimer systems would be very intriguing.

From a purely theoretical point of view, the calculation of the three-body recombination rate for $L = 1$ at finite temperatures should be possible. A similar computation was conducted for $L = 0$ in Ref. [BHKP08] deriving universal functions for the atom-dimer phase shifts, which were subsequently used to calculate the three-body recombination rate. This principle should carry over to P-waves and could be implemented in existing calculations in a straightforward way.

The calculations for the three identical particles in two dimensions can also be generalized to heteronuclear systems. This was done in a zero range universal calculation for the three-body bound states very recently [Be$^+$11]. Our formalism allows for a calculation of the bound states up to next-to-leading order and to derive the heteronuclear atom-dimer scattering properties and three-body recombination rates. This could be beneficial for current experiments in lower dimensions as are conducted, for example, in Chin's group [HZGC11].

Also interesting is whether the Efimov effect survives in dipolar systems. It has been positively answered for bosonic dipoles by Wang and coworkers using hyperspherical model potentials [WDG11a]. Also fermionic dipoles show universal behavior in this approach [WDG11b]. A dipole interaction can also be incorporated into the EFT method used in this thesis. This would serve as an independent test to the validity of the found results. Besides, dipolar molecules are currently under experimental investigation (see, e.g., [Zi$^+$08, Web$^+$08]).

It should be relatively straightforward to calculate the range effects to the tetramer binding

energies in $2D$ by combining the formulae shown in Chapter 7 with the method used in Ref. [PHM04]. It would be especially interesting to see if unnaturally large prefactors are also found in the perturbative expansion for these binding energies.

Furthermore, the field of Efimov physics is still far from being completely explored. Apart from the three-body effects, which were the main focus of this work, there are two tetramers associated with each Efimov trimer [HP07, vSDG09]. Their existence has been confirmed experimentally [Fe$^+$09] and further signatures have been seen in other experiments, e.g., [PDH09]. This sequence of bound states might continue further [vSt11]. Cluster states of Efimov character have been predicted [vSt10], as well as the equivalent of the heteronuclear Efimov effect for four particles in a narrow range of the mass ratio [CMP10]. The Efimov effect should also be present in systems in mixed dimensions such as two-dimensional layers of one atomic species being immersed in a larger three-dimensional sample of another species [NT11]. It could also be seen in atom-trimer [De10] or dimer-dimer scattering [PSS05, De11]. This list is far from complete and even though a few questions were investigated in detail in this thesis, the field of Efimov physics is constantly growing. It will remain an active field with many more challenges to be solved in the future.

Appendix A

Heteronuclear Integral Equation

In this appendix, we want to give an extensive derivation of the heteronuclear integral equations (5.3) and (6.3) used in the Chapters 5 and 6. We also deduce the subtracted equation, used in Subsections 5.2.2 and 5.2.4, and show more details of the computation of s_L from Section 6.2.

A.1 Derivation

To calculate the STM equation, we start by deriving the full heteronuclear dimer propagator (5.2). Feynman rules for the heteronuclear case of Lagrangian (5.1) are given in Table A.1. Note that we first only consider bosons, the fermionic case is discussed at the end of this section. The full dimer propagator is shown in Fig. A.1 and is given by

$$\begin{aligned} iD(E) &= iD^{(0)}(E) + iD^{(0)}(E)\big(-i\Sigma(E)\big)iD^{(0)}(E) + \cdots \\ &= iD^{(0)}(E)\left[1 - \Sigma(E)iD^{(0)}(E)\right]^{-1}, \end{aligned} \tag{A.1}$$

Description	Feynman rule
Propagator for atom i	$i/(k_0 - \frac{k^2}{2m_i} + i\epsilon)$
Dimer propagator, $iD^{(0)}$	i/g_2
(A_1-A_2 $\rightarrow$ D)–vertex, (D $\rightarrow$ A_1-A_2)–vertex	$-ig_2$
(A_2-D $\rightarrow$ A_2-D)–vertex	$-ig_3/4$

Table A.1: Feynman rules for the heteronuclear case.

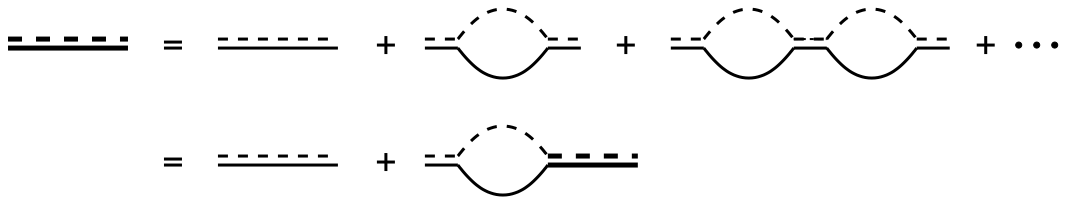

Figure A.1: Infinite bubble sum or integral equation for the dimer propagator. Solid (dashed) lines denote atom species 2 (1). Mixed double lines denote the bare dimer propagator; thick mixed double lines denote the full dimer propagator.

where $iD^{(0)}(E)$ denotes the bare dimer propagator and $i\Sigma(E)$ the self-energy. This self-energy is given by

$$\begin{aligned}
-i\Sigma(E) &= (-ig_2)^2 \int \frac{d^3q}{(2\pi)^3}\frac{dq_0}{2\pi}\frac{i}{q_0 - q^2/(2m_1) + i\epsilon}\frac{i}{E - q_0 - q^2/(2m_2) + i\epsilon} \\
&= -ig_2^2 \int \frac{d^3q}{(2\pi)^3}\frac{1}{E - q^2/2\mu + i\epsilon} \\
&= -i2\mu g_2^2 \int \frac{d\Omega}{4\pi}\int_0^\Lambda \frac{dq}{2\pi^2}\frac{q^2}{2\mu E - q^2 + i\epsilon} \\
&= -i\frac{\mu g_2^2}{\pi^2}\left(-\Lambda + \int_0^\Lambda dq \frac{2\mu E}{2\mu E - q^2 + i\epsilon}\right) \\
&\approx i\frac{\mu g_2^2}{\pi^2}\left(\Lambda - \frac{\pi}{2}\sqrt{-2\mu E - i\epsilon}\right),
\end{aligned} \tag{A.2}$$

where we neglected a term proportional to $1/\Lambda$ in the very last step. Inserting this into Eq. (A.1) and multiplying by $(-ig_2)^2$ to account for the vertices leads to the two-body amplitude

$$\mathcal{A}_2(E) = -g_2\left[1 + \frac{\mu g_2}{\pi^2}\left(\Lambda - \frac{\pi}{2}\sqrt{-2\mu E - i\epsilon}\right)\right]^{-1}. \tag{A.3}$$

The scattering length and the coupling g_2 can now be deduced

$$a = -\frac{\mu}{2\pi}\mathcal{A}_2(0) = \frac{\mu g_2}{2\pi}\left[1 + \frac{\mu g_2 \Lambda}{\pi^2}\right]^{-1} \quad \Longleftrightarrow \quad g_2 = \frac{2\pi a}{\mu}\left[1 - \frac{2a\Lambda}{\pi}\right]^{-1}. \tag{A.4}$$

Substituting $E = P_0 - \frac{P^2}{2M}$ and multiplying by $(-ig_2)^{-2}$, we thus can give the full dimer propagator,

$$\begin{aligned}
D(P_0, \vec{P}) &= \frac{1}{g_2}\left[1 + \frac{\mu g_2}{\pi^2}\left(\Lambda - \frac{\pi}{2}\sqrt{-2\mu\Big(P_0 - P^2/(2M)\Big) - i\epsilon}\right)\right]^{-1} \\
&= \frac{1}{g_2}\left[1 + \frac{\mu}{\pi^2}\frac{2\pi a}{\mu}\frac{1}{1 - 2a\Lambda/\pi}\left(\Lambda - \frac{\pi}{2}\sqrt{-2\mu\Big(P_0 - P^2/(2M)\Big) - i\epsilon}\right)\right]^{-1} \\
&= \frac{2\pi}{\mu g_2^2}\left[-1/a + \sqrt{-2\mu\Big(P_0 - P^2/(2M)\Big) - i\epsilon}\right]^{-1},
\end{aligned} \tag{A.5}$$

corresponding to Eq. (5.2). The wave function renormalization is given by

$$Z_{\mathrm{D}}^{-1} = i\frac{\partial}{\partial P_0}\big(iD(P_0,P)\big)^{-1}\Big|_{P_0=-1/(2\mu a^2),P=0} = \frac{\mu^2 g_2^2\, a}{2\pi}\,. \tag{A.6}$$

Subsequently, we make use of this dimer propagator to derive the atom-dimer amplitude pictured in Fig. 5.1,

$$\begin{aligned}
\mathcal{A}(p,k;E) &= -g_2^2\left[\frac{1}{E-p^2/(2m_2)-k^2/(2m_2)-(\vec{p}+\vec{k})^2/(2m_1)+i\epsilon}+\frac{g_3}{4g_2^2}\right] \\
&\quad -g_2^2\frac{2\pi}{g_2^2\mu}\int\frac{d^3q}{(2\pi)^3}\int\frac{dq_0}{2\pi}\left[\frac{1}{E-p^2/(2m_2)-q_0-(\vec{p}+\vec{q})^2/(2m_1)+i\epsilon}+\frac{g_3}{4g_2^2}\right] \\
&\quad \times\frac{i}{q_0-q^2/(2m_2)+i\epsilon}\,\frac{\mathcal{A}(p,q;E)}{-1/a+\sqrt{-2\mu(E-q^2/(2m_2)-q^2/(2M))-i\epsilon}} \\
&= -g_2^2\left[\frac{1}{E-p^2/(2\mu)-k^2/(2\mu)-\vec{p}\cdot\vec{k}/m_1+i\epsilon}+\frac{g_3}{4g_2^2}\right] \\
&\quad -\frac{4\pi}{\mu}\int\frac{d^3q}{(2\pi)^3}\left[\frac{1}{E-p^2/(2\mu)-q^2/(2\mu)-\vec{p}\cdot\vec{q}/m_1+i\epsilon}+\frac{g_3}{4g_2^2}\right] \\
&\quad \times\frac{\mathcal{A}(p,q;E)}{-1/a+\sqrt{-2\mu(E-q^2/(2m_2)-q^2/(2M))-i\epsilon}} \\
&= -g_2^2\left[\frac{2\mu}{2\mu E-p^2-k^2-2\vec{p}\cdot\vec{k}\frac{\mu}{m_1}+i\epsilon}+\frac{g_3}{4g_2^2}\right] \\
&\quad -\frac{2\pi}{\mu}\int\frac{d^3q}{(2\pi)^3}\left[\frac{2\mu}{2\mu E-p^2-q^2-2\vec{p}\cdot\vec{q}\frac{\mu}{m_1}+i\epsilon}+\frac{g_3}{4g_2^2}\right] \\
&\quad \times\frac{\mathcal{A}(p,q;E)}{-1/a+\sqrt{-2\mu(E-q^2/(2m_2)-q^2/(2M))-i\epsilon}}\,.
\end{aligned} \tag{A.7}$$

We now first concentrate on the S-wave case. Therefore, we average the equation over $x=\cos\big(\angle(\vec{p},\vec{k})\big)$ to project the amplitude on its S-wave part,

$$\int_{-1}^{1}\frac{dx}{2}\,\frac{2\mu}{2\mu E-p^2-k^2-2pkx\frac{\mu}{m_1}+i\epsilon} = -\frac{m_1}{2pk}\ln\left[\frac{p^2+k^2+2pk\frac{\mu}{m_1}-2\mu E-i\epsilon}{p^2+k^2-2pk\frac{\mu}{m_1}-2\mu E-i\epsilon}\right]. \tag{A.8}$$

At the same time, we multiply the amplitude with the wave function renomalization factor (A.6). We thus arrive at Eq. (5.3) which can then be rewritten using $H(\Lambda)/\Lambda^2 = -g_3/(4m_1g_2^2)$ (Eq. (5.5)),

$$\begin{aligned}
\mathcal{A}_S(p,k;E) &= \frac{2\pi m_1}{a\mu^2}\left[\frac{1}{2pk}\ln\left[\frac{p^2+k^2+2pk\frac{\mu}{m_1}-2\mu E-i\epsilon}{p^2+k^2-2pk\frac{\mu}{m_1}-2\mu E-i\epsilon}\right]+\frac{g_3}{4m_1g_2^2}\right] \\
&\quad +\frac{m_1}{\pi\mu}\int^{\Lambda}dq\,q^2\left[\frac{1}{2pq}\ln\left[\frac{p^2+q^2+2pq\frac{\mu}{m_1}-2\mu E-i\epsilon}{p^2+q^2-2pq\frac{\mu}{m_1}-2\mu E-i\epsilon}\right]+\frac{g_3}{4m_1g_2^2}\right] \\
&\quad \times\frac{\mathcal{A}_S(q,k;E)}{-1/a+\sqrt{-2\mu\Big(E-q^2/(2\mu_{\mathrm{AD}})\Big)-i\epsilon}}
\end{aligned}$$

$$
\begin{aligned}
= \quad & \frac{2\pi m_1}{a\mu^2}\left[\frac{1}{2pk}\ln\left[\frac{p^2+k^2+2pk\frac{\mu}{m_1}-2\mu E-i\epsilon}{p^2+k^2-2pk\frac{\mu}{m_1}-2\mu E-i\epsilon}\right]+\frac{H(\Lambda)}{\Lambda^2}\right] \\
& +\frac{m_1}{\pi\mu}\int^{\Lambda} dq\, q^2\left[\frac{1}{2pq}\ln\left[\frac{p^2+q^2+2pq\frac{\mu}{m_1}-2\mu E-i\epsilon}{p^2+q^2-2pq\frac{\mu}{m_1}-2\mu E-i\epsilon}\right]+\frac{H(\Lambda)}{\Lambda^2}\right] \\
& \times\frac{\mathcal{A}_S(q,k;E)}{-1/a+\sqrt{-2\mu\Big(E-q^2/(2\mu_{\mathrm{AD}})\Big)-i\epsilon}}\,. \qquad \text{(A.9)}
\end{aligned}
$$

As for identical bosons, $H(\Lambda)$ should fulfill Eq. (3.15) to ensure renormalization but can be set to zero in the practical calculations.

If instead of considering only S-waves, we want to derive the STM equation for general L, we project Eq. (A.7) with the help of Legendre polynomials onto the Lth partial wave,

$$
Q_L(z)=\frac{1}{2}\int_{-1}^{1} dx\,\frac{P_L(x)}{z-x}, \qquad \text{(A.10)}
$$

where $Q_L(z)$ is a Legendre polynomial of the second kind. Directly neglecting $H(\Lambda)$, this yields

$$
\begin{aligned}
\mathcal{A}_L(p,k;E) \quad = \quad & \frac{2\pi m_1}{a\mu^2}\frac{1}{pk}(-1)^L Q_L\left(\frac{p^2+k^2-2\mu E}{2pk\mu/m_1}\right) \\
& +\frac{m_1}{\pi\mu}\int_0^{\Lambda_{\mathrm{c}}} dq\,\frac{q}{p}(-1)^L Q_L\left(\frac{p^2+q^2-2\mu E}{2pq\mu/m_1}\right) \\
& \times\frac{\mathcal{A}_L(q,k;E)}{-1/a+\sqrt{-2\mu(E-q^2/(2\mu_{\mathrm{AD}}))}}\,, \qquad \text{(A.11)}
\end{aligned}
$$

as given in Eq. (6.3) for bosons.

If the particles of species 2 are fermionic, both summands on the right hand side acquire an additional factor of (-1) due to Fermi statistics.

A.2 Subtracted Equation

Here, the subtracted integral equation (5.15) is derived. For $k=0$, $E=0$, and the three-body force being zero, the S-wave STM equation (5.3) simplifies to

$$
\mathcal{A}_S(p)=\frac{4\pi}{a\mu p^2}+\frac{m_1}{2\pi\mu}\int_0^{\Lambda} dq\frac{q}{p}\ln\left[\frac{p^2+q^2+2pq\frac{\mu}{m_1}}{p^2+q^2-2pq\frac{\mu}{m_1}}\right]\frac{\mathcal{A}_S(q)}{-1/a+\sqrt{\frac{\mu}{\mu_{\mathrm{AD}}}}q}\,. \qquad \text{(A.12)}
$$

To obtain the subtracted and hence infrared finite amplitude $\bar{\mathcal{A}}_S$, the first three exchange terms have to be subtracted, as they contain the divergencies.

1. Tree diagram, $S1$

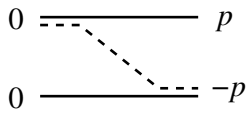

$$S1 = \frac{(-ig_2)^2}{-p^2/(2m_1) - p^2/(2m_2) + i\epsilon} = \frac{2\mu g_2^2}{p^2}\,. \tag{A.13}$$

2. One-loop diagram, $S2$

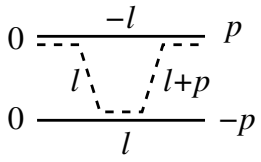

$$\begin{aligned} S2 \;=\; & (-ig_2)^4 \int \frac{dl_0}{2\pi}\,\frac{d^3l}{(2\pi)^3}\,\frac{i}{-l_0 - l^2/(2m_2) + i\epsilon}\,\frac{i}{l_0 - l^2/(2m_1) + i\epsilon} \\ & \times \frac{i}{l_0 + p_0 - (\vec{l}+\vec{p})^2/(2m_1) + i\epsilon}\,\frac{2\pi/(g_2^2\mu)}{1/a - \sqrt{-2\mu\,(-l_0 + l^2/(2M)) - i\epsilon}}\,. \end{aligned} \tag{A.14}$$

For the integration over l_0, we close the contour in the upper half plane and thus include the pole at $l_0 = -l^2/(2m_2) + i\epsilon$. We insert the on-shell energy $-p_0 = p^2/(2m_2)$ and expand the dimer propagator $a/\left(1 - a\sqrt{-2\mu l^2/(2\mu_{\rm AD}) - i\epsilon}\right) \approx a\left(1 + al\sqrt{\mu/\mu_{\rm AD}}\right)$. This leads to

$$S2 = -8\pi g_2^2 a\mu \int \frac{d^3l}{(2\pi)^3}\,\frac{1}{l^2 - i\epsilon}\,\frac{1}{l^2 + p^2 + 2\vec{p}\cdot\vec{l}\frac{\mu}{m_1} - i\epsilon}\left(1 + al\sqrt{\mu/\mu_{\rm AD}}\right)\,. \tag{A.15}$$

Now, we make use of a Feynman parameter to further develop the integral. The auxiliary calculation is:

$$\begin{aligned} \frac{1}{l^2}\,\frac{1}{l^2 + p^2 + 2\vec{p}\cdot\vec{l}\frac{\mu}{m_1}} &= \int_0^1 dz\left[(1-z)l^2 + z\left(l^2 + p^2 + 2\vec{p}\cdot\vec{l}\frac{\mu}{m_1}\right)\right]^{-2} \\ &= \int_0^1 dz\left[l^2 + zp^2 + 2z\vec{p}\cdot\vec{l}\frac{\mu}{m_1}\right]^{-2} \\ &= \int_0^1 dz\left[l^2 + p^2 z\left(1 - z\left(\frac{\mu}{m_1}\right)^2\right)\right]^{-2}\,, \end{aligned} \tag{A.16}$$

where, in the last step, the substitution $\vec{l} \to \vec{l} - \vec{p}z\frac{\mu}{m_1}$ was used. This yields

$$\begin{aligned} S2 &= -\frac{8\pi g_2^2 a\mu}{(2\pi)^3} 4\pi \int dl \int_0^1 dz\left[\frac{l^2}{[l^2 + p^2 z(1 - z(\frac{\mu}{m_1})^2)]^2} + \frac{al^3\sqrt{\mu/\mu_{\rm AD}}}{[l^2 + p^2 z(1 - z(\frac{\mu}{m_1})^2)]^2}\right] \\ &= -\frac{4g_2^2 a\mu}{\pi}\left[\int_0^1 dz \frac{\pi}{2p}\,\frac{1}{2\sqrt{z - z^2(\frac{\mu}{m_1})^2}}\right. \end{aligned}$$

$$
\begin{aligned}
& -a\sqrt{\frac{\mu}{\mu_{\rm AD}}}\int_0^1 dz\frac{1}{2}\left\{1+\ln\left(p^2 z\left(1-z\left(\frac{\mu}{m_1}\right)^2\right)\right)\right\}\Bigg] \\
= & -\frac{4g_2^2 a\mu}{\pi}\left[\frac{\pi}{2p}\arcsin\left(\frac{\mu}{m_1}\right)\frac{m_1}{\mu}-a\sqrt{\frac{\mu}{\mu_{\rm AD}}}\ln(p)\right]. \qquad \text{(A.17)}
\end{aligned}
$$

3. Two-loop diagram, $S3$

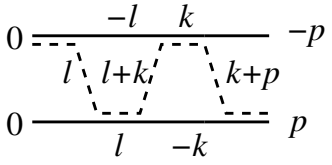

$$
\begin{aligned}
S3 = & (-ig_2)^6\int\frac{dl_0}{2\pi}\frac{d^3l}{(2\pi)^3}\int\frac{dk_0}{2\pi}\frac{d^3k}{(2\pi)^3}\frac{i}{l_0-l^2/(2m_1)+i\epsilon}\frac{i}{-l_0-l^2/(2m_2)+i\epsilon} \\
& \times\frac{i}{-k_0-k^2/(2m_2)+i\epsilon}\frac{i}{l_0+k_0-(\vec{l}+\vec{k})^2/(2m_1)+i\epsilon} \\
& \times\frac{i}{k_0+p_0-(\vec{k}+\vec{p})^2/(2m_2)+i\epsilon}\,i\left(\frac{2\pi}{g_2^2\mu}\right)^2 \\
& \times\frac{1}{1/a-\sqrt{-l_0+l^2/(2M)-i\epsilon}}\frac{1}{1/a-\sqrt{-k_0+k^2/(2M)-i\epsilon}}. \qquad \text{(A.18)}
\end{aligned}
$$

For the l_0 integration, we close the contour on the upper half plane and have to consider the poles $l_0=-l^2/(2m_2)+i\epsilon$ and $k_0=-k^2/(2m_2)+i\epsilon$. We make use of the on-shell condition $-p_0=p^2/(2m_2)$ and expand the two dimer propagators, yielding the prefactor times a^2. We obtain

$$
\begin{aligned}
S3 = & -g_2^2a^2\frac{(2\pi)^2}{\mu^2}\int\frac{d^3l}{(2\pi)^3}\int\frac{d^3k}{(2\pi)^3}\frac{-2\mu}{l^2-i\epsilon}\frac{-2\mu}{l^2+k^2+2\vec{l}\cdot\vec{k}\frac{\mu}{m_1}}\frac{-2\mu}{p^2+k^2+2\vec{p}\cdot\vec{k}\frac{\mu}{m_1}} \\
= & \frac{g_2^2\mu a^2}{2\pi^4}(2\pi)^2\int dk\,k^2\int_{-1}^1 dx_1\int dl\,l^2\int_{-1}^1 dx_2\frac{1}{l^2}\frac{1}{l^2+k^2+2lkx_1\frac{\mu}{m_1}} \\
& \times\frac{1}{p^2+k^2+2pkx_2\frac{\mu}{m_1}} \\
= & \frac{2g_2^2\mu a^2}{\pi^2}\int dk\,k^2\int dl\,l^2\frac{1}{l^2}\frac{m_1}{2lk\mu}\ln\left[\frac{l^2+k^2+2lk\frac{\mu}{m_1}}{l^2+k^2-2lk\frac{\mu}{m_1}}\right]\frac{m_1}{2pk\mu} \\
& \times\ln\left[\frac{p^2+k^2+2pk\frac{\mu}{m_1}}{p^2+k^2-2pk\frac{\mu}{m_1}}\right] \\
= & \frac{g_2^2a^2m_1^2}{2\mu\pi^2p}\int dk\ln\left[\frac{p^2+k^2+2pk\frac{\mu}{m_1}}{p^2+k^2-2pk\frac{\mu}{m_1}}\right]\int dl\,\frac{1}{l}\ln\left[\frac{l^2+k^2+2lk\frac{\mu}{m_1}}{l^2+k^2-2lk\frac{\mu}{m_1}}\right], \qquad \text{(A.19)}
\end{aligned}
$$

where we used Eq. (A.8) twice. First, we consider the l-integral and rewrite it using $\tilde{l}=l/k$,

$$
\int\frac{dl}{l}\ln\left[\frac{l^2+k^2+2lk\frac{\mu}{m_1}}{l^2+k^2-2lk\frac{\mu}{m_1}}\right]=\int\frac{d\tilde{l}}{\tilde{l}}\ln\left[\frac{\tilde{l}^2+1+2\tilde{l}\frac{\mu}{m_1}}{\tilde{l}^2+1-2\tilde{l}\frac{\mu}{m_1}}\right]=2\pi\arcsin\left(\frac{\mu}{m_1}\right), \qquad \text{(A.20)}
$$

which is valid for $0 < \frac{\mu}{m_1} = \frac{m_2}{M} < 1$ being naturally fulfilled. The second integral to be considered is

$$\int dk \ln\left[\frac{p^2+k^2+2pk\frac{\mu}{m_1}}{p^2+k^2-2pk\frac{\mu}{m_1}}\right] = -4\frac{\mu}{m_1}\ln(p)p\,. \tag{A.21}$$

Therefore, we obtain

$$S3 = -\frac{4g_2^2a^2m_1}{\pi}\arcsin\left(\frac{\mu}{m_1}\right)\ln(p)\,. \tag{A.22}$$

The subtracted equation we want to derive is now given by

$$\begin{aligned}\bar{\mathcal{A}}_S(p) &= \mathcal{A}_S(p) - Z_{\rm D}\,(S1+S2+S3)\\ &= \mathcal{A}_S(p) - \frac{4\pi}{a\mu p^2} + \frac{4\pi m_1}{p\mu^2}\arcsin\left(\frac{\mu}{m_1}\right)\\ &\quad +\frac{8a}{\mu}\left[\arcsin\left(\frac{\mu}{m_1}\right)\frac{m_1}{\mu} - \sqrt{\frac{\mu}{\mu_{\rm AD}}}\right]\ln(p)\,.\end{aligned} \tag{A.23}$$

Solving Eq. (A.23) for $\mathcal{A}_S$ and inserting this into Eq. (A.12), we find the final equation

$$\begin{aligned}\bar{\mathcal{A}}_S(p) &= -\frac{4\pi}{a\mu p^2} + \frac{4\pi m_1}{p\mu^2}\arcsin\left(\frac{\mu}{m_1}\right) + \frac{8a}{\mu}\left[\arcsin\left(\frac{\mu}{m_1}\right)\frac{m_1}{\mu} - \sqrt{\frac{\mu}{\mu_{\rm AD}}}\right]\ln(p)\\
&\quad +\frac{4\pi}{a\mu p^2} + \frac{m_1}{2\pi\mu}\int_0^\Lambda dq\frac{q}{p}\ln\left[\frac{p^2+q^2+2pq\frac{\mu}{m_1}}{p^2+q^2-2pq\frac{\mu}{m_1}}\right]\frac{\bar{\mathcal{A}}_S(q)}{-1/a+\sqrt{\frac{\mu}{\mu_{\rm AD}}}\,q}\\
&\quad +\frac{m_1}{2\pi\mu}\int_0^\Lambda dq\frac{q}{p}\ln\left[\frac{p^2+q^2+2pq\frac{\mu}{m_1}}{p^2+q^2-2pq\frac{\mu}{m_1}}\right]\frac{1}{-1/a+\sqrt{\frac{\mu}{\mu_{\rm AD}}}\,q}\\
&\quad \times\left\{\frac{4\pi}{a\mu q^2} - \frac{4\pi m_1}{q\mu^2}\arcsin\left(\frac{\mu}{m_1}\right) - \frac{8a}{\mu}\left[\arcsin\left(\frac{\mu}{m_1}\right)\frac{m_1}{\mu} - \sqrt{\frac{\mu}{\mu_{\rm AD}}}\right]\ln(q)\right\}\\
&= -\int_0^\Lambda dq\frac{q}{p}\ln\left[\frac{p^2+q^2+2pq\frac{\mu}{m_1}}{p^2+q^2-2pq\frac{\mu}{m_1}}\right]\frac{\arcsin\left(\frac{\mu}{m_1}\right)\frac{m_1}{\mu} - \sqrt{\frac{\mu}{\mu_{\rm AD}}}}{-1/a+\sqrt{\frac{\mu}{\mu_{\rm AD}}}\,q}\frac{4am_1}{\pi\mu^2}\\
&\quad \times\left(\ln(q) + \sqrt{\frac{\mu}{\mu_{\rm AD}}}\frac{\pi}{2}\right)\\
&\quad +\frac{2am_1}{\mu^2}\left(\arcsin\left(\frac{\mu}{m_1}\right)\frac{m_1}{\mu} - \sqrt{\frac{\mu}{\mu_{\rm AD}}}\right)\left\{2\sqrt{1-\left(\frac{\mu}{m_1}\right)^2}\arctan\left(\frac{-\frac{\mu}{m_1}+\frac{p}{\Lambda}}{\sqrt{1-\left(\frac{\mu}{m_1}\right)^2}}\right)\right.\\
&\quad -2\sqrt{1-\left(\frac{\mu}{m_1}\right)^2}\arctan\left(\frac{\frac{\mu}{m_1}+p/\Lambda}{\sqrt{1-\left(\frac{\mu}{m_1}\right)^2}}\right) + 4\frac{\mu}{m_1}\ln(\Lambda)\\
&\quad \left.+\left(\frac{\mu}{m_1}+\frac{\Lambda}{p}\right)\ln\left(1+2\frac{\mu}{m_1}\frac{p}{\Lambda}+\frac{p^2}{\Lambda^2}\right) + \left(\frac{\mu}{m_1}-\frac{\Lambda}{p}\right)\ln\left(1-2\frac{\mu}{m_1}\frac{p}{\Lambda}+\frac{p^2}{\Lambda^2}\right)\right\}\end{aligned}$$

$$
\begin{aligned}
&-\frac{2m_1}{\mu^2 p}\Bigg(\mathrm{Li}_2\Big(-e^{i\arccos(\frac{\mu}{m_1})}\frac{p}{\Lambda}\Big)+\mathrm{Li}_2\Big(-e^{-i\arccos(\frac{\mu}{m_1})}\frac{p}{\Lambda}\Big)\\
&-\mathrm{Li}_2\Big(e^{i\arccos(\frac{\mu}{m_1})}\frac{p}{\Lambda}\Big)-\mathrm{Li}_2\Big(e^{-i\arccos(\frac{\mu}{m_1})}\frac{p}{\Lambda}\Big)\Bigg)\\
&+\frac{m_1}{2\pi\mu}\int_0^\Lambda dq\,\frac{q}{p}\,\ln\left[\frac{p^2+q^2+2pq\frac{\mu}{m_1}}{p^2+q^2-2pq\frac{\mu}{m_1}}\right]\frac{\bar{\mathcal{A}}_S(q)}{-1/a+\sqrt{\frac{\mu}{\mu_{\mathrm{AD}}}}\,q}\,,
\end{aligned}
\tag{A.24}
$$

where we left out a few calculational details on the very last step. The function $\mathrm{Li}_2(z)$ is the dilogarithm defined as

$$
\mathrm{Li}_2(z)=\int_0^z dt\,\frac{\mathrm{Li}_1(t)}{t}=\int_0^z dt\,\frac{-\ln(1-t)}{t}\,. \tag{A.25}
$$

For the numerical evaluation, it can be taken from the GNU Scientific Library where it is implemented as a special function [gsl].

A.3 Determining s_L

In this section, we want to give a few further details on the derivation of Eq. (6.6). We start directly from Eq. (6.5), which is already simplified for large momenta. It is given by

$$
\tilde{\mathcal{A}}_L(p)=(\pm1)(-1)^L\frac{m_1}{\pi\mu}\sqrt{\frac{\mu_{\mathrm{AD}}}{\mu}}\int_0^\infty\frac{dq}{q}\,P_L\left(\frac{p^2+q^2}{2pq\mu/m_1}\right)\,Q_0\left(\frac{p^2+q^2}{2pq\mu/m_1}\right)\tilde{\mathcal{A}}_L(q)\,, \tag{A.26}
$$

where

$$
\sin\phi=\frac{1}{\delta+1}=\frac{\mu}{m_1}\quad\Longleftrightarrow\quad\cos\phi=\frac{\sqrt{\delta(\delta+2)}}{\delta+1}=\sqrt{\frac{\mu}{\mu_{\mathrm{AD}}}}\,, \tag{A.27}
$$

and $\tilde{\mathcal{A}}_L(p)=p\mathcal{A}_L(p,k;E)\propto p^{\pm is_L}$.

Furthermore, we make use of the series representation of P_L,

$$
P_L(x)=\sum_{k=0}^{k_{\max}}(-1)^k\frac{(2L-2k)!\;x^{L-2k}}{(L-k)!\;(L-2k)!\;k!\;2^L}\,, \tag{A.28}
$$

where

$$
k_{\max}=\begin{cases}L/2 & \text{if } L \text{ is even}\\ (L-1)/2 & \text{if } L \text{ is odd}\end{cases}\,. \tag{A.29}
$$

The Mellin transform of a function $f(x)$ is defined as

$$
\mathcal{M}[f;s]:=\int_0^\infty dx\,x^{s-1}\,f(x)\quad\text{if}\quad\int_0^\infty\frac{dx}{x}\,|f(x)|^2\ \text{exists}\,. \tag{A.30}
$$

The Mellin transform of the zeroth order Legendre function of the second kind Q_0 is given by [EMOT54]

$$
\mathcal{M}\left[\ln\left(\frac{1+x^2+2x\sin\phi}{1+x^2-2x\sin\phi}\right);s\right]=\frac{2\pi}{s}\,\frac{\sin[s\phi]}{\cos[s\pi/2]}\,, \tag{A.31}
$$

and we know [EMOT54]

$$\mathcal{M}[x^a f(x); s] = \mathcal{M}[f; s+a]\,. \tag{A.32}$$

Including the binomial expansion

$$(x+x^{-1})^j = \sum_m^j \frac{j!}{m!\,(j-m)!} x^{j-m} y^{-m}\,, \tag{A.33}$$

we have all formulae at hand to obtain

$$\begin{aligned} 1 \;=\; & \pm \frac{(-1)^L}{\sin(2\phi)} \sum_{k=0}^{k_{\max}} \frac{(2L-2k)!}{(L-k)!\,k!} \frac{(-1)^k}{2^{2L-2k}(\sin\phi)^{L-2k}} \\ & \times \sum_{m=0}^{L-2k} \frac{1}{m!\,(L-2k-m)!} \frac{2}{is_L+2m-L+2k} \frac{\sin\left[(is_L+2m-L+2k)\phi\right]}{\cos\left[(is_L+2m-L+2k)\frac{\pi}{2}\right]}\,, \end{aligned} \tag{A.34}$$

corresponding to Eq. (6.6).

Note that there is another method to derive s_L. We start with

$$\tilde{\mathcal{A}}_L(p) \;=\; (\pm 1)(-1)^L \frac{m_1}{\pi\mu} \sqrt{\frac{\mu_{\rm AD}}{\mu}} \int_0^\infty \frac{dq}{q}\, Q_L\left(\frac{p^2+q^2}{2pq\mu/m_1}\right) \tilde{\mathcal{A}}_L(q)\,, \tag{A.35}$$

and insert the hyperspherical representation of $Q_L\left((x+x^{-1})/(2\sin\phi)\right)$ along the lines of [Gr05]. This leads to

$$\begin{aligned} 1 \;=\; & (\pm 1)(-1)^L \frac{2^{L+1}}{\pi} \frac{(\sin\phi)^L}{\cos\phi} \frac{\Gamma\left(\frac{L+1+is_L}{2}\right)\Gamma\left(\frac{L+1-is_L}{2}\right)}{\Gamma\left(\frac{3+2L}{2}\right)} \\ & \times {}_2F_1\left(\frac{L+1+is_L}{2}, \frac{L+1-is_L}{2}; \frac{3+2L}{2}; \sin^2\phi\right)\,, \end{aligned} \tag{A.36}$$

which is completely equivalent to Eq. (117) of [NFJG01]. However, both equations, (A.34) and (A.36) yield the same results for s_L up to about 12 digits for all tested values of L and δ.

Appendix B

Integration Elements and Phase Space Factors

Here, we want to show how to calculate hyperspherical integration elements and phase space factors in two and three spatial dimensions. The case of $2D$ is used in Chapter 7. For $3D$, the derived equations are not used in the thesis but could, in principle, be helpful for an extension to Chapter 6 for the calculation of three-body recombination rates at finite temperatures.

B.1 Integration Elements

For the general hyperspherical integration element, the first coordinate transformations to Jacobi coordinates are given by

$$\begin{aligned} p_{\mathrm{tot}} &= p_1 + p_2 + p_3 \,, \\ p_{12} &= \frac{m_1+m_2}{2m_1}\, p_1 - \frac{m_1+m_2}{2m_2}\, p_2 \,, \\ p_{3,12} &= p_3 - \frac{m_2}{m_1+m_2}\,(p_1+p_2) \,. \end{aligned} \tag{B.1}$$

Subsequently, the collision energy and the hyperangle are introduced as

$$\begin{aligned} E &= \frac{2m_1m_2}{(m_1+m_2)^3}\, p_{12}^2 + \frac{m_1+m_2}{2m_2(m_1+2m_2)}\, p_{3,12}^2 \,, \\ \alpha &= \arctan\left(\frac{2\sqrt{m_1 m_2^2 (m_1+2m_2)}}{(m_1+m_2)^2}\, \frac{p_{12}}{p_{3,12}} \right) \,, \end{aligned} \tag{B.2}$$

and we do not need to change the center-of-mass momentum. Calculating the determinants of the corresponding Jacobi matrices leads to the integration elements. For $3D$, we obtain

$$d^3p_1\, d^3p_2\, d^3p_3 = \frac{m_2\sqrt{m_1+2m_2}\,(m_1+m_2)^2}{4\sqrt{m_1}}\, \sin^2 2\alpha\, d\alpha\, E^2\, dE\, d\Omega_{12}\, d\Omega_{3,12}\, d^3p_{\mathrm{tot}} \,. \tag{B.3}$$

And for $2D$, the result (now for three identical bosons, $m_1 = m_2 = m$) is given by

$$d^2p_1\, d^2p_2\, d^2p_3 = m^2\, \sin(2\alpha_3)\, d\alpha_3\, E\, dE\, d\varphi_{12}\, d\varphi_{3,12}\, d^2p_{\mathrm{tot}} \,, \tag{B.4}$$

corresponding to Eq. (7.19).

B.2 Phase Space Factors

For two different atomic species in $3D$, the three-atom phase space is given by

$$\begin{aligned} PS_{\mathrm{AAA}}^{(3D)} &= \int \frac{d^3p_1}{(2\pi)^3}\frac{d^3p_2}{(2\pi)^3}\frac{d^3p_3}{(2\pi)^3}(2\pi)^4\,\delta^3\left(\vec{p}_1+\vec{p}_2+\vec{p}_3\right)\,\delta\left(\frac{p_1^2}{2m_1}+\frac{p_2^2}{2m_2}+\frac{p_3^2}{2m_2}-E\right) \\ &= \frac{m_2^3\,E^2}{32\pi^3\left(2\,m_2/\mu-1\right)^{3/2}}\int d\Omega\,. \end{aligned} \tag{B.5}$$

The atom-dimer phase space is

$$\begin{aligned} PS_{\mathrm{AD}}^{(3D)} &= \int \frac{d^3p_{\mathrm{A}}}{(2\pi)^3}\frac{d^3p_{\mathrm{D}}}{(2\pi)^3}(2\pi)^4\,\delta^3\left(\vec{p}_{\mathrm{A}}+\vec{p}_{\mathrm{D}}\right)\,\delta\left(\frac{p_{\mathrm{A}}^2}{2m_2}+\frac{p_{\mathrm{D}}^2}{2M}-E\right) \\ &= \frac{\mu_{\mathrm{AD}}}{4\pi^2}\,k\int d\Omega\,, \end{aligned} \tag{B.6}$$

and the atom-dimer relative velocity is

$$v_{\mathrm{AD}}^{(3D)} = \frac{k}{\mu_{\mathrm{AD}}}\,. \tag{B.7}$$

The relation between the hyperangular average of the three-body recombination rate and the atom-dimer inelastic scattering cross section, when no deep dimers are present, is then given by

$$\begin{aligned} K^{(3D)}(E) &= 2\,v_{\mathrm{AD}}^{(3D)}\,\frac{PS_{\mathrm{AD}}^{(3D)}}{PS_{\mathrm{AAA}}^{(3D)}}\,\sigma_{\mathrm{AD}}^{(\mathrm{inel},3D)}(E) \\ &= \frac{32\pi\hbar^3\mu_{AD}\left(E+E_{\mathrm{D}}\right)\left(\frac{2m_2}{\mu}-1\right)^{3/2}}{m_2^3\,E^2}\,\sigma_{AD}^{(\mathrm{inel},3D)}(E)\,. \end{aligned} \tag{B.8}$$

where the factor of 2 arises because there are two ways to choose one of the two indistinguishable particles to form a dimer.

In $2D$, the analogous considerations (now for three identical particles) yield

$$\begin{aligned} PS_{\mathrm{AAA}}^{(3D)} &= \int \frac{d^2p_1}{(2\pi)^2}\frac{d^2p_2}{(2\pi)^2}\frac{d^2p_3}{(2\pi)^2}(2\pi)^3\,\delta^2\left(\vec{p}_1+\vec{p}_2+\vec{p}_3\right)\,\delta\left(\frac{p_1^2}{2m}+\frac{p_2^2}{2m}+\frac{p_3^2}{2m}-E\right) \\ &= \frac{m^2E}{6\pi}\,, \end{aligned} \tag{B.9}$$

$$\begin{aligned} PS_{\mathrm{AD}}^{(2D)} &= \int \frac{d^2p_{\mathrm{A}}}{(2\pi)^2}\frac{d^2p_{\mathrm{D}}}{(2\pi)^2}(2\pi)^3\,\delta^3\left(\vec{p}_{\mathrm{A}}+\vec{p}_{\mathrm{D}}\right)\,\delta\left(\frac{p_{\mathrm{A}}^2}{2m_2}+\frac{p_{\mathrm{D}}^2}{2M}-E\right) \\ &= \frac{2m}{3}\,, \end{aligned} \tag{B.10}$$

$$v_{\mathrm{AD}}^{(2D)} = \frac{3k}{2m}\,, \tag{B.11}$$

and

$$\begin{aligned} K^{(2D)}(E) &= 3!\, v_{\mathrm{AD}}^{(2D)} \frac{PS_{\mathrm{AD}}^{(2D)}}{PS_{\mathrm{AAA}}^{(2D)}} \sigma_{\mathrm{AD}}^{(\mathrm{inel},2D)}(E) \\ &= \frac{36\pi\hbar^2}{m^2 E}\, k\, \sigma_{\mathrm{AD}}^{(\mathrm{inel},2D)}(E)\,, \end{aligned} \tag{B.12}$$

where $3! = 6$ accounts for the three indistinguishable particles and the resulting equation corresponds to Eq. (7.20).

Appendix C

Numerical Procedure

Most of the results presented in this thesis have been derived numerically. Therefore, we give a short account on the numerical procedure in this appendix. We start with general remarks on the discretization followed by two strategies to deal with functions that have poles.

C.1 General Remarks

Quite generally, the integral equation we want to solve is of the form known as a *Fredholm equation of the second kind*,

$$f(p) = h(p) + \int_0^\Lambda dq\, K(p,q)\, f(q)\,, \tag{C.1}$$

with the kernel $K(p,q)$. The first step for the numerical solution of this equation consists in discretizing the above equation,

$$\begin{aligned} f(p_i) &= h(p_i) + \sum_{j=1}^{N} w_j\, K(p_i,q_j)\, f(q_j) \\ \Longleftrightarrow \quad f_i &= h_i + \sum_{j=1}^{N} w_j\, K_{ij}\, f_j\,, \end{aligned} \tag{C.2}$$

where at the same time the integral is replaced by a weighted sum with w_j denoting the weights. The kernel is now given by the matrix K_{ij}. We make use of the *Gauss-Legendre* integration to determine the points p_i with the corresponding weights w_j. The algorithm for Gauss-Legendre integration, its implementation, and more details can be found in Chapter 4 of Ref. [PTVF92].

This Fredholm equation can now be rewritten as

$$\left(\delta_{ij} - \sum_{j=1}^{N} w_j\, K_{ij}\right) f_j = h_j\,. \tag{C.3}$$

For a well behaved kernel, it can be solved numerically according to the procedure described in Chapter 18 of Ref. [PTVF92].

Whenever a scattering amplitude $\mathcal{A}$ is computed in the presence of the Efimov effect, it shows log-periodic behavior. It is therefore very useful to choose the mesh points for the Gaussian integration on a logarithmic grid. This was done with the help of the following substitution,

$$\tilde{p} = \ln(p+1) \quad \Leftrightarrow \quad p = e^{\tilde{p}} - 1\,. \tag{C.4}$$

The interval translates from $0 \leq p \leq \Lambda$ to $0 \leq \tilde{p} \leq \ln(\Lambda+1)$. The integration element is given by

$$dp = e^{\tilde{p}}\, d\tilde{p}\,. \tag{C.5}$$

If an integration should span the interval from zero to infinity for x, we used the following substitution,

$$x' = \frac{x}{1+x} \quad \Leftrightarrow \quad x = \frac{x'}{1-x'}\,, \tag{C.6}$$

for $0 \leq x' \leq 1$. The integration element is then given by

$$dx = \frac{1}{(1-x')^2}\, dx'\,. \tag{C.7}$$

C.2 Poles with Direct Procedure

The scattering amplitudes $\mathcal{A}$ we are interested in usually contain kernels with a pole. To treat them adequately, there are two possible strategies and we made use of both for the derivation of all numerical results, depending on the exact requirements of each case.

To include a pole at $q = q_0 + i\epsilon$ directly, we rewrite Eq. (C.1),

$$f(p) = h(p) + \int_0^\Lambda dq\, \frac{\tilde{K}(p,q)}{q - q_0 - i\epsilon}\, f(q)\,, \tag{C.8}$$

and thus separate the pole structure from the kernel, $K(p,q) = \frac{\tilde{K}(p,q)}{q-q_0-i\epsilon}$. Now, we can make use of the Sokhatsky-Weierstrass theorem,

$$\lim_{\epsilon\to 0^+} \int_a^b \frac{f(x)}{x \pm i\epsilon}\, dx = \mp i\pi\, f(0) + \mathcal{P}\int_a^b \frac{f(x)}{x}\, dx\,, \tag{C.9}$$

where $\mathcal{P}$ denotes the principal value. Adding a zero leads to

$$f(p) = h(p) + \int_0^\Lambda dq\, \frac{\tilde{K}(p,q)f(q) - \tilde{K}(p,q_0)f(q_0)}{q-q_0} + \tilde{K}(p,q_0)\, f(q_0)\left(i\pi + \mathcal{P}\int_0^\Lambda \frac{dq}{q-q_0}\right). \tag{C.10}$$

The last integral is just given by $\ln\left(\frac{\Lambda-q_0}{q_0}\right)$. Implementing this equation in the numerical procedure, we now need one more mesh point to incorporate the pole position, $q_{N+1} \equiv q_0$. This yields

$$f_i = h_i + \sum_{j=1}^N w_j\, K_{ij}\, f_j + \tilde{K}_{iN+1}\, f_{N+1}\left(i\pi + \ln\left(\frac{\Lambda-q_0}{q_0}\right) - \sum_{k=1}^N \frac{w_k}{p_k - p_{N+1}}\right). \tag{C.11}$$

These are N equations for $N+1$ unknown functions f_i, so we can set up the $N+1$th equation,

$$f_{N+1} = h_{N+1} + \sum_{j=1}^{N} w_j \, K_{N+1j} \, f_j + \tilde{K}_{N+1N+1} \, f_{N+1} \left(i\pi + \ln\left(\frac{\Lambda - q_0}{q_0}\right) - \sum_{k=1}^{N} \frac{w_k}{p_k - p_{N+1}} \right) . \tag{C.12}$$

The equivalent of Eq. (C.3) now looks like

$$\left(\delta_{ij} - \sum_{j=1}^{N+1} \mathcal{M}_{ij} \right) f_j = h_j \, , \tag{C.13}$$

with $1 \leq i \leq N+1$ and the matrix $\mathcal{M}$ being defined as

$$\mathcal{M}_{ij} = \begin{cases} w_j \, K_{ij} & \text{for } j \leq N \\ \tilde{K}_{iN+1} \, f_{N+1} \left(i\pi + \ln\left(\frac{\Lambda - q_0}{q_0}\right) - \sum_{k=1}^{N} \frac{w_k}{p_k - p_{N+1}} \right) & \text{for } j = N+1 \end{cases} . \tag{C.14}$$

C.3 Poles with Contour Deformation

If the kernel has more than one pole or a complicated structure, the procedure described in the previous section might not be easily applicable. Another way to deal with the singularities numerically is contour deformation as a rotation into the complex plane. With this procedure, it is possible to circumvent the pole. The desired result should not depend on the angle of rotation. However, for the inclusion of deeply bound dimers with the help of a complex cutoff containing the parameter η_*, it is actually obligatory to use a deformed contour and the rotation angle then acquires a physical meaning. Therefore, in this case, the rotation has to be counterclockwise, because this corresponds to a positive value of η_*, using $e^{i\eta_*/s_L}$ as rotation.

For the implementation, we start again with Eq. (C.1) and rotate the momenta p and q with a general rotation angle φ,

$$f(pe^{i\varphi}) = h(pe^{i\varphi}) + \int_0^\Lambda dq \, e^{i\varphi} \, K(pe^{i\varphi}, qe^{i\varphi}) \, f(qe^{i\varphi}) \, . \tag{C.15}$$

If during the rotation no pole is hit (e.g., if the pole lies in the upper half plane and the rotation uses a negative angle), this equation can be discretized and used along the lines of Section C.1. In a final step, an interpolation with the help of the now known function f back onto the real axis is used. If, however, one crosses a pole in the rotation procedure, its contribution has to be accounted for. This can be done via the residual theorem or a direct inclusion with the help of Section C.2. Note that we only consider functions where it is not necessary to close the contour explicitly.

Bibliography

[Ad86] S.K. Adhikari, *Quantum scattering in two dimensions*, Am. J. Phys. **54**, 362 (1986).

[AG92] S.K. Adhikari and W.G. Gibson, *Low-energy behavior of few-particle scattering amplitudes in two dimensions*, Phys. Rev. A **46**, 3967 (1992).

[AN72] R.D. Amado and J.V. Noble, *Efimov's Effect: A New Pathology of Three-Particle Systems. II*, Phys. Rev. D **5**, 1992 (1972).

[An$^+$95] M.H. Anderson, J.R. Ensher, M.R. Matthews, C.E. Wieman, and E.A. Cornell, *Observation of Bose-Einstein Condensation in a Dilute Atomic Vapor*, Science **269**, 198 (1995).

[Bi] M. Birse, private communication.

[Bl] D. Blume, private communication.

[Bl05] D. Blume, *Threshold behavior of bosonic two-dimensional few-body systems*, Phys. Rev. B **72**, 094510 (2005) [arXiv:cond-mat/0507729].

[Bo24] S. Bose, *Plancks Gesetz und Lichtquantenhypothese*, Zeitschr. f. Physik, **26**, 178 (1924) [DOI: 10.1007/BF01327326].

[BBH00] P.F. Bedaque, E. Braaten, and H.-W. Hammer, *Three-body recombination in Bose gases with large scattering length*, Phys. Rev. Lett. **85**, 908 (2000) [arXiv:cond-mat/0002365].

[BDZ08] I. Bloch, J. Dalibard, and W. Zwerger, *Many-Body Physics with Ultracold Gases*, Rev. Mod. Phys. **80**, 885 (2008) [arXiv:0704.3011 [cond-mat.other]].

[BH03] E. Braaten and H.-W. Hammer, *Universality in the Three-Body Problem for ^{4}He Atoms*, Phys. Rev. A **67**, 042706 (2003) [arXiv:cond-mat/0203421].

[BH04] E. Braaten and H.-W. Hammer, *Enhanced Dimer Relaxation in an Atomic and Molecular BEC*, Phys. Rev. A **70**, 042706 (2004) [arXiv:cond-mat/0303249].

[BH06] E. Braaten and H.-W. Hammer, *Universality in Few-body Systems with Large Scattering Length*, Phys. Rept. **428**, 259 (2006) [arXiv:cond-mat/0410417].

[BH07a] E. Braaten and H.-W. Hammer, *Resonant Dimer Relaxation in Cold Atoms with a Large Scattering Length*, Phys. Rev. A **75**, 052710 (2007) [arXiv:cond-mat/0610116], see Erratum in Phys. Rev. A **79**, 039905(E) (2009).

[BH07b] E. Braaten and H.-W. Hammer, *Efimov Physics in Cold Atoms*, Annals Phys. **322**, 120 (2007) [arXiv:cond-mat/0612123].

[BHKP08] E. Braaten, H.-W. Hammer, D. Kang, and L. Platter, *Three-Body Recombination of Identical Bosons with a Large Positive Scattering Length at Nonzero Temperature*, Phys. Rev. A **78**, 043605 (2008) [arXiv:0801.1732 [cond-mat.other]].

[BHKP09] E. Braaten, H.-W. Hammer, D. Kang, and L. Platter, *Three-body Recombination of Lithium-6 Atoms with Large Negative Scattering Lengths*, Phys. Rev. Lett. **103**, 073202 (2009) [arXiv:0811.3578 [cond-mat.other]].

[BHKP10] E. Braaten, H.-W. Hammer, D. Kang, and L. Platter, *Efimov Physics in 6Li Atoms*, Phys. Rev. A **81**, 013605 (2010) [arXiv:0908.4046 [cond-mat.quant-gas]].

[BHvK99a] P.F. Bedaque, H.-W. Hammer, and U. van Kolck, *Renormalization of the Three-Body System with Short-Range Interactions*, Phys. Rev. Lett. **82**, 463 (1999) [arXiv:nucl-th/9809025].

[BHvK99b] P.F. Bedaque, H.-W. Hammer, and U. van Kolck, *The Three-Boson System with Short-Range Interactions*, Nucl. Phys. A **646**, 444 (1999) [arXiv:nucl-th/9811046].

[BKP07] E. Braaten, D. Kang, and L. Platter, *Universality Constraints on Three-Body Recombination for Cold Atoms: from 4He to 133Cs*, Phys. Rev. A **75**, 052714 (2007) [arXiv:cond-mat/0612601].

[BP07] V.A. Babenko and N.M. Petrov, *Determination of Low-Energy Parameters of Neutron–Proton Scattering on the Basis of Modern Experimental Data from Partial-Wave Analyses*, Phys. Atom. Nucl. **70**, 669 (2007) [arXiv:0704.1024 [nucl-th]].

[BSTH95] C.C. Bradley, C.A. Sackett, J.J. Tollett, and R.G. Hulet, *Evidence of Bose-Einstein Condensation in an Atomic Gas with Attractive Interactions*, Phys. Rev. Lett. **75**, 1687 (1995).

[BT79] L.W. Bruch and J.A. Tjon, *Binding of three identical bosons in two dimensions*, Phys. Rev. A **19**, 425 (1979).

[Ba^+09] G. Barontini, C. Weber, F. Rabatti, J. Catani, G. Thalhammer, M. Inguscio, and F. Minardi, *Observation of Heteronuclear Atomic Efimov Resonances*, Phys. Rev. Lett. **103**, 043201 (2009) [arXiv:0901.4584 [cond-mat.other]], see Erratum in Phys. Rev. Lett. **104**, 059901(E) (2010).

[Be^+11] F.F. Bellotti, T. Frederico, M.T. Yamashita, D.V. Fedorov, A.S. Jensen, and N.T. Zinner, *Scaling and universality in two dimensions: three-body bound states with short-ranged interactions*, arXiv:1107.3017 [cond-mat.quant-gas] (2011).

[Br$^+$06] I.V. Brodsky, M.Yu. Kagan, A.V. Klaptsov, R. Combescot, and X. Leyronas, *Exact diagrammatic approach for dimer-dimer scattering and bound states of three and four resonantly interacting particles*, Phys. Rev. A**73**, 032724 (2006).

[Ch09] C. Chin, *Few-body universality of Ultracold Atomic Gases in the strong interaction regime*, talk presented at the ITAMP workshop "Efimov States in Molecules and Nuclei: Theoretical Methods and New Experiments", Rome, 19-21 Oct. 2009, available at http://www.cfa.harvard.edu/itamp/efimovschedule.html

[CMP10] Y. Castin, C. Mora, and L. Pricoupenko, *Four-body Efimov effect*, Phys. Rev. Lett. **105**, 223201 (2010) [arXiv:1006.4720 [cond-mat.quant-gas]].

[CT11] Y. Castin and E. Tignone, *Trimers in the resonant 2+1 fermionic problem on a narrow Feshbach resonance: From Efimovian Dawn to Hydrogenoid Twilight*, arXiv:1107.1881 [cond-mat.quant-gas] (2011).

[Da61] G.S. Danilov, Sov. Phys. JETP **13**, 349 (1961).

[De10] A. Deltuva, *Efimov physics in bosonic atom-trimer scattering*, Phys. Rev. A **82**, 040701(R) (2010) [arXiv:1009.1295 [physics.atm-clus]].

[De11] A. Deltuva, *Universality in bosonic dimer-dimer scattering*, arXiv:1107.3956 [physics.atom-ph] (2011).

[DE06a] J.P. D'Incao and B.D. Esry, *Mass Dependence of Ultracold Three-Body Collision Rates*, Phys. Rev. A **73**, 030702(R) (2006) [arXiv:physics/0508119].

[DE06b] J.P. D'Incao and B.D. Esry, *Enhancing the Observability of the Efimov Effect in Ultracold Atomic Gas Mixtures*, Phys. Rev. A **73**, 030703(R) (2006) [arXiv:cond-mat/0508474].

[DGE09] J.P. D'Incao, C.H. Greene, and B.D. Esry, *The short-range three-body phase and other issues impacting the observation of Efimov physics in ultracold quantum gases*, J. Phys. B: At. Mol. Opt. Phys. **42**, 044016 (2009) [arXiv:cond-mat/0703269].

[DJ99] B. DeMarco and D.S. Jin, *Onset of Fermi degeneracy in a trapped atomic gas*, Science **285**, 1703 (1999).

[DMZC08] B. Deh, C. Marzok, C. Zimmermann, and Ph.W. Courteille, *Feshbach resonances in mixtures of ultracold ^6Li and ^{87}Rb gases*, Phys. Rev. A **77**, 010701(R) (2008) [arXiv:0709.4554 [cond-mat.other]].

[DSE04] J.P. D'Incao, H. Suno, and B.D. Esry, *Limits on Universality in Ultracold Three-Boson Recombination*, Phys. Rev. Lett. **93**, 123201 (2004) [arXiv:physics/0403080].

[Da$^+$95] K.B. Davis, M.-O. Mewes, M.R. Andrews, N.J. van Druten, D.S. Durfee, D.M. Kurn, and W. Ketterle, *Bose-Einstein Condensation in a Gas of Sodium Atoms*, Phys. Rev. Lett. **75**, 3969 (1995).

[De+08] J. Deiglmayr, A. Grochola, M. Repp, K. Mörtlbauer, C. Glück, J. Lange, O. Dulieu, R. Wester, and M. Weidemüller, *Formation of ultracold polar molecules in the rovibrational ground state*, Phys. Rev. Lett. **101**, 133004 (2008) [arXiv:0807.3272 [quant-ph]].

[Ef70] V. Efimov, *Energy Levels Arising from Resonant Two-body Forces in a Three-body System*, Phys. Lett. B **33**, 563 (1970).

[Ef72] V. Efimov, *Level Spectrum of Three Resonantly Interacting Particles*, JETP Lett. **16**, 34 (1972).

[Ef73] V. Efimov, *Energy levels of three resonantly interacting particles*, Nucl. Phys. A **210**, 157 (1973).

[Ef93] V. Efimov, *Effective interaction of three resonantly interacting particles and the force range*, Phys. Rev. C **47**, 1876 (1993).

[Ei24] A. Einstein, *Quantentheorie des einatomigen idealen Gases*, Sitzungsberichte der Preussischen Akademie der Wissenschaften **1**, 261 (1924) [http://jptp.uni-bayreuth.de/vorlesungen/bec/einstein24.pdf].

[Es10] T. Esslinger, *Fermi-Hubbard physics with atoms in an optical lattice* , Ann. Rev. Cond. Mat. Phys. **1**, 070909 (2010) [arXiv:1007.0012 [cond-mat.quant-gas]].

[EGB99] B.D. Esry, C.H. Greene, and J.P. Burke, *Recombination of Three Atoms in the Ultracold Limit*, Phys. Rev. Lett. **83**, 1751 (1999).

[EMOT54] A. Erdélyi, W. Magnus, F. Oberhettinger, and F.G. Tricomi, *Tables of Integral Transforms*, Vol. I, McGraw-Hill Book Company, New York (1954).

[ENU11] S. Endo, P. Naidon, and M. Ueda, *Universal physics of 2+1 particles with non-zero angular momentum*, Few-Body Syst. (2011) [DOI: 10.1007/s00601-011-0229-6, arXiv:1103.2606 [physics.atom-ph]].

[Ef+09] M.A. Efremov, L. Plimak, B. Berg, M.Yu. Ivanov, and W.P. Schleich, *Efimov states in atom-molecular collisions*, Phys. Rev. A **80**, 022714 (2009) [arXiv:0905.3974 [quant-ph]].

[FG10] F. Ferlaino and R. Grimm, *Forty years of Efimov physics: How a bizarre prediction turned into a hot topic*, Physics **3**, 9 (2010).

[Fe+09] F. Ferlaino, S. Knoop, M. Berninger, W. Harm, J.P. D'Incao, H.-C. Nägerl, and R. Grimm, *Evidence for Universal Four-Body States Tied to an Efimov Trimer* , Phys. Rev. Lett. **102**, 140401 (2009) [arXiv:0903.1276 [cond-mat.other]].

[gsl] http://www.gnu.org/software/gsl/manual/html_node/

[Gr05] H.W. Grießhammer, *Naive Dimensional Analysis for Three-Body Forces Without Pions*, Nucl. Phys. A **760**, 110 (2005) [arXiv:nucl-th/0502039].

[GSKK09] N. Gross, Z. Shotan, S. Kokkelmans, and L. Khaykovich, *Observation of universality in ultracold ^7Li three-body recombination*, Phys. Rev. Lett. **103**, 163202 (2009) [arXiv:0906.4731 [cond-mat.other]].

[GSKK10] N. Gross, Z. Shotan, S. Kokkelmans, and L. Khaykovich, *Nuclear-spin-independent short-range three-body physics in ultracold atoms*, Phys. Rev. Lett. **105**, 103203 (2010) [arXiv:1003.4891 [cond-mat.quant-gas]].

[Go+99] D.E. Gonzáles Trotter et al., *New Measurement of the 1S0 Neutron-Neutron Scattering Length Using the Neutron-Proton Scattering Length as a Standard*, Phys. Rev. Lett. **83**, 3788 (1999).

[Gri+00] R.E. Grisenti, W. Schöllkopf, J.P. Toennies, G.C. Hegerfeldt, T. Köhler, and M. Stoll, *Determining the Bond Length and Binding Energy of the Helium Dimer by Diffraction from a Transmission Grating*, Phys. Rev. Lett. **85**, 2284 (2000).

[Gro+11] N. Gross, Z. Shotan, O. Machtey, S. Kokkelmans, and L. Khaykovich, *Study of Efimov physics in two nuclear-spin sublevels of 7Li*, Comptes Rendus Physique **12**, 4 (2011) [arXiv:1009.0926 [cond-mat.quant-gas]].

[HH09] K. Helfrich and H.-W. Hammer, *Resonant atom-dimer relaxation in ultracold atoms*, Europhys. Lett. **86**, 53003 (2009) [arXiv:0902.3410 [cond-mat.other]].

[HH11a] K. Helfrich and H.-W. Hammer, *Resonant three-body physics in two spatial dimensions*, Phys. Rev. A **83**, 052703 (2011), Copyright (2011) by the American Physical Society, [arXiv:0902.3410 [cond-mat.other]].

[HH11b] K. Helfrich and H.-W. Hammer, *On the Efimov Effect in Higher Partial Waves*, J. Phys. B: At. Mol. Opt. Phys. **44**, 215301 (2011) [arXiv:1107.0869 [cond-mat.quant-gas]].

[HHH11] P. Hagen, H.-W. Hammer, and C. Hanhart, *Two- and three-body structure of the Y(4660)*, Phys. Lett. B **696**, 103 (2011) [arXiv:1007.1126 [hep-ph]].

[HHP10] K. Helfrich, H.-W. Hammer, and D.S. Petrov, *Three-body problem in heteronuclear mixtures with resonant interspecies interaction*, Phys. Rev. A **81**, 042715 (2010), Copyright (2010) by the American Physical Society, [arXiv:1001.4371 [cond-mat.quant-gas]].

[HL09] H.-W. Hammer and D. Lee, *Causality and universality in low-energy quantum scattering*, Phys. Lett. B **681**, 500 (2009) [arXiv:0907.1763 [nucl-th]].

[HL10] H.-W. Hammer and D. Lee, *Causality and the effective range expansion*, Annals Phys. **325**, 2212 (2010) [arXiv:1002.4603 [nucl-th]].

[HLP07] H.-W. Hammer, T. A. Lähde, and L. Platter, *Effective Range Corrections to Three-Body Recombination for Atoms with Large Scattering Length*, Phys. Rev. A **75**, 032715 (2007) [arXiv:cond-mat/0611769].

[HM01] H.-W. Hammer and T. Mehen, *A renormalized equation for the three-body system with short-range interactions*, Nucl. Phys. A **690**, 535 (2001) [arXiv:nucl-th/0011024].

[HP07] H.-W. Hammer and L. Platter, *Universal Properties of the Four-Body System with Large Scattering Length*, Eur. Phys. J. A **32**, 113 (2007) [arXiv:nucl-th/0610105].

[HS04] H.-W. Hammer and D.T. Son, *Universal Properties of Two-Dimensional Boson Droplets*, Phys. Rev. Lett. **93**, 250408 (2004) [arXiv:cond-mat/0405206].

[HZGC11] C.-L. Hung, X. Zhang, N. Gemelke, and C. Chin, *Observation of scale invariance and universality in two-dimensional Bose gases*, Nature **470**, 236 (2011) [arXiv:1009.0016 [cond-mat.quant-gas]].

[Har+11] H. Hara, Y. Takasu, Y. Yamaoka, J.M. Doyle, and Y. Takahashi, *Quantum degenerate mixtures of alkali and alkaline-earth-like atoms*, Phys. Rev. Lett. **106**, 205304 (2011) [arXiv:1104.4430 [physics.atom-ph]].

[Han+11] A.H. Hansen, A. Khramov, W.H. Dowd, A.O. Jamison, V.V. Ivanov, and S. Gupta, *Quantum Degenerate Mixture of Ytterbium and Lithium Atoms*, Phys. Rev. A **84**, 011606(R) (2011) [arXiv:1105.5751 [cond-mat.quant-gas]].

[Hu+09] J.H. Huckans, J.R. Williams, E.L. Hazlett, R.W. Stites, and K.M. O'Hara, *Three-Body Recombination in a Three-State Fermi Gas with Widely Tunable Interactions*, Phys. Rev. Lett. **102**, 165302 (2009) [arXiv:0810.3288 [physics.atom-ph]].

[Is10] M. Iskin, *Dimer-atom scattering between two identical fermions and a third particle*, Phys. Rev. A **81**, 043634 (2010) [arXiv:1003.0106 [cond-mat.quant-gas]].

[IS08] M. Iskin and C.A.R. Sá de Melo, *Fermi-Fermi mixtures in the strong-attraction limit*, Phys. Rev. A **77**, 013625 (2008) [arXiv:0709.4424 [cond-mat.supr-con]].

[In+98] S. Inouye, M.R. Andrews, J. Stenger, H.-J. Miesner, D.M. Stamper-Kurn, and W. Ketterle, *Observation of Feshbach resonances in a Bose–Einstein condensate*, Nature **392**, 151 (1998).

[Iv+11] V.V. Ivanov, A. Khramov, A.H. Hansen, W.H. Dowd, F. Muenchow, A.O. Jamison, S. Gupta, *Sympathetic Cooling in an Optically Trapped Mixture of Alkali and Spin-Singlet Atoms*, Phys. Rev. Lett. **106**, 153201 (2011) [arXiv:1101.5142 [physics.atom-ph]].

[Jo06] S. Jonsell, *Efimov states for systems with negative scattering lengths*, Europhys. Lett. **76**, 8 (2006).

[Ju09] P.S. Julienne, *Ultracold molecules from ultracold atoms: a case study with the KRb molecule*, Faraday Discuss. **142**, 361 (2009) [arXiv:0812.1233 [physics.atom-ph]].

[JPP10] C. Ji, L. Platter, and D.R. Phillips, *Beyond universality in three-body recombination: an Effective Field Theory treatment*, Europhys. Lett. **92**, 13003 (2010) [arXiv:1005.1990 [cond-mat.quant-gas]].

[JPP11] C. Ji, D.R. Phillips, and L. Platter, *The three-boson system at next-to-leading order in the pionless EFT*, arXiv:1106.3837 [nucl-th] (2011).

[Kn] S. Knoop, private communication.

[KDSK99] W. Ketterle, D.S. Durfee, and D.M. Stamper-Kurn, *Making, probing and understanding Bose-Einstein condensates*, in *Bose-Einstein condensation in atomic gases, Proceedings of the International School of Physics "Enrico Fermi", Course CXL*, edited by M. Inguscio, S. Stringari and C.E. Wieman, IOS Press, Amsterdam (1999) [arXiv:cond-mat/9904034].

[KM06] O.I. Kartavtsev and A.V. Malykh, *Universal low-energy properties of three two-dimensional bosons*, Phys. Rev. A **74**, 042506 (2006) [arXiv:physics/0606013].

[KM07a] O.I. Kartavtsev and A.V. Malykh, *Low-energy three-body dynamics in binary quantum gases*, J. Phys. B: At. Mol. Opt. Phys. **40**, 1429 (2007) [arXiv:physics/0610261].

[KM07b] O.I. Kartavtsev and A.V. Malykh, *Universal description of the rotational-vibrational spectrum of three particles with zero-range interactions*, Pis'ma ZhETF **86**, 713 (2007) [JETP Lett. **86**, 625 (2008), arXiv:0709.4151 [physics.atom-ph]].

[KZ08] W. Ketterle and M. Zwierlein, *Making, probing and understanding ultracold Fermi gases*, in *Ultracold Fermi Gases, Proceedings of the International School of Physics "Enrico Fermi", Course CLXIV, Varenna, 20 - 30 June 2006*, edited by M. Inguscio, W. Ketterle, and C. Salomon, IOS Press, Amsterdam (2008) [arXiv:0801.2500 [cond-mat/other]].

[Kn+09] S. Knoop, F. Ferlaino, M. Mark, M. Berninger, H. Schöbel, H.-C. Nägerl, and R. Grimm, *Observation of an Efimov-like resonance in ultracold atom-dimer scattering*, Nature Phys. **5**, 227 (2009) [arXiv:0807.3306 [cond-mat.other]].

[Kr+06] T. Kraemer, M. Mark, P. Waldburger, J.G. Danzl, C. Chin, B. Engeser, A.D. Lange, K. Pilch, A. Jaakkola, H.-C. Nägerl, and R. Grimm, *Evidence for Efimov quantum states in an ultracold gas of caesium atoms*, Nature **440**, 315 (2006) [arXiv:cond-mat/0512394].

[Le06] D. Lee, *Large-N droplets in two dimensions*, Phys. Rev. A **73**, 063204 (2006) [arXiv:physics/0512085].

[LL85] L.D. Landau and E.M. Lifschitz, *Lehrbuch der theoretischen Physik, Band 3, Quantenmechanik*, Akademie-Verlag, Berlin (1985).

[LP11] J. Levinsen and D.S. Petrov, *Atom-dimer and dimer-dimer scattering in fermionic mixtures near a narrow Feshbach resonance*, [arXiv:1101.5979 [cond-mat.quant-gas]].

[LTWP09] J. Levinsen, T.G. Tiecke, J.T.M. Walraven, and D.S. Petrov, *Atom-Dimer Scattering and Long-Lived Trimers in Fermionic Mixtures*, Phys. Rev. Lett. **103**, 153202 (2009) [arXiv:0907.5523 [cond-mat.quant-gas]].

[La$^+$10] G. Lamporesi, J. Catani, G. Barontini, Y. Nishida, M. Inguscio, and F. Minardi, *Scattering in Mixed Dimensions with Ultracold Gases*, Phys. Rev. Lett. **104**, 153202 (2010) [arXiv:1002.0114 [cond-mat.quant-gas]].

[Lo$^+$10a] T. Lompe, T.B. Ottenstein, F. Serwane, K. Viering, A.N. Wenz, G. Zürn, and S. Jochim, *Atom-Dimer Scattering in a Three-Component Fermi Gas*, Phys. Rev. Lett. **105**, 103201 (2010) [arXiv:1003.0600 [cond-mat.quant-gas]].

[Lo$^+$10b] T. Lompe, T.B. Ottenstein, F. Serwane, A.N. Wenz, G. Zürn, and S. Jochim, *Radio Frequency Association of Efimov Trimers*, Science **330**, 940 (2010) [arXiv:1006.2241 [cond-mat.quant-gas]].

[Mi] F. Minardi, private communication.

[MKSP08] B. Marcelis, S.J.J.M.F. Kokkelmans, G.V. Shlyapnikov, and D.S. Petrov, *Collisional properties of weakly bound heteronuclear dimers*, Phys. Rev. A **77**, 032707 (2008) [arXiv:0711.4632 [cond-mat.stat-mech]].

[MNS90] G.A. Miller, B.M.K. Nefkens, and I. Šlaus, *Charge symmetry, quarks and mesons*, Phys. Rept. **194**, 1 (1990).

[MS08] P. Massignan and H.T.C. Stoof, *Efimov states near a Feshbach resonance*, Phys. Rev. A **78**, 030701(R) (2008) [arXiv:cond-mat/0702462v4].

[Ma$^+$09] C. Marzok, B. Deh, C. Zimmermann, Ph.W. Courteille, E. Tiemann, Y.V. Vanne, and A. Saenz, *Feshbach resonances in an ultracold ^7Li and ^{87}Rb mixture*, Phys. Rev. A **79**, 012717 (2009) [arXiv:0808.3967 [cond-mat.other]].

[NFJ99] E. Nielsen, D.V. Fedorov, and A.S. Jensen, *Structure and Occurrence of Three-Body Halos in Two Dimensions*, Few-Body Syst. **27**, 15 (1999).

[NFJG01] E. Nielsen, D.V. Fedorov, A.S. Jensen, and E. Garrido, *The three-body problem with short-range interactions*, Phys. Rep. **347**, 373 (2001).

[NM99] E. Nielsen and J.H. Macek, *Low-energy Recombination of Identical Bosons by Three-Body Collisions*, Phys. Rev. Lett. **83**, 1566 (1999).

[NT08] Y. Nishida and S. Tan, *Universal Fermi gases in mixed dimensions*, Phys. Rev. Lett. **101**, 170401 (2008) [arXiv:0806.2668 [cond-mat.other]].

[NT10] Y. Nishida and S. Tan, *Confinement-induced p-wave resonances from s-wave interaction*, Phys. Rev. A **82**, 062713 (2010) [arXiv:1011.0033 [cond-mat.quant-gas]].

[NT11] Y. Nishida and S. Tan, *Liberating Efimov physics from three dimensions*, Few-Body Syst. (2011) [DOI: 10.1007/s00601-011-0243-8, arXiv:1104.2387 [cond-mat.quant-gas]].

[Na+10] S. Nakajima, M. Horikoshi, T. Mukaiyama, P. Naidon, and M. Ueda, *Nonuniversal Efimov Atom-Dimer Resonances in a Three-Component Mixture of 6Li*, Phys. Rev. Lett. **105**, 023201 (2010) [arXiv:1003.1800 [cond-mat.quant-gas]].

[Na+11] S. Nakajima, M. Horikoshi, T. Mukaiyama, P. Naidon, and M. Ueda, *Measurement of an Efimov trimer binding energy in a three-component mixture of ^6Li*, Phys. Rev. Lett. **106**, 143201 (2011) [arXiv:1010.1954 [cond-mat.quant-gas]].

[Ne+09] N. Nemitz, F. Baumer, F. Münchow, S. Tassy, and A. Görlitz, *Production of heteronuclear molecules in an electronically excited state by photoassociation in a mixture of ultracold Yb and Rb*, Phys. Rev. A **79**, 061403(R) (2009).

[Ot+08] T.B. Ottenstein, T. Lompe, M. Kohnen, A.N. Wenz, and S. Jochim, *Collisional stability of a three-component degenerate Fermi gas*, Phys. Rev. Lett. **101**, 203202 (2008) [arXiv:0806.0587 [cond-mat.other]].

[Pe03] D.S. Petrov, *Three-body problem in Fermi gases with short-range interparticle interaction*, Phys. Rev. A **67**, 010703(R) (2003) [arXiv:cond-mat/0209246].

[Pe04] D.S. Petrov, *Three-boson problem near a narrow Feshbach resonance*, Phys. Rev. Lett. **93**, 143201 (2004) [arXiv:cond-mat/0404036].

[PBS03] D.S. Petrov, M.A. Baranov, and G.V. Shlyapnikov, *Superfluid transition in quasi-two-dimensional Fermi gases*, Phys. Rev. A **67**, 031601(R) (2003) [arXiv:cond-mat/0212061].

[PDH09] S.E. Pollack, D. Dries, and R.G. Hulet, *Universality in three- and four-body bound states of ultracold atoms*, Science **18**, 1683 (2009) [arXiv:0911.0893 [cond-mat.quant-gas]].

[PHM04] L. Platter, H.-W. Hammer, and Ulf-G. Meißner, *Universal Properties of the Four-Boson System in Two Dimensions*, Few-Body Syst. **35**, 169 (2004) [arXiv:cond-mat/0405660].

[PHS00] D.S. Petrov, M. Holzmann, and G.V. Shlyapnikov, *Bose-Einstein Condensation in Quasi-2D Trapped Gases*, Phys. Rev. Lett. **84**, 2551 (2000) [arXiv:cond-mat/9909344].

[PJP09] L. Platter, C. Ji, and D.R. Phillips, *Range Corrections to Three-Body Observables near a Feshbach Resonance*, Phys. Rev. A **79**, 022702 (2009) [arXiv:0808.1230 [cond-mat.other]].

[PO07] L. Pricoupenko and M. Olshanii, *Stability of two-dimensional Bose gases in the resonant regime*, J. Phys. B: At. Mol. Opt. Phys. **40**, 2065 (2007) [arXiv:cond-mat/0205210].

[PP06] L. Platter and D.R. Phillips, *The Three-Boson System at Next-To-Next-To-Leading Order*, Few-Body Syst. **40**, 35 (2006) [arXiv:cond-mat/0604255].

[PS01] D.S. Petrov and G.V. Shlyapnikov, *Interatomic collisions in a tightly confined Bose gas*, Phys. Rev. A **64**, 012706 (2001) [arXiv:cond-mat/0012091].

[PS08] L. Platter and J.R. Shepard, *Scaling functions applied to three-body recombination of ^{133}Cs atoms*, Phys. Rev. A **78**, 062717 (2008) [arXiv:0711.1908 [cond-mat.other]].

[PSS04] D.S. Petrov, C. Salomon, and G.V. Shlyapnikov, *Weakly Bound Dimers of Fermionic Atoms*, Phys. Rev. Lett. **93**, 090404 (2004) [arXiv:cond-mat/0309010].

[PSS05] D.S. Petrov, C. Salomon, and G.V. Shlyapnikov, *Scattering properties of weakly bound dimers of fermionic atoms*, Phys. Rev. A **71**, 012708 (2005) [arXiv:cond-mat/0407579].

[PTVF92] W.H. Press, S.A. Teukolsky, W.T. Vetterling, and B.P. Flannery, *Numerical Recipes in C, The Art of Scientific Computing*, Second Edition, Cambridge University Press, Cambridge (1992) [available online: http://apps.nrbook.com/c/index.html]

[Sh07] J.R. Shepard, *Calculations of recombination rates for cold ^{4}He atoms from atom-dimer phase shifts and determination of universal scaling functions*, Phys. Rev. A **75**, 062713 (2007) [arXiv:cond-mat/0702290].

[STM57] G.V. Skorniakov and K.A. Ter-Martirosian, *Three Body Problem for Short Range Forces. 1. Scattering of Low Energy Neutrons by Deuterons*, Sov. Phys. JETP **4**, 648 (1957) [J. Exptl. Theoret. Phys. (U.S.S.R.) 31, 775 (1956)].

[Si$^+$05] C. Silber, S. Günther, C. Marzok, B. Deh, Ph.W. Courteille, and C. Zimmermann, *Quantum-Degenerate Mixture of Fermionic Lithium and Bosonic Rubidium Gases*, Phys. Rev. Lett. **95**, 170408 (2005) [arXiv:cond-mat/0506217].

[TSGS10] M.K. Tey, S. Stellmer, R. Grimm, and F. Schreck, *Double-degenerate Bose-Fermi mixture of strontium*, Phys. Rev. A **82**, 011608(R) (2010) [arXiv:1006.1131 [cond-mat.quant-gas]].

[Ta$^+$10] S. Tassy, N. Nemitz, F. Baumer, C. Höhl, A. Batär, and A. Görlitz, *Sympathetic cooling in a mixture of diamagnetic and paramagnetic atoms*, J. Phys. B: At. Mol. Opt. Phys. **43**, 205309 (2010).

[ucan] http://ucan.physics.utoronto.ca/News

[vSDG09] J. von Stecher, J.P. D'Incao, and C.H. Greene, *Four-body legacy of the Efimov effect*, Nature Phys. **5**, 417 (2009) [arXiv:0810.3876v1 [physics.atom-ph]].

[vSG07] J. von Stecher and C.H. Greene, *Spectrum and Dynamics of the BCS-BEC crossover from a few-body perspective*, Phys. Rev. Lett. **99**, 090402 (2007) [arXiv:cond-mat/0701044].

[vSGB07] J. von Stecher, C.H. Greene, and D. Blume, *BEC-BCS Crossover of a Trapped Two-Component Fermi Gas with Unequal Masses*, Phys. Rev. A **76**, 053613 (2007) [arXiv:0705.0671 [cond-mat.other]].

[vSt10] J. von Stecher, *Weakly Bound Cluster States of Efimov Character*, J. Phys. B: At. Mol. Opt. Phys. **43**, 101002 (2010) [arXiv:0909.4056 [cond-mat.quant-gas]].

[vSt11] J. von Stecher, *Universal Five- and Six-Body Droplets Tied to an Efimov Trimer*, arXiv:1106.2319 [cond-mat.quant-gas] (2011).

[VdGVvdE84] B.J. Verhaar, L.P.H. de Goey, E.J.D. Vredenbregt, and J.P.H.W. van den Eijnde, *Scattering length and effective range in two dimensions; application to adsorbed hydrogen atoms*, J. Phys. A: Math. Gen. **17**, 595 (1984).

[WDG11a] Y. Wang, J.P. D'Incao, and C.H. Greene, *The Efimov effect for three interacting bosonic dipoles*, Phys. Rev. Lett. **106**, 233201 (2011) [arXiv:1103.1406 [physics.atom-ph]].

[WDG11b] Y. Wang, J.P. D'Incao, and C.H. Greene, *Universal three-body physics for fermionic dipoles*, arXiv:1106.6133 [physics.atom-ph] (2011).

[Web+08] C. Weber, G. Barontini, J. Catani, G. Thalhammer, M. Inguscio, and F. Minardi, *Association of ultracold double-species bosonic molecules*, Phys. Rev. A **78**, 061601(R) (2008) [arXiv:0808.4077 [cond-mat.other]].

[Wen+09] A.N. Wenz, T. Lompe, T.B. Ottenstein, F. Serwane, G. Zürn, and S. Jochim, *A Universal Trimer in a Three-Component Fermi Gas*, Phys. Rev. A **80**, 040702(R) (2009) [arXiv:0906.4378 [cond-mat.quant-gas]].

[Wi+09] J.R. Williams, E.L. Hazlett, J.H. Huckans, R.W. Stites, Y. Zhang, and K.M. O'Hara, *Evidence for Ground- and Excited-State Efimov Trimers in a Three-State Fermi Gas*, Phys. Rev. Lett. **103**, 130404 (2009) [arXiv:0908.0789 [quant-ph]].

[YFT07] M.T. Yamashita, T. Frederico, and L. Tomio, *Three-boson recombination at ultralow temperatures*, Phys. Lett. A **363**, 468 (2007) [arXiv:cond-mat/0608542].

[Za+09] M. Zaccanti, B. Deissler, C. D'Errico, M. Fattori, M. Jona-Lasinio, S. Müller, G. Roati, M. Inguscio, and G. Modugno, *Observation of an Efimov spectrum in an atomic system*, Nature Phys. **5**, 586 (2009) [arXiv:0904.4453 [cond-mat.quant-gas]].

[Zi+08] J.J. Zirbel, K.-K. Ni, S. Ospelkaus, J.P. D'Incao, C.E. Wieman, J. Ye, and D.S. Jin, *Collisional stability of fermionic Feshbach molecules*, Phys. Rev. Lett. **100**, 143201 (2008) [arXiv:0710.2479 [cond-mat.other]].

Danksagung

Zu guter Letzt möchte ich mich noch bei all denen bedanken, die mich auf dem Weg zur Promotion begleitet und dabei zum Gelingen dieser Arbeit beigetragen haben.

An erster Stelle ist dabei Hans-Werner zu nennen. Danke, dass Du mir dieses Thema vorgeschlagen und mich bei der Bearbeitung kontinuierlich unterstützt hast. Du hattest immer eine offene Tür, hast mir die Teilnahme an vielen Konferenzen ermöglicht, an meine Fähigkeiten geglaubt und für eine sehr angenehme, nette Arbeitsatmosphäre gesorgt; das ist nicht selbstverständlich und ich weiß das sehr zu schätzen.

Weiterhin möchte ich mich bei Herrn Prof. Rosch dafür bedanken, dass er sich bereit erklärt hat, mein zweiter Gutachter zu sein. Auch für die Möglichkeit, in Ihrem Gruppenseminar vorzutragen und für Ihre Offenheit meiner Arbeit gegenüber bedanke ich mich.

Natürlich gilt mein Dank auch Herrn Prof. Meschede und Herrn Prof. Vöhringer, die sich bereitwillig als weitere Kommissionsmitglieder zur Verfügung gestellt haben.

Meine Kollegen des dritten Stocks im HISKP sollen auch nicht unerwähnt bleiben, danke für die vielen gemeinsamen Mensabesuche, die *social event* Abende, das *lunch seminar* und die hilfsbereite, offene Atmosphäre. Besonders danken möchte ich meinen Bürokollegen David C., Kathryn, Konstantin und Patrick, der ganzen Arbeitsgruppe Hammer, und auch besonders Simon K., Sebastian K., Mark, Matthias und Bastian.

I am also grateful for discussions with and comments on my work by V. Efimov, D.S. Petrov, L. Platter, D. Lee, and D. Phillips. Furthermore, I would like to thank the Institute for Nuclear Theory, Seattle, and the Chalmers University, Gothenburg, for their hospitality.

Der *Bonn-Cologne Graduate School of Physics and Astronomy* und der *Studienstiftung des deutschen Volkes* danke ich für die finanzielle und ideelle Unterstützung. Der BCGS bin ich vor allem für die unkomplizierte Zuteilung der Reisemittel dankbar, die mir viele Dienstreisen ermöglicht hat. Von der Aufnahme in die Studienstiftung konnte ich vor allem durch viele Kontakte, die spannenden Doktorandenforen und natürlich die Sommerakademien enorm profitieren.

Nun möchte ich mich noch bei meinen “Bonner” Freunden bedanken, die mich größtenteils auch schon durch das ganze Studium hindurch begleitet, motiviert und unterstützt haben. Danke Bernhard, David C., David M., Eike, Elena, Friedemann, Karim, Katja, Markus-J., Martina, Nils, Sebastian B., Stefan, Theresa und auch denen, die ich jetzt hier nicht aufzählen kann.

Großer Dank gilt auch den Korrekturlesern dieser Arbeit, David C., Klaus, Sebastian K. und Stefan.

Meiner Familie möchte ich für ihre stete Unterstützung danken.

Klaus, was kann ich schon schreiben, danke für alles.